A Novel USD-Modelling Tool for Chromatography Design - Specification of Resin Properties

A thesis submitted to University College London for the degree of Doctor of Philosophy

By

Alison Tang

Department of Biochemical Engineering
University College London
Torrington Place
London
WC1E 7JE

2010

I, Alison Tang confirm that the work presented in this thesis is my own. Where information has been derived from other sources, I confirm that this has been indicated in the thesis.

Signed ……

Date …….

Abstract

In the early stages of downstream process development there is typically only limited availability of process material. Novel methods to obtain information from fewest experiments are essential to make informed choices between processing alternatives at the earliest stage. Design of chromatographic separation initially involves scouting of appropriate matrix type, mobile phase compositions followed by test runs at lab scale and verified at pilot scale.

Traditional small-scale methods for chromatography development focus on the screening of separation media and feedstock conditions. It is still necessary to predict chromatography performance at different scales and operating conditions. In this work a new method has been developed to predict performance of larger scale columns using an ultra scale-down approach. The strategy breaks traditional geometric scaling rules, using models to correct for the differences in performance and also for prediction of the effect of changes in operating conditions. Micro-scale columns were used to scale down lab scale runs further challenging the traditional scale down strategies.

The characteristics of antibody fragments in *E.coli* lysate were identified in terms of pH, precipitation and ionic strength to determine good binding conditions. Chromatography studies were carried out at laboratory scale (1 mL) to investigate the flowrate effects on the adsorption of antibody fragments on a strong cation exchange resin. The effect was successfully predicted using a general rate model, which describes the physical and chemical forces of resin-protein interactions but with modifications to allow for deviations noted in experimental performance possibly due to fouling and long loading times changing the rate of protein transfer. Further studies were carried out using micro-scale tip chromatography, mimicking the results obtained at 1 mL scale. A similar effect of flowrate was observed and the scale up factor to predict the performance of laboratory 1 mL scale from 40 μL micro-scale was investigated.

Acknowledgement

Firstly I wish to thank my supervisors Professor Mike Hoare and advisor Dr. Dan Bracewell for their guidance and invaluable advices throughout the project. I would also like to express my gratitude towards my family for their support. Without them this PhD would not be successful.

I would also like to acknowledge all biochemical engineers who helped and supported me during the course of my PhD. On a personal level I would like to thank all members of the department especially the cheerful people from vineyard office, Roberts 107 and colonnades office.

Table of contents

List of figures

List of Tables

Nomenclature

C	protein breakthrough concentration	$mg\ mL^{-1}$
C_0	initial protein concentration	$mg\ mL^{-1}$
C_{bi}	bulk phase concentration of component i	$mol\ m^{-3}$
C_{fi}	Feed concentration profile of component I, a tie dependent variable	$mol\ m^{-3}$
C_{pi}	Concentration of component i in the stagnant fluid phase inside particle macropores	$mol\ m^{-3}$
D_{ax}	Axial or radial dispersion coefficient of component i	$m^2\ s^{-1}$
D_b	intra-particle bead diffusivity	$m^2\ s^{-1}$
d_m	molecular diameter	m
D_m	molecular diffusivity	
dp	pore diameter	m
Fab'	fragment antigen binding with hinge sequence	
		$m^3\ mol^{-1}$
k_{ads}	Adsorption rate constant	s^{-1}
K_d	Langmuir constant	
k_d	Desorption rate constant for component i	s^{-1}
k_i	film mass transfer coefficient of component i	$m\ s^{-1}$
P	modified protein breakthrough concentration	$mg\ mL^{-1}$
P_0	modified protein concentration	$mg\ mL^{-1}$
Q_{eq}	Dynamic binding capacity	$mg\ mL^{-1}$
Q_{max}	Maximum binding capacity	$mg\ mL^{-1}$
R	coordinates for particle	
R_p	Particle radius	m
t	Time	s
v	Interstitial velocity	$cm\ h^{-1}$
V_l	volume of liquid	mL
V_m	volume of resin	mL
Z	Axial coordinate	
ε_b	Bed void volume fraction	
ε_p	Partical porosity	
λ	dm/D_p	
τ	tortuosity	

1. Introduction

The purpose of the project was to reduce the number of experiments required to be performed when optimising an adsorption step of chromatography by using computer modelling. In addition to minimising experimental effort, the project also opens the opportunity to scale-down the unit operation using micro-scale chromatography columns; reduce the amount of feedstock required to explore a design space and at the same time shorten the time required to complete one experiment due to the fact that a smaller column is used.

The technology aims to narrow down a large design space, allowing subsequent optimisation experiment upon points that are closer to the operating hot spot hence making process optimisation more efficient in terms of feed stock utilisation. This is especially useful during early process development where feedstock and time is limited.

Because antibodies and its recombinant forms are popular therapeutic choices, therefore Fab' fragments expressed by an *E.coli* system was used in this project to mimic a real process feed-stream.

1.1 Antibodies and antibody fragments

1.1.1 Function of antibodies

Antibodies are a major protein component of the vertebrate immune system. This system can be roughly divided into two types of immunity; Cellular immunity and humoral immunity. Cellular immunity is mediated by T lymphocytes of T cells. The system guards against intracellular pathogens for example viruses and bacteria, and hinders fungi, parasites, cancerous cells and foreign tissues. Humoral immunity is mediated by the group of proteins of interest – antibodies. Antibodies are also known as immunoglobulin and are produced by B lymphocytes and B cells. This type of immunity is most effective against bacterial infections and extra cellular viral infections (Voet, 1995).

Antibodies bind to pathogenic or foreign bodies in order to fulfil their biological function. The specific binding site of an antibody is called an antigen, with great specificity and strength. Antibodies can bind their targets with affinities between 10^8 and 10^{11} M^{-1}. Once bound to the target antigen, antibodies contribute to immunity in three main ways, depending on the antibody isotype. Firstly they can halt pathogens from entering or damaging host cells by binding to them and blocking contact with cells and tissues. This structural mode of action is known as neutralization. Secondly they can trigger the pathogen's destruction by activating the complement pathways (Ravetch, 2001).Thirdly they can coat the pathogen and trigger a range of effector functions such as phagocytosis by phagocytes, degranulation by mast cells and neutrophils, and release of cytokines and cytotoxic molecules by natural killer cells (Janeway, 2001). The appropriate immune mechanisms for distinct pathogens are selected by the isotype of antibody.

Human antibodies come in five different isotypes or classes: IgA, IgD, IgE, IgG and IgM. These are described in Table 1.1. There are also four further subclasses of IgG and two of IgA. Although different isotypes have different effector functions and biological functions, mediated by differences in the structure of specific constant region of the protein, they all bind antigens in the same way and share a common immunoglobulin fold.

1.1.2 Antibody structure

The basic unit of each antibody is the immunoglobulin (Ig) monomer. This is a Y shaped tetrameric molecule consisting of four polypeptide chains; two identical heavy (H) chains and two identical light (L) chains. These are connected by disulphide bonds. Each chain is composed of a number of domains known as Ig domains, each consisting of about 70-110 amino acid residues. They fold in a characteristic β-sheet pattern known as the Ig fold, where two domains are held together in a sandwich shape by conserved cysteines and non-covalent bonds. The structure is shown in Figure 1.1. The H and L chains consist of a mixture of constant (C) and variable domains (V). Each H chain has three

constant regions (C_H1, C_H2, and C_H3) and a single variable region (V_H). Each L chain has a single constant region (C_L) and a single variable region (V_L) (Voet, 1995).

The variable domains, located at the N-terminal tip of the Ig monomer, are extremely variable in amino acid sequence, and form the unique antigen-recognition site of each antibody. V_L and V_H are not uniformly variable however; as all variable chains share conserved amino acid residues to form the Ig fold. Variability is focused into three short hypervariable sequences, each a few residues in length. These hypervariable sequences line the antigen-binding sites, and determine the antibodies binding specificity. Therefore they are also known as complementarily-determining regions (CDRs) (Janeway, 2001).

There are two measures of the strength of binding of any particular antibody for its antigen: affinity and avidity. Affinity measures the strength with which a single Fab binds to an antigen. However, as an antibody, and indeed an antigen, may possess multiple binding sites that may contribute to increase the strength of antibody-antigen binding, the term avidity is used to describe the total strength at which a particular antibody binds its antigen. Avidity is the combined strength of multiple bond interactions; therefore the avidity of an antibody may be several orders of magnitude higher than its affinity, especially in the case of multimeric antibody isotypes such as IgM.

The constant regions are different between antibody isotypes and determine the antibodies structure and effector functions. For example, IgM constant region cause association of five Ig monomers to form a pentamer. The IgE constant region can initiate mast cell degranulation when complexed with an antigen.

A typical Ig monomer is depicted in Fig. 1.1, illustrating all the regions discussed above. Also depicted are the three regions of the protein: Fc, Fab, and Fv. These are defined by proteolytic digestion of the Ig monomer. Treatment of the Ig monomer with the enzyme papain results in the cleavage of the molecule at the hinge region (also shown) into two Fab fragments and one Fc fragment. The Fc region contains only constant domains, and is named historically ‘fragment crystallisable’. F_c region is responsible for the immune response for a given antigen; this is achieved by binding to a specific class of F_c

receptors and other immune molecules, for example complement proteins. The Fab fragments, which each consist of one complete light chain and C_H1 and V_H from the heavy chain, contain the antibody binding site. Hence they are known as 'fragment antigen binding'. The Fab fragment can be further cleaved by enzymatic approaches, yielding the Fv (fragment variable) fragment. This fragment contains only the variable domains of the H and L chains (Brinkmann et al, 1997). It is the smallest antibody fragment that retains antigen binding activity, but generally Fv fragments by themselves are unstable as the V_H and V_L domains can dissociate, often accompanied by aggregation (Glockshuber et al, 1990)

Table 1.1 A list of antibody isotypes and their corresponding functions and number of Ig monomers

Isotype	Function	No. of Ig monomers
IgA	Prevents colonization of mucosal zones by pathogens (Underdown, 1986)	Two (dimer)
IgD	B cells antigen receptor (Geisberger, 2006)	One (monomer)
IgE	Protects against parasitic worms. Binds to allergens and induces histamine release by mast cells (Gerald Pier, 2004)	One (monomer)
IgG	Fights antigens by providing majority of antibody based immunity against foreign bodies. Found in four subtypes (Gerald Pier, 2004)	One (monomer)
IgM	Expressed on the surface of B cells as well as in secreted form. Eliminates pathogens in early phase of adaptive immune response before sufficient IgG can be produced (Geisberger, 2006; Gerald Pier, 2004)	Five (pentamer)

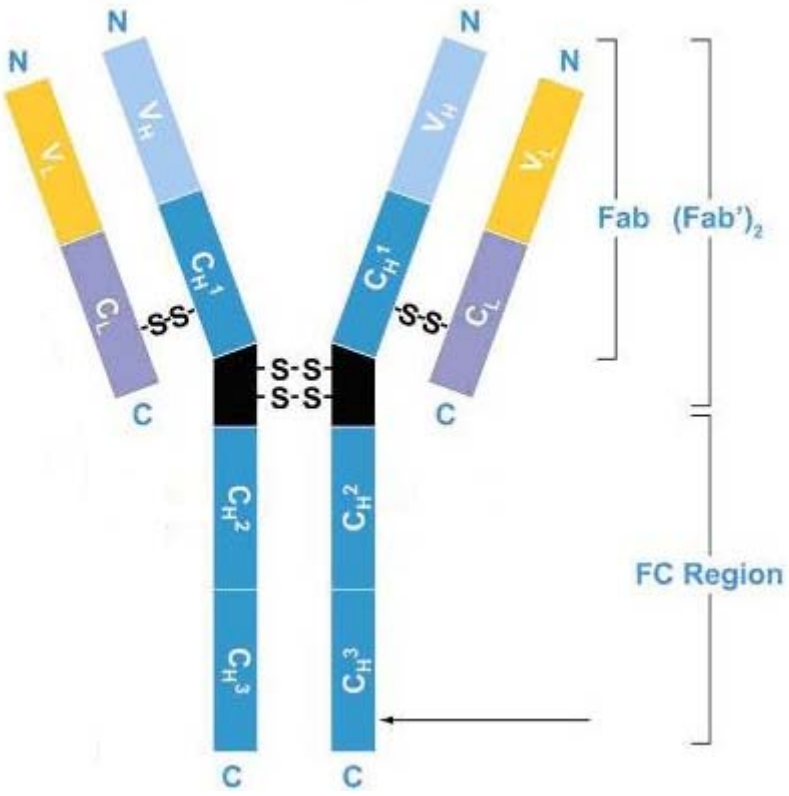

Figure 1.1 Structure of an antibody. See text for details.

1.1.3 Antibodies in Biotechnology

Antibodies have many structural and functional features that make them valuable reagents for research, therapy, and other biotechnological applications. Their key property is their ability to form highly specific interactions with a wide variety of ligands. Functional domains providing specific antigen-binding (Fab or Fv) or effector functions (Fc) can be exchanged between molecules, expressed as separate biologically active fragments, or expressed as components of novel fusion proteins (Morrison, 1992; Chester, 1995).

Either polyclonal or monoclonal antibodies are used in biotechnology. Polyclonal antibodies are multiple variant forms of antibody binding the same target; they are produced by different V (D) J recombination in different producing cells, or clones. Monoclonal antibodies are identical in their protein 1^0 structure, all produced from a single clone.

Monoclonal antibodies are more commonly used in biotechnology as they can be fully characterised, defined and optimised.

As well as whole antibodies, antibody fragments, such as Fab or Fv, are also commonly used in biotechnology (Joosten et al., 2003) as they can be more easily produced in recombinant systems, have reduced molecular weight, and lack the effector functions of the Fc region. These usually have a single binding interaction with an antigen they tend to be monovalent. Hence, although they would have the same binding affinity as the antibody from which they are derived, they have less avidity than whole antibody with multiple Fab regions.

Antibody fragments were historically produced by enzymatic cleavage of whole antibodies, but are now more commonly produced by recombinant organisms, A variety of antibody fragment configurations have been developed. For example, the basic Fab region can be produced as two separate polypeptide chains. Fab' (Figure 1.2) fragments are standard Fab fragments but with the heavy chain extended to include one or more

hinge region cysteine residues. In order to increase binding avidity the di-Fab ($F(ab')_2$) can be created by linking two Fab' arms with a disulphide bond (Carter, 2006) or thioester bridge (Rodrigues, 1993) or by constructing a linear $(F(ab')_2$ comprising tandem repeats of the heavy chain fragment V_H-C_H1-V_HC_H1 (Zapata, 1995). The Fv region has also been produced recombinantly, although the lack of cross-linking cysteine residues causes a tendency to dissociate into V_H and V_L upon dilution (Glockshuber, 1990). Therefore both a single chain Fv (scFv), with a polypeptide linker inserted between the V_H and V_L domains, and a disulphide stabilized Fv have been designed to increase stability (Raag, 1995).

As well as simple antibody fragments, the basic antibody monomer has been rearranged and engineered to form a myriad of different structures. The creation and isolation of specific antibodies to specific antigens in biotechnology is a complex matter. Antibodies were first produced in a polyclonal form, purified from the blood of animals immunised against the desired antigen. The development of hybridoma technology allowed the conversion of B cells from immunised mice into cell lines that can proliferate and produce monoclonal antibody indefinitely (Kohler, 1975). The immunogenicity of these antibodies in humans, and the complexity of protein engineering in mammalian cells then lead to the development of antibody genetic manipulation in bacteria. Although the complex structure and large size of IgG molecules makes expression in bacteria exceedingly difficult, the Fab region (Better et al., 1998) or a single chain Fv fragment (Skerra, 1988) can be produced. These methods allowed antibodies to be cloned, expressed and optimised with respect to affinity, stability and specificity. They can also be 'humanised' by the transfer of antigen binding sites into a human antibody framework (Carter, 2006). This retains antibody binding specificity while reducing the potential of immunogenicity. The development of display technologies permitted precise control over antibody selection conditions by the use of bacteriophages or yeast to create antibodies, rather than mice. These techniques rely on rapid cloning of immunoglobulin gene segments to create libraries of antibodies with slightly different amino acid sequences. These are then 'displayed' at the surface of the yeast or bacteriophage to allow affinity selection of the desired antibodies (Hoogenboom, 2005; Sidhu, 2006). Most recently a bacterial *E.coli* system has been developed that allows combination of full-length IgG and surface-displayed molecules, to further speed antibody development (Mazor et al., 2007).

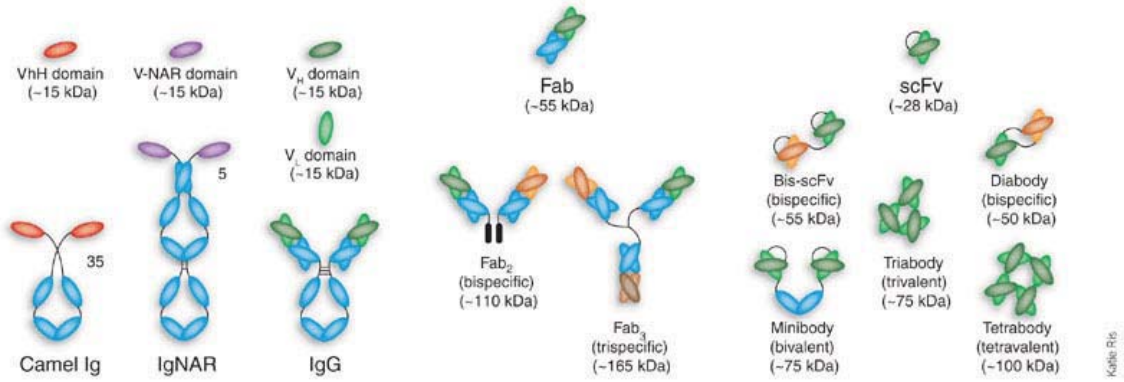

Figure 1.2 Forms of an antibody that are being produced recombinantly taken from review by Hollinger & Hudson, Nature Biotechnology (2005) vol 23, 1126-36

1.1.4 Biotechnological applications of antibodies and antibody fragments

The three major areas of application of antibodies are medical diagnosis, medical therapy and scientific research. Several immunodiagnostic methods based on detection of typical disease biomarkers are used to diagnose infectious diseases, for example ELISA, immunofluorescence, Western blot, immunodiffusion, and immunoelectrophoresis. Two examples are the detection of indicators of cancer (Krauss, 2003) and rheumatoid arthritis (Bizzaro, 2007).

The ability of antibodies to bind to a single antigen with high specificity leads to their therapeutic power. There are currently over 200 antibody based biopharmaceuticals under development, and 31 monoclonal antibody FDA-approved therapies (Strohl, 2009). Although monoclonal antibody therapies still are difficult to produce and deliver safely to patients, they remain a promising method in providing specific cures to certain diseases. (Hale, 2006; Koths, 1995; Reichert, 2005)

Research application stem around identification, location, and quantification of proteins of interest (Filpula, 2007). For example, antibodies are used in flow cytometry to differentiate cell types and life stage by the type of proteins they express (Brehm-Stecher, 2004). They are used in Western blot analysis to identify proteins separated by electrophoresis (Kurien, 2006). ELISA assays use antibodies to quantify proteins (Reen, 1994). The techniques of immunohistochemistry and immunofluorescence can be used to examine protein expression in tissue sections or to locate proteins within cells in diagnostics (Brehm-Stecher, 2004; Boswell, 2007).

Other suggested applications are treatment of wastewater (Costantini, 2007), counter-bioterrorism and bio-defence, biosensors (Conroy, 2009) and the food industry. Antibodies (Joosten, 2003) and antibody fragments are also considered as components of a variety of consumer goods. For example, antibody fragments could be used in shampoos to prevent formation of dandruff (Dolk, 2005), or in toothpaste to protect against cavities (Kupper, 2005).

1.2 Developing biopharmaceuticals

Today, biopharmaceuticals account for between 10% and 15% of the world pharmaceutical market (more than $10 billions) (Ashton, 2001; DiMasi, 2007). Monoclonal antibody drugs represent a primary sector of the biopharmaceuticals market, this trend is likely to continue and grow in the coming years (Pavlou, 2005). The specificity of mAbs against antigens has tremendous clinical value, making them effective therapeutic agents.

Blockbusters – drugs with $1 billion annual sales or more - constitute the "backbone" of the pharmaceutical industry, providing high revenue streams over relatively long periods. All the major pharmaceutical companies depend heavily upon blockbuster products. In that manner, leading companies underpin their corporate presence, influence and branding, high revenue flows, profitability and attractiveness to investors. Furthermore, specialised companies – especially in biotechnology – are increasingly involved with blockbuster and potential blockbuster products, both directly and as commercial partners.

Current and potential blockbuster revenues are seriously threatened by patent expiry, regulatory hurdles, reduced R&D efficiency, increasing competition, formidable therapeutic challenges and healthcare payers influencing pricing (Wheelwright, 1994; Clark, 2004). Nevertheless, there are strong drivers of growth including unmet therapeutic needs, rising incidence of many diseases, aging populations, rising living standards and fast-developing geographical markets. The future of current and potential blockbusters is therefore vitally important to all companies in the pharmaceutical sector, especially in this uncertain period of economic changes and pressures (Foot, 2010).

Figure 1.3 is brief Gantt chart of a typical biopharmaceutical development timeline. All pharmaceutical companies aim to launch their product as early as possible to generate profits (Struck, 1994). Getting a product onto the market before competitors is of particular importance since "first-to-market" often gain better recognition from customers (Wheelwright, 1994). However this market domination effect will be over after patent protection expires (Schellekens, 2004). Following the traditional trend, the launch of a biopharmaceutical will fall after the patent expires. In other words if the

product launches before patent expires, and the niche position of the drug in the market will last longer.

1.2.1 Upstream processing

The primary aim of the fermentation unit operation in antibody fragment production in *E.coli* is the cost–effective production of the antibody fragment by high productivity low-cost fermentation, where productivity is the amount of product formed per unit volume per time. A secondary aim is the design of the fermentation to allow facile and inexpensive downstream processing (DSP). The usual strategy to fulfil this primary goal is the growth of the *E.coli* cells to high cell densities, and the optimisation of the amount of Fab' produced per cell.

Apart from fulfilling the economic criteria of antibody production, upstream processing also involves cell line development. A well defined cell line co-produces the least amount of contaminants that might potentially interfere with the downstream processing.

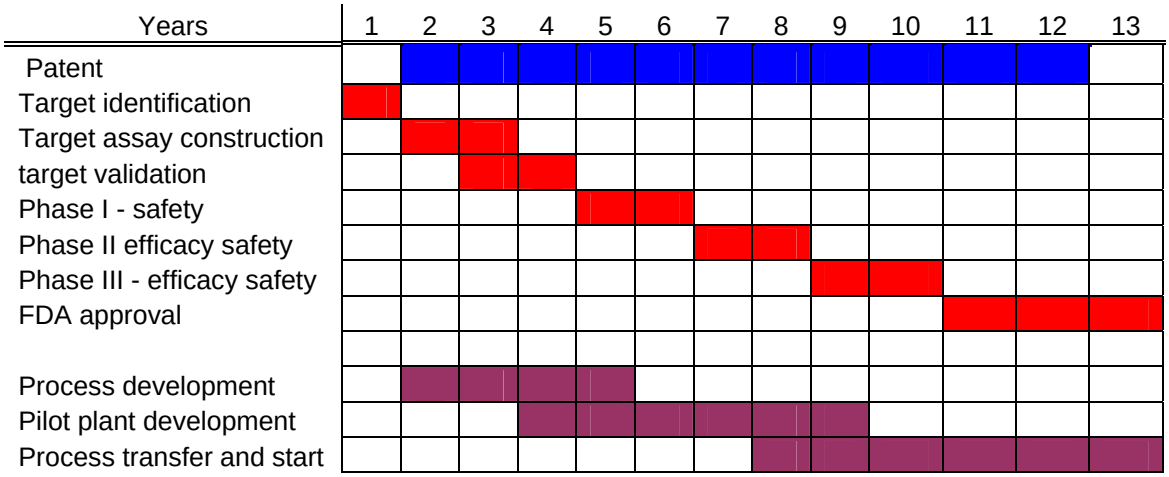

Figure 1.2 Gantt chart visualising the approval stages and development of an antibody in the biopharmaceutical industry.

1.2.2 Downstream process – purification strategies

Downstream processing involves the use of a sequence of unit operation to isolate protein product from cell culture from fermentation. Advances have been made over the last century (Becker, 1983) and still evolving. Design of downstream processing is highly dependant on the expression system, protein of interest, and location of expression. Here we will only consider processing steps relevant to the production of antibody fragments in the *E.coli* periplasm, the system of interest. Cytosolic production and extensive solubilisation and re-naturation stages required for protein recovery from exclusion bodies are not considered as this has been found to be less cost-effective than periplasmic production (Farid, 2007).

Processing may be divided into a number of stages including release of intracellular product, primary capture, purification, finishing and formulation. In the capture step the product is isolated and concentrated before it is further processed. In the purification section, bulk impurities are removed. The final purity is achieved in the polishing section.

For this purpose several unit operations can be used which have different separation mechanisms and capacities. In downstream processing of biological products, mainly chromatographic and membrane filtration units are used (Shukla, 2007).

1.2.2.1 Separation of biomass

In this thesis, downstream processing techniques for intracellular products are discussed. Recovery of proteins from *E.coli* fermentation broths begins with separation of the solids from the liquid phase of the fermentation broth, followed by chemical lysis of cells to release target protein that is contained inside the cells, finally removing the remaining cell debris. The leading methods for this are centrifugation and microfiltration.

Centrifugation separates on the basis of the particle size and density difference between solids and liquids or two liquids. The density gradient is amplified through the application of centrifugal force by high-speed rotation. In bioproessing centrifugation

can be used for the removal of whole cells, cell debris, sepheroplasts, and inclusion bodies from the liquid phase. Therefore it can be used both for initial recovery of the cells/liquid from the raw fermentation broth and also later on for separation of post intracellular product release. In the biotechnology industry three different types of centrifuge are commonly used: disc-stack, multi-chamber bowl, and tubular bowl centrifuges (Boychyn, 2004).

Centrifugation is preferred over other harvesting technologies due to its scalability and economical operation for large volumes (typically 2-150,000 L/batch). Large scale centrifugation acts as the primary harvesting step but cannot accomplish complete removal of cells and cell debris, which must be removed prior to chromatography (van Reis, 2001).

Because of the incomplete removal of particulates from a commercial scale centrifugation, depth filtration step(s) need to be employed to remove residual cellular debris (Low, 2007). Depth filtration refers to the use of a porous medium that is capable of retaining particulates throughout its matrix rather than just on its surface. Depth filters employed in bioprocessing typically consist of a fibrous bed of cellulose or polypropylene fibres along with filter aid (diatomaceous earth) and binders. The flat sheets are packed into single-use cartridges that can be stacked in housing and pressurized to drive fluid flow through the system (Jordan, 1996).

Depth filters typically do not come with an absolute pore size rating unless they include a membrane layer at the end of the flow path. The depth filter is followed by a filter with an absolute pore size rating that ensures the removal of solid particulates from the cell culture harvest supernatant.

1.2.2.2 Primary Capture – Chromatography

For purification of antibodies, different chromatographic techniques are used for the purpose of capturing protein products or polishing for quality. The major types of chromatography for primary capture are affinity chromatography (Shukla, 2007) and ion

exchange chromatography. Regardless of the type of chromatographic separation, all comprise of several steps. Before the column can be used, it must be equilibrated to ensure that the conditions within the column are homogenous, that is all parts of the column are equilibrated to the same condition with lowest elution strength. After equilibration, the column is loaded with the feedstock of choice. The column is then washed to remove some impurities and unbound/loosely bound proteins, before the target protein is eluted from the column by a stepwise or continuous change of the elution strength of the mobile phase. Afterwards, the column is washed again to remove the remaining impurities. Before the next batch can be processed, the column has to be regenerated and sanitised (Levison, 2003).

1.2.2.2.1 Affinity Chromatography

Affinity chromatography can provide very high enrichment factors in one step due to its high selectivity nature. For the purification of antibodies, the most common type of affinity ligands are immobilised bacterial cell wall proteins – e.g. staphylococcal protein A or streptococcal protein G.

The interaction of these two proteins occurs primarily through the Fc region of the antibodies but can also interact through secondary binding sites. Both Protein A and Protein G are available in recombinant forms in which non-essential regions have been removed leaving four binding sites for IgG intact.

Feedstocks can be loaded into a Protein A column directly without conditioning due to the high selectivity of the resin and feedstocks are normally close to neutral pH. The product is eluted from the column at low pH. A wash step introduced between column load and elution is often at an intermediate pH and removes host cell proteins and other contaminants. Finally the column is stripped and regenerated using high concentrations of chaotropes such as urea or guanidine hydrochloride. However eluting at low pH means target protein will be exposed to low pH conditions and can result in the formation of soluble high molecular weight aggregates and/or insoluble precipitate formation during product elution. High molecular weight aggregate formation can lead to a reduction in

product yield if a significant level of the product species aggregate (Cromwell, 2006). This also places an added burden on the polishing steps to achieve clearance since aggregate species can be potentially antigenic. Insoluble aggregate formation can be the result of either the product species or impurities such as host cell proteins precipitating. Both cases increase the risk of reduction in column lifetime, and at the same time affecting the product activity (Shukla, 2007; Bermudez, 2004) Regardless of the disadvantage the purity of the resulting eluant is >99 % pure.

A disadvantage of protein A or protein G usage is that there is always a small degree of leakage of the protein ligand, these leaked ligands are harmful to patients if present in the final drug product. For this reason, therapeutic products requires additional purification steps to remove these toxic ligands. Moreover, there are non-specific interactions resulting in a contamination of the target protein with impurities that are retained by the affinity matrix due to hydrophobic or ion exchange effects. The different bound species of proteins were eluted together with the target protein. This reduces the selectivity and more importantly reduces the access of target proteins to the affinity matrix ligands, hence reduces the binding capacity of the matrix. Another disadvantage of Protein A chromatography is the high cost of the matrix, which can be up to 10 times as expensive as conventional chromatographic supports (Sommerfeld, 2005). The high cost of the resin often leads to an operating strategy in which a smaller Protein A column is cycled several times while purifying a batch of cell culture supernatant is loaded on a relatively smaller column (Shukla, 2010).

1.2.2.2.2 Ion Exchange Chromatography

Basis for ion exchange chromatography (IEX) is the competition of the protein and a salt for the binding sites on the surface of the ion exchanger. The strength of binding is proportional to the charge of the protein for an oppositely charged ion exchanger. The charge of the protein depends on the pH value of the solution. The pH value at which net charge of the protein is zero is called isoelectric point (pI value). Ion exchangers with

negatively charged groups are cation exchangers because they bind positively charged proteins (cations) when mobile phase pH value is below pI value of the protein. Conversely, anion exchangers are positively charged. Because of the nature of the matrix, protein and stationary phase are charged oppositely is determined by the pH value of the mobile phase (Newcombe, 2008). Salt concentration of the mobile phase will determine if protein binding occurs as both salt and protein compete for the charged sites of the stationary phase, even small amounts of salt ions in the feed solution can significantly lower the resin binding capacity in ion exchange chromatography (Cramer and Brooks, 1992)

For a platform process, an ion exchange step is used to reduce host cell protein impurities, high molecular weight aggregates, low molecular weight clipped species, DNA and leached Protein A that remain after the Protein A chromatographic step to acceptably low levels that assure safety of the product (Low, 2007; Shukla, 2007; Sommerfeld, 2005). In other words IEX is currently widely used as a polishing step rather than a primary recovery step.

1.2.2.3 Nonaffinity process vs platform process

A generic process which assumes that a pre-defined purification process works for all antibodies is called a platform process (Shukla, 2007). Process development can often be the rate-limiting step in the introduction of biopharmaceuticals into clinical trials. The increasing numbers of antibodies entering clinical trials, there is a clear driver for employing a templated approach to process development.

In theory a platform approach can reduce process development effort, however significant physicochemical differences exist among different antibodies making this approach either impractical or resulting in a non-robust process.

Within the upstream section the major optimisation potential is to increase the product titre. This can be achieved by raising the specific production rate of the cells or by having a high cell number over a long fermentation period. Purification processes for antibodies have improved progressively over the last 20 years, giving a more than 50-

fold increase in cell culture productivity (Blanca Lain, 2009). To cope with the upstream improvement, Protein A primary capture step needs to be able to handle the increasing antibody titre. A typical protein A affinity chromatography resins have a dynamic binding capacity of around 40 g L^{-1} and depend highly on residence time, whereas recent developments have led to CEX resins with high dynamic binding capacity of 100 grams of protein per liter of resin. The cost of IEX resins are 10 times less expensive than protein A resins, this makes platform processes a less attractive choice financially (Sommerfeld, 2005).

Developments in antibody engineering capabilities have resulted in significant diversity in antibody-based therapeutics, allowing for fusion molecules, immunoadhesins, Fab and F(ab)2 structures which may or may not contain Fc portions or engineered bioaffinity sites, so that Protein A no longer provides a platform solution. An upcoming trend of peptide based drugs will be good additional example of non-affinity products (Vlieghe, 2010). Furthermore, protein A shows some variability in binding to antibodies, which appears to be due to interactions with the variable region, for instance the presence of specific sequences in the heavy chain.

Although production are mainly based on using an affinity process (platform process), due to the above reasons a non-affinity process needs to be adopted to satisfy the ever improving upstream development. Several methods have been proposed and tested to increase the process capacity of the primary recovery step. The affinity chromatography can be replaced by hydroxyapitite chromatography, ion-exchange chromatography and filtration (Subramanian, 2005).

Ion exchange is certainly amenable to the large scale purification of antibodies and is used as the primary capture step in at least one commercial process. Capacities are higher and cleaning and sanitisation steps are simpler, the chief trade-off is a greater burden on the subsequent steps for purification and clearance of host cell protein and potential virus contamination. In a comparison between a protein A process and a three step non-affinity processes (Figure 1.4), similar levels of host cell protein clearance could be achieved by both approaches. There is much potential in non-affinity processes, only limited to intensive optimisation of binding and elution conditions (Alahari Arunakumari,

2007; G.M. Ferreira, 2007; Wang, 2008). If a good and efficient optimisation routine is established to ensure the quality of the product from ion-exchange chromatography which can rival a protein A based process, a non-affinity process can be utilised more broadly (Follman, 2004). In figure 1.5 a table listing the functions of the unit operation described above is presented.

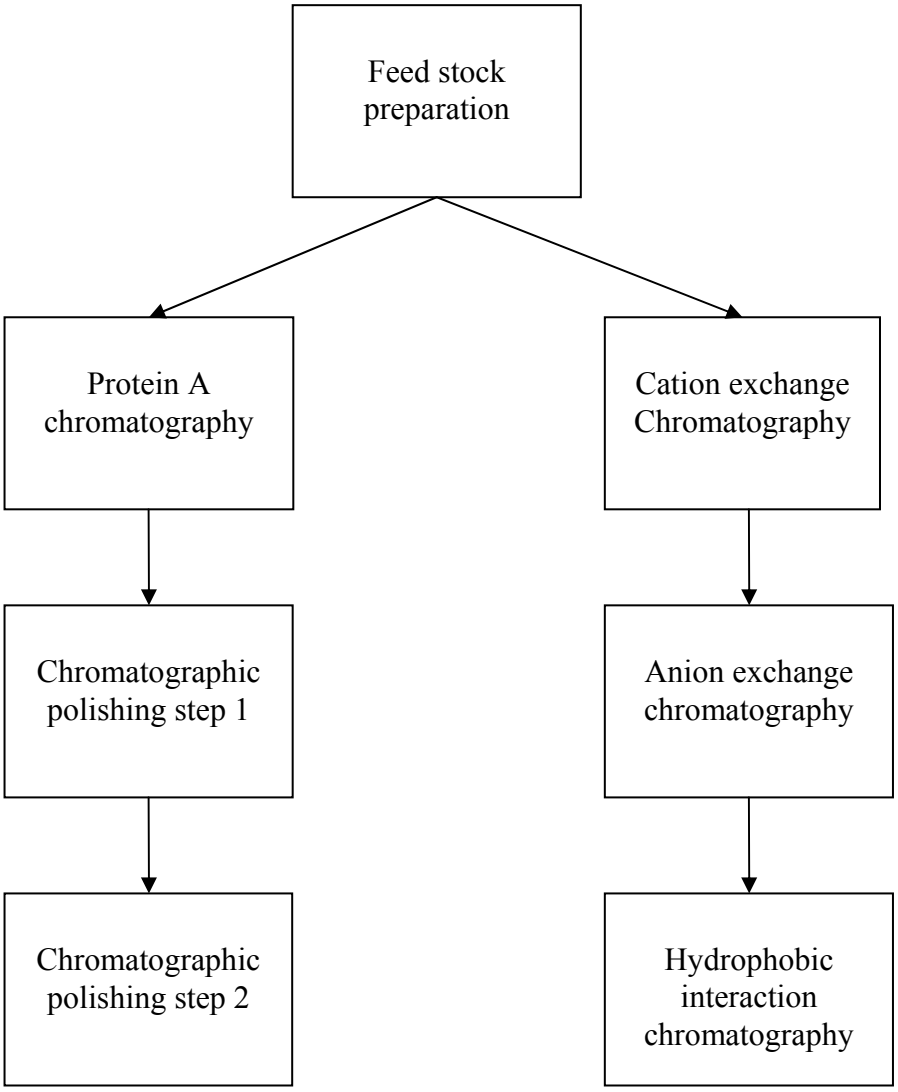

Figure 1.3 Two major routes for antibody purification from a feedstock; an affinity process (left) and non-affinity process. (righ

Table 1.2 Upstream and downstream unit operations and their corresponding functions.

Unit operation	Contaminants introduced	Contaminants removed
Fermentation (Low, 2007)	Amino acid Inorganic salts Glucose Intact cells Cell debris Host cell proteins Viruses DNA Lipids Endotoxins Other culture medium compositions	N/A
Centrifugation (Low, 2007)	Shear induced aggregates	Intact Cells High MW cell debris
Depth Filtration (Roush, 2008)	Filter aid	Low MW cell debris Low MW aggregates
Dead end filtration		Low MW cell debris Low MW aggregates Filter aid
Protein A chromatography (Shukla, 2007)	Leached protein A High MW aggregates	Host cell protein Viruses Endotoxins
Ion-exchange chromatography (Shukla, 2007)		High MW aggregates Host cell impurities DNA Viruses Endotoxins

1.2.3 Validation

The biopharmaceutical manufacturing industry is highly regulated having to meet strict regulations. After the drug has been approved, most regulatory agencies such as the FDA require that the drug product be tested for its identity, potency, quality, purity and stability before it can be released for use (Doblhoff-Dier and Bliem, 1999). Because of the above reason, process controls are crucial to ensure that a specific process will consistently produce a product which meets its predetermined specifications and quality attributes at various critical stages of a manufacturing process. A quality by design approach was used to determine the process parameters to ensure lot-to-lot consistency (Geigert 1997); quality control, quality assurance and batch documentation thus form key parts of the in-process validation procedure for any biopharmaceutical. A diagram explaining the chronological sequence of product development is presented in figure 1.3.

Information obtained about the unit operation during development phase of a bioprocess is not enough to justify the setting of validation criteria. Therefore the response of a process output to variations in input parameters is investigated in some detail before process validation in a process characterisation phase. Defining the design space of bioprocess is crucial to validation, working within the space is not considered as change, however working outside of the space would initiate regulatory disapproval (ICH, 2006a). Setting the operating range to be too narrow would underestimate the accidental deviations of operating conditions in the bioprocess. However if the range is too wide, the product might fail to meet the acceptance criteria.

1.2.4 Validation of chromatography

Chromatography performance is affected by a wide range of variables, such as pH and ionic strength, linear velocity, column load volume and quality, ligand density, bed height, gradient slope. All these parameters are important to the outcome of the eluate. To investigate the effects of all these parameters will lead to large experimental designs and substantial analytical support as each experiment may have to be analysed with several assays to test for purity of the protein with respect to product variants, host cell contaminants and process impurities. Apart from developing the optimised operation for chromatography, a series of experiments is also required to examine the sensitivity of the system. In general validation of chromatography is to ensure the quality of the eluate is reproducible for every operating cycle and in addition the number of cycles the resin can endure before the batch of resin needs to be discarded (Müller-Späth, 2009).

Due to the fact that there are many different parameters present that are likely to affect the performance of chromatography; validation requires the developers to perform extensive number of experiments to justify the quality of their products. Because of this reason, methods need to be developed to reduce the experimental effort and at the same time provide enough evidence to ensure the robustness of the process.

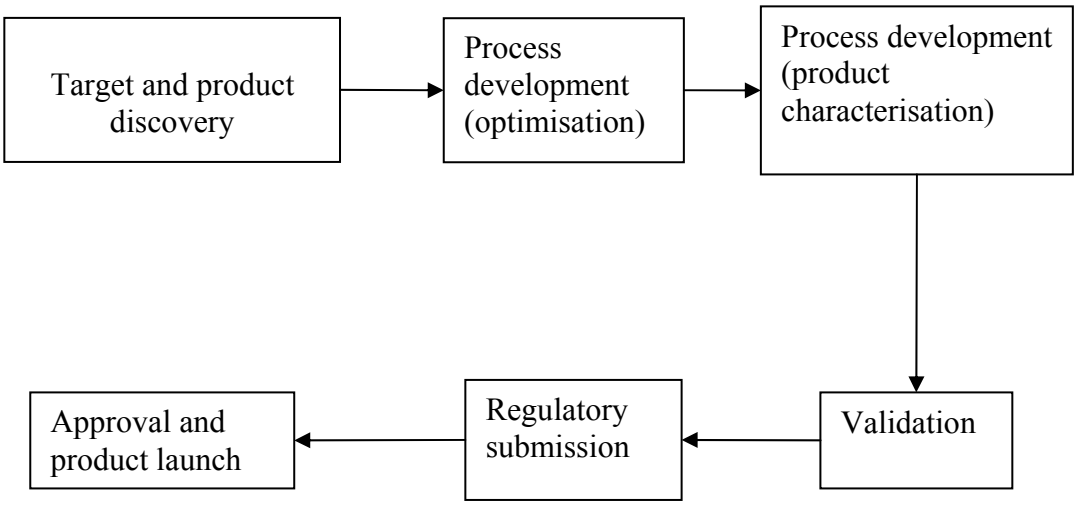

Figure 1.5 A typical path of a drug candidate will follow from identification to launch

1.3 Modelling

1.3.1 Whole process modelling

With an increasing number of international and national regulations, companies bringing new drugs to market face additional burdens of ensuring and improving quality, each being expensive and time-consuming activities.

Modelling plays an important role in bioprocess development for design and scale-up. Predictive models can also be used in biopharmaceutical manufacturing to assist decision-making either to maintain process consistency or to identify optimal operating conditions (Gao, 2010).

Modelling complete flowsheets requires purpose-built software such as Extend and Superpro designer. Simulations can be used to tackle many problems, from initial design and proof-of-concept studies through operation (Gosling, 2005; Petrides, 1989) and validation. The ultimate goal of modelling of a bioprocess is to develop more robust processes faster and at a lower cost resulting in higher quality products by comparing process alternatives (Rouf, 2001). Through modelling potential resource problem can be identified and anticipated before setup.

1.3.2 Unit operation modelling

Key unit operations of a bioprocess often determine the quality of the product produced by a process. The performance of these key unit operations is often determined by a large number of operating variables. If the design and performance characteristics of these units can be compiled into a mathematical representation, then potential problems can be investigated through modelling, reducing the need for expensive experimentation. This will reduce the time and cost of process development and ensure the developed process is robust and has the ability to handle variability and deliver a predefined quality as regards yield, purity and productivity within the defined design space. (Gosling, 2005; Yu, 2008) In addition, accurate prediction of a unit operation allows accurate prediction of its economics hence the whole process economics.

A lot of mathematical models still require users to provide some experimental data as critical input data. The quality of this data will often determine the usefulness of the model, but it has been shown that combining some experimental data with process models can improve their accuracy significantly. If process models can reliably predict unit performance then they will undoubtedly gain wide spread use since the savings in time and resources can be substantial.

1.4 Scale-down methods

From the above sections, it is explained that due to the requirements of regulatory agencies and process optimisation, a large number of experiments are required to generate enough evidence to prove the robustness of the process.

During the early stages of R&D, cell lines are not optimised hence target protein production is not expressed in large quantity. Since target protein is scarce, the number of experiments that be conducted at normal laboratory scale is limited. To alleviate this problem, smaller scale unit operations or innovative approach to obtain the necessary parameters for models can be used. The ultra scale-down methods and high throughput screening are examples of such strategy. The net result can be a reduction in the time needed to get a functioning process into a facility and the early resolution of other issues such as the sizing of ancillary process-support equipment. Furthermore, given the relatively inexpensive nature of microscale experimentation, if a product fails subsequently in clinical trials, then the money spent using these devices in development studies can be written off more readily. Because of these advantages, microscale approaches are seen increasingly as a powerful way to accelerate bioprocess development and have been applied to steps such as fermentation and microfiltration.

1.4.1 Ultra scale-down

Ultra scale-down is a novel nonlinear scaling approach; this method reduces the volume of test material required whilst maintaining the relevance of data collection. The experimental philosophy of USD methodology involves the characterisation of the critical regimes of a large scale unit operation and then using miniature devices to obtain data on the impact of the process material properties. An example of a successful utilisation of this method is demonstrated by (Boychyn, 2004; Chan, 2006). The authors mimicked the performance of a process scale centrifuge using a bench top device. This was done by reproducing the shear condition identical at the entry point of a process scale centrifuge using a rotating disc shear device, making the feed material constant across both scales. This approach enables reliable centrifugation scale-down of several orders of magnitude. There are other examples of ultra scale-down for different unit operations such as depth filtration, (Reynolds, 2003) and centrifugation using micro-titre plates. (Tait, 2009)

The main purpose of the ultra scale-down method is to allow the experimenter to generate data at small scale with least amount of materials to predict performances of the unit operation at industrial scale. The philosophy of the experimentation is to mimic the physics of the hardware and reproduce the quality of the feed material.

1.4.2 High throughput screening

High throughput screening is an experimentation method designed for drug discovery purposes. This technique has a wide range of applications this includes ELISA, cell based assay development, protein stability and protein–protein interaction studies. (Fernandes, 1998; Capelle, 2007).

High throughput microliter scale-down approaches reduce sample requirements by an order of magnitude - below the mL scale volumes employed at present for laboratory columns. These microscale techniques ideally suited to accommodate the limited quantities of feed stocks that are available early in process development. The technology allows early stage evaluation of many process strategies in parallel, thus

reducing development costs and allowing later pilot work to be more highly focused upon the most feasible option (Bensch, 2005; Bergander, 2008; Chhatre, 2009). In other words, this technique provides a platform to reduce the size of design spaces, filtering out the non-feasible options at an early stage.

High throughput screening involves the use of micro-titre plates; each well of the plate(s) represents an independent experiment. The multi-well nature of a 96 well-plate the plate provides a design space for a series of discreet experiments. Due to the size of the design space, the number of discreet experiments can be very large this leads to the need of a well defined analytical technique to process the large array of results obtained.

1.5 Chromatography – scale down and modelling

Adsorption of protein products under complex conditions i.e. real feedstock is regarded as a non-linear system. In the age of rapid development of biotechnology, preparative and large scale chromatography becomes increasingly important for product manufacturing; in addition, Unlike analytical chromatography, dispersion and mass transfer effects are often significant in preparative and large scale chromatography; this causes difficulty in predicting the performance of chromatography without intensive experimental work.

Small preparative columns are very time consuming to experiment with and in addition, due to the size of these columns, the feed material requirement to complete the experimentation to obtain the desirable results remains high. Because of the above reason high throughput screening is particularly useful in scouting conditions either for binding or elution stages of the unit operation (Mazza, 2002; Kramarczyk, 2008; Kelley, 2008; Bensch, 2005). There are also efforts in using this technology to aide the optimisation of the unit operation (Susanto, 2009; Susanto, 2008; Bergander, 2008; Wiendahl, 2008).

1.5.1 Modelling

Because obtaining information experimentally through quality by design method is very time consuming and labour intensive even when using a high throughput screening (HTS) technique due to the size of the design space. Mathematical models can be used to identify the sensitive parameters of the systems, this requires a well developed model that has the ability to represent the system sufficiently enough to simulate the performance of chromatography. The main objective of modelling in this case is to reduce significantly the size of the design space. Since the design space is reduced in size, experimental effort will also decrease for validation (Mollerup, 2009). The adsorption of protein materials into the resin bead follows the two film theory developed by Lewis and Whitman in 1924. In chromatography terms the film theory means that for any substance to reach the ligand in the porous resin particle it must first enter the stagnant film of the resin particle before it can diffuse into the intra-particle space. The general rate model is a model that utilizes the film theory together with intra-particle diffusions to simulate the performance of chromatography. There is also another model that takes into account protein-protein interaction of a system into account on top of the general rate model (Berninger, 1991;Whitley, 1991).

Apart from adsorption theory of target proteins onto the resin, there are other parameters that need to be identified to complete the models. Such as adsorption rates (Velayudhan, 1994), mass transfer coefficient (Persson, 2004; Liapis, 2008}, intra particle diffusivity (Kempe, 2006; Tyn, 1990), axial dispersion (Farkas, 1979) and molecular diffusivity (Gallant, 2004). A lot of effort has been put into estimating the necessary parameters to complete the models and understanding their underlying meaning to the system. For example confocal microscopy has been used to understand the intra particle diffusion (Susanto, 2007).

Another way to estimate the parameters is by lumping the parameters in order to reduce the effort to estimate the necessary parameters for modelling (Martin, 2005)

1.5.2 Scale up

Modelling not only serves as a performance prediction tool, it also provides opportunity to predict the performance of the unit operation at different scales. A traditional way to scale up a chromatography column is by maintaining the column height while increasing the radius of the column. By doing so, the residence time of the feedstock remains unchanged when the linear velocity is constant at both scales. However, as the radius of the column increases, the wall support of the center of the resin decreases; this limits the maximum running flowrate to preserve the packing and structure of the resin bed. The extent of compression of the resin correlates to the pressure drop with the aspect ratio of the packed beds and the superficial velocity (Stickel, 2001). Using the Stickel rule to scale-down a column will result in a relatively long column (at least 30 cm), resulting in a relatively large column volume.

1.6 Introduction to project

From the above sections, the structure of an antibody and its potential use in the biopharmaceutical industry is presented. There is a market for these therapeutic proteins; however the research and development together with the regulatory requirements hinders the commercialisation of such products. Process validation by quality by design method for down-stream purification strategies requires extensive experimental efforts due to the large number of process variables. It is necessary to develop methods to reduce the design space of the experiments and at the same time optimise the unit operation to identify the operating window.

In this project an ultra scale-down approach for chromatography will be performed and discussed. The feedstock used in the project will be a *E.coli* heat lysate (generated by heating during periplasmic extraction) containing Fab' fragments and the resin of choice is a generic cation exchange resin. The chromatography step serves as a primary capture step. Performance of chromatography is judged by breakthrough curves because breakthrough curves represent adsorption of target protein onto the resin under column conditions.

The first aim of the project is to identify the parameters that are sensitive to the system followed by developing a general rate based model that can predict the performance of a laboratory scale chromatography under different condition. The condition of choice in this project is flowrate, because it is the easiest parameter to change at process scale and also this parameter will aid the optimisation of loading time.

The second aim of the project is to discover the scale down opportunities of the model. A micro-scale tip column will be used to challenge the traditional geometric scaling rule. Breakthrough curves will be obtained using micro-scale tips and by using the breakthrough curves the scale up opportunities to predict the performance of laboratory 1 mL scale from 40 μL micro-scale will be investigated.

Chapter 2 - Materials and Methods

2.1. *E.coli* lysate feedstock preparation

In this section, a full methodology for *E.coli* lysate feedstock preparation will be presented. The key steps implemented to prepare the *E.coli* lysate are illustrated in figure 2.1. The cell feedstock preparation involves fermentation to grow *E.coli* cells for expressing Fab' fragments because the Fab' fragments are intracellular product. Centrifugation was implemented to recover the cells in the form of a cell paste. The cell paste was then resuspended in a lysis buffer and heated to release the Fab' fragments accumulated in the periplasm and at the same time break down some of the intracellular protein contaminants. The cell debris and lysate mixture from the periplasmic extraction was spun down in a centrifuge to remove cell debris resulting in a heat clarified lysate. The heat clarified lysate was then concentrated and conditioned to the right pH. The conditioned *E.coli* lysate was filtered through dead end filtration before loading into an ion-exchange column.

2.1.1. Chemicals

All chemicals were purchased from Sigma-Aldrich Co. Ltd (Dorset, UK) unless otherwise specified. All chemicals are of analytical grade. These are tested where appropriate in the following sections.

2.1.2. Fermentation

A humanised Fab' antibody fragment was produced by fed-batch *E.coli* fermentation. The *E.coli* cell strain is W3110 transformed with the plasmid pAGP-4. The protocol and cell strain was obtained from UCB Celltech and is strictly proprietary. The

fermentation was carried out in a 20 L vessel (Applikon Biotechnology, Schiedam, Netherlands)

The *E.coli* cells were first incubated at 30 ^{0}C in shake flasks before inoculated into the 20L vessel with 10L of SM6c defined media that contains the bare minimum nutritional requirements for *E.coli* cells. The cells were controlled and monitored to grow until stationary phase. After stationary phase was reached, isopropyl β-D-1-thiogalactopyranoside (IPTG) was added to the cells to initiate Fab' expression (detailed protocol is strictly confidential). The cells express Fab' antibody fragments under transcriptional control of the *E.coli tac* promoter. Each antibody chain was preceded by the *E.coli* ampA signal sequence to direct expression to the periplasmic space. The expression of Fab' was terminated when Fab' fragments were detected in the media. Samples were taken every two hours of the fermentation; cell growth was monitored using light microscopy at 380 nm whereas Fab' fragments were quantified using protein G HPLC assay.

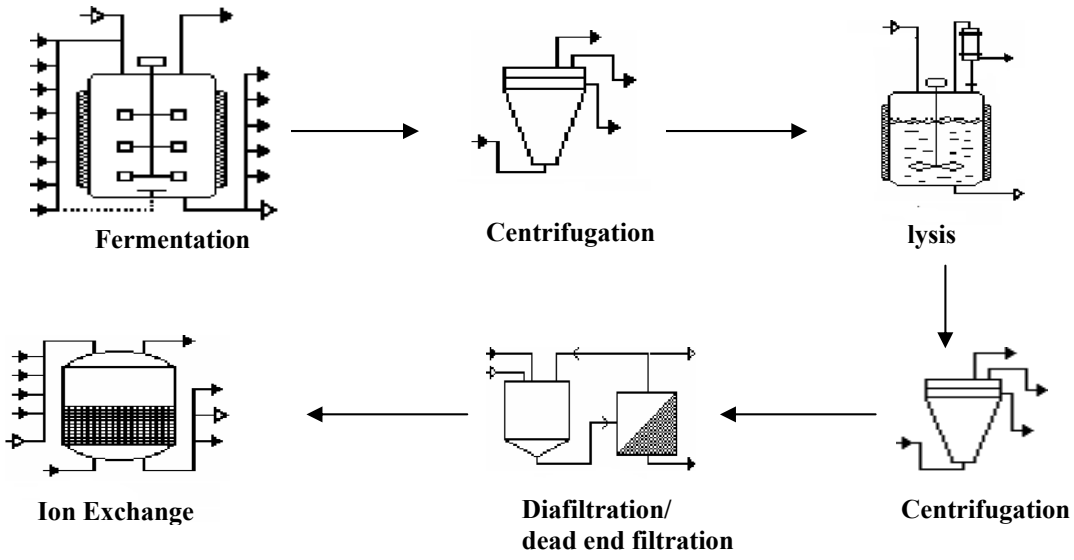

Figure 2.1 Steps to prepare *E.coli* lysate. The steps in chronological order: fermentation, centrifugation, chemical lysis, second centrifugation, a diafiltration followed by a dead end filtration and finally ion exchange chromatography.

2.1.3. Centrifugation

The cells were harvested from the fermenter and separated from the media by extraction; using a CARR P6 solid bowl centrifuge with automated solids discharge (Kendro, Asheville, NC, USA). The centrifuge was operated at 15,200 rpm with a feed rate of 45 L h^{-1}. The centrifugation was done immediately after the completion of the fermentation to prevent product leaking into the cell broth. The cell paste harvested was stored at -80 ^{0}C.

2.1.4. Heat lysis

A heat lysis step was used to release the periplasmic proteins; this was done by adding a detergent to dissolve the cell wall, making the cell "leaky"; heating the lysate makes the non heat resistant proteins denature (the Fab' fragments expressed by this system is heat resistant). Hence proteins are able to escape from the cells while keeping the cells intact. This method of releasing intra-cellular product reduces the requirements of the subsequent down stream processing unit operations, however the Fab' fragment release is only 40 % of total Fab' fragments expressed. Although the Fab' released is not 100%; the Fab' fragments released is of higher purity compared to homogenisation where all whole cell proteins are being released; in other words less truncated versions of Fab' fragments are present in clarified lysate.

The harvested cell paste from centrifugation was resuspended in 10 L of lysis buffer consists of 100mM Tris-HCl and 10 mM EDTA adjusted to pH 7.4 with hydrochloric acid. The mixture was then incubated in a 20 L vessel at 55 ^{0}C, agitated at 350 rpm overnight for 16 hours.

2.1.5. Centrifugation

The lysed cells were removed from the 20L vessel. The Fab' fragments from the perplasmic space were released into the lysis buffer. To extract the product, spheroplasts and cell debris were removed by laboratory scale Beckman Avanti J-HC centrifugation **(**Beckman Coulter,UK) at 10,000 rpm for 45 min, the supernatant was collected as Fab' fragment heat lysate.

2.1.6. Concentration

A concentration step was performed to reduce the feed volume for easy storage and at the same time allowed leeway for dilution to reduce the conductivity of the clarified lysate for subsequent chromatography experiments.

The conditions of the heat lysate was firstly adjusted by concentrating three-folds using a 0.1 m^2 Pellicon 2 mini 10 kd cut off cartridge filter mounted on a Proflux system (Millipore, Bedford, MA, USA). The concentration was completed in a tangential flow manner; pressure was kept constant at 1 bar. (Diagram of the diafiltration system is shown in fig 2.2). All proteins were retained and recycled during the process while salts were eliminated through the permeate stream. The retentate was collected and adjusted to pH 5.2 using concentrated HCl; the reason behind the pH adjustment will be explained in chapter 4.2.2.

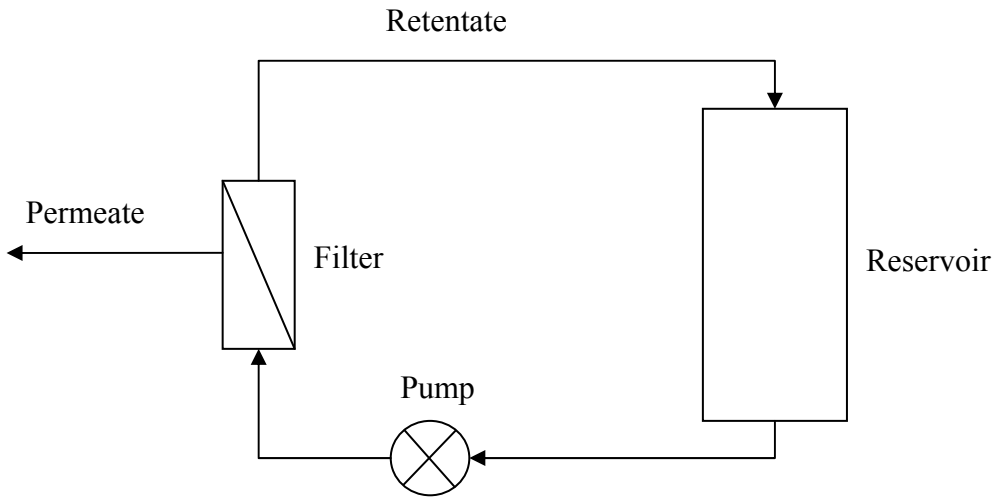

Figure 2.2 Flow diagram of the concentration of *E.coli* lysate using an ultrafiltration membrane. Salts and water transmit through the filter and exit the system from the permeate stream whereas the Fab' fragments and other proteins recycle into the reservoir.

2.1.7. Filtration

During the process of diafiltration and pH adjustment, particulates were formed. It is necessary to remove these particulates prior to chromatography step, as these particulates will cause blockage the top frit of the column and at the same time interfere with the adsorption of protein onto the resin particles. To remove these particulates; a dead end filtration step was performed using a 0.22 μm vacuum filter. The resultant filtrate is free from particulates and is ready to be loaded into a cation exchange column. In chapter 4.4 the composition of the particulates were analysed. The clarified lysate was stored in 50 mL aliquots in Falcon tubes (Greiner, Stonehouse, UK) at -4 ^{0}C.

2.2. Protein G assay

Due to the complexity of the *E.coli* lysate, the assay technique needs to be specific to Fab' fragments, in other words, the least amount of interference from non-Fab' fragment proteins. Within the periplasmic space of the *E.coli* cell, the Fab' fragment is the only protein that can bind to a protein G immunoglobulin-binding protein. The Fab' fragment by its nature is expressed without the presence of the F_c region but still has the ability to bind to protein G through secondary binding sites. Although this secondary binding site is not specific to Fab' fragment, the binding is strong enough to maintain high binding capacity. Using this specificity, the concentration of Fab' fragment can be determined.

To determine the concentration of Fab' fragments in a sample, a 1mL HiTrap protein G HP (GE Healthcare) column was used on an Agilent 1200 HPLC system (Agilent technologies, Berkshire, UK). The HiTrap column was first equilibrated with 5 CV of equilibration buffer consists of 50 mM di-sodium hydrogen phosphate adjusted to pH 7.4 with 85% phosphoric acid. After equilibration, 100 μL of sample was loaded into the column. After loading, 5 CV of equilibration buffer was used to wash away any unbound materials. Straight after washing is elution; this was done by running 2

CV of elution buffer through the column. The wash and elution step were repeated to ensure any bound materials were disassociated from the ligand. To regenerate the resin, 5 CV of equilibration buffer was loaded through column. The whole cycle was run at a flowrate of 2 mL min^{-1} and the total time required to complete the analysis of a sample was approximately 9 minutes. A chromatogram of the analysis was recorded from loading till regeneration. Fab' fragment was eluted at approximately 3 minutes into the analysis. The concentration of Fab' fragment in the sample is directly proportional to the peak area. The peak area is integrated by Chemstation. (Agilent Technologies, Berkshire,UK). The same method was used to intergrate the peak areas of the chromatogram throughout the project.

2.2.1.1. Pure Fab' fragments preparation

The peak area from the Protein G assay alone is insufficient to determine the concentration of protein in a sample. To translate peak area into concentration, a standard curve needs to be obtained. Pure Fab' fragments at different concentrations were used to obtain a standard curve. After the standard curve was determined, the sensitivity of the assay was examined to aid the planning of the subsequent chromatography experiments.

Pure Fab' fragments were produced by purifying heat lysate with a Protein A column. A XK50 column was packed with 200 mL of rProtein A resin (GE healthcare) at 65 mL min^{-1}.

To prepare the lysate for Protein A chromatography, 1 M of glycine was added to the lysate after the removal of all the cell debris from the heat lysate. The pH of the glycine-lysate mixture was adjusted to pH 7.5 using 50% (w/v) sodium glycinate. The conditioned lysate was filtered through a 0.22 μm filter.

The column was equilibrated with 5 CV of 50mM sodium phosphate buffer at pH 7.4. The purification was continued by loading conditioned lysate into the packed protein A column at 155 cm h^{-1}. Excess lysate was loaded onto the column to ensure the column was saturated. The column was then washed with at least 5 CV of equilibration buffer until UV signal detected returned to zero. A step elution was

achieved by passing 50 mM sodium phosphate buffer at pH 2.5 through the column until a distinct peak was observed. The eluted materials were collected in 5 mL fractions. The column was then sanitised with 1 CV of 6M guanidine hydrochloride solution and immediately flushed with 10 CV of equilibration buffer.

The most concentrated eluted fractions (maximum peak height using OD280) were pooled together; Tris was added to adjust the pH from 2.5 to 7.4. The stabilised pure Fab' was buffer exchanged into pH 5 sodium acetate with 1% sodium azide for long term storage.

2.2.1.2. Fab' fragment standard curve using HPLC

The purified Fab' was quantified using an ELISA (protocol not included as experimentation was performed by Helen Baldacini) previously, with the concentration determined; a standard curve can be obtained using HPLC. The purified Fab' was diluted with 50 mM di-sodium hydrogen phosphate adjusted to pH 7.4 (equilibration buffer to protein G column) into 10 μg mL^{-1}, 20 μg mL^{-1}, 50 μg mL^{-1}, 100 μg mL^{-1}, 200 μg mL^{-1}, 300 μg mL^{-1}, 400 μg mL^{-1} and 500 μg mL^{-1} fractions. These fractions were then analysed using the method described in section 2.2.1.

E.coli lysate consists of many different proteins and the interaction between these proteins is unknown, especially under different pH and conductivity. An analysis was done under different pH and low conductivity for the purpose of screening the appropriate binding conditions for cation exchange chromatography.

2.2.2. Precipitation analysis

Particulates formed when lysate pH was reduced. Particulates form as the net charge of the proteins in the lysate changes due to pH shift, hence promoting interaction between proteins. The composition of the particulates was examined. The result aids the determination of lysate pH prior to the cation exchange step.

The *E.coli* lysate was separated into seven 10 mL aliquots. The pH of the aliquots was adjusted to 2, 2.5, 3, 3.5, 4, 4.5 and 5 using HCl. The pH adjusted *E.coli* lysates were spun down using a bench top centrifuge (Eppendorf) at 10,000 rpm for 30 minutes to separate the solid and liquid phases. The liquid phases were decanted into separate Eppendorf tubes for analysis. The pellets left behind were rinsed with 10 mM sodium phosphate buffer of their corresponding pH to rinse off the remaining liquid phase that was not removed during decantation. Because the pellets were disturbed during the rinsing stage, the mixture was centrifuged at 10,000 rpm for 10 minutes. After the excess buffer was removed, 1.5 mL of 10 mM phosphate buffer at pH 8.5 was added to each of the aliquots. The pellets and buffer mixtures were left on an Eppendorf thermomixer for 2 hours to allow all the pellets to re-dissolve.

The dissolved pellets and the liquid phases of the *E.coli* lysate were analysed using reducing sodium dodecyl sulfate polyacrylamide gel electrophoresis (SDS-PAGE). 500 μL of each of the samples were separated into individual Eppendorf tubes. 500 μL of Tris-Glycine SDS sample buffer containing 1% 2-mercaptoethanol was added to each of the Eppendorf tubes. The conditioned samples were heated to 90^0C for 10 minutes. The Eppendorf tubes were briefly centrifuged for 10 seconds at 5000 rpm to re-collect the condensation 15 μL samples were then loaded into two separate Novex® 4-12% tris-glycine Gels (Invitrogen) and run simultaneously using the same power pack at 125 V for 90 minutes.

The gels were developed for 2 hours using Coomassie® G-250 SimplyBlue Safe-Stain. (Invitrogen) The gels were then de-stained using deionised water overnight until distinct bands can be seen.

The same protocol was used for all SDS-PAGE analysis done in this project. For non-reducing gels, the 1% 2-mercaptoethanol was not added to the running buffer before heating.

2.3. Measuring chromatographic performance

In this section methods used to determine the binding conditions of prepared *E.coli* lysate onto SP Sepharose FF resin and the method for obtaining the breakthrough data for modelling will be presented.

2.3.1. Adsorption isotherm

Adsorption isotherms were obtained to investigate the adsorption of Fab' fragments on SP Sepharose FF resin with different net charges in the lysate; the net charge of Fab' fragments were altered by adjusting the lysate pH.

2.3.1.1.Dry resin weight analysis

The resin dry weights were determined at different aspirate volumes. This was to confirm, within the experimental space, the amount of resin taken from bulk resin suspension is directly proportional to the volume aspirated. Firstly the same volume of resin was repeatedly aspirated and dispensed to demonstrate the reproducibility of each batch system. Secondly different volumes of resin were aspirated and dispensed to prove that each batch adsorption system contains the correct amount of resin. Particular attention was paid to error analysis at very small volumes. 10 mL of resin was poured inside a Falcon tube and then 20% ethanol was added to the Falcon tube up to 50 mL mark. The Falcon tube was centrifuged at 4000 rpm for 20 minutes. The percentage of resin to ethanol was adjusted to 25% (v/v ethanol) by changing the volume of 20% ethanol.

While agitating the mixture, 40 μL, 50 μL, 60 μL, 100 μL, 200 μL, 400 μL and 600 μL of the resin-ethanol suspension was slowly pipetted onto pre-weighed weighing boats the volumes correspond to matrix volume of 10 μL, 12.5 μL, 15 μL, 25 μL, 50 μL, 100 μL and 150 μL respectively. The same

volumes of deionised water were added to each of the weighing boats to spread the resin out into a flat sheet. The weighing boats were subsequently incubated inside a 45^0C oven for 2 hours to remove all moisture. The weighing boats were then weighed to calculate the dried resin weight.

2.3.1.2.Batch adsorption

100 µL of resin suspension was dosed into 14 wells of a 96 filter well-plate (with 0.22 µm filter). The well plate was centrifuged at 4000 rpm for 10 min to remove excess 20 % ethanol. 100 µL of 10mM sodium acetate buffer at pH 5.2 was added to the wells. The excess equilibration buffer was removed by centrifugation at 4000 rpm for 10 min.

The equilibrated resin cakes were then transferred into Eppendorfs (≤ 1mL experiments) and Falcon tube (> 1mL experiments). 100 µL of lysate was added into each well, transferring the resin into the Eppendorf tubes and Falcon tubes. The pipette tips used were all wide bore to ensure all resin particles can be taken up by the tips. Lysate was added to the transferred resin-lysate mixture to a total volume of 0.25mL, 0.5 mL, 0.75 mL, 1 mL, 5 mL, 10 mL and 20 mL. The individual containers were left overnight on a rocker.

The fully saturated resin particles were separated from the lysate by centrifugation at 4000 rpm for 20 minutes. The liquid phases were assayed to determine the concentration of Fab' fragments.

2.3.2. Breakthrough curve

2.3.2.1 Millilitre scale with HiTrap columns

Chromatography was performed using a 1 mL HiTrap SP Sepharose FF column on an AKTA-Basic system (GE healthcare, Uppsala, Sweden). Breakthrough of Fab' was determined at an operating flowrate of 1 mL min^{-1}, 1.5 mL min^{-1} and 2 mL min^{-1} which are equivalent to linear velocities of 310 cm h^{-1}, 232 cm h^{-1} and 155 cm h^{-1} respectively. Fresh columns were used for each flowrates to nullify the effect of any irreversible interactions between feedstock proteins and resin due to column overloading. All columns were equilibrated with 10 CV equilibration buffer composed of 20 mM sodium acetate at pH 5.2.

Lysate prepared using method described in section 2.1 were allowed to defrost at 4^0C before being brought up to room temperature. The room temperature lysate was diluted to 2 mS cm^{-1} using deionised water. The concentration of Fab' lysate was assayed prior to loading.

The conditioned lysate was loaded into the column. During loading, the column effluent was collected in fractions of 10 mL (10 CV). The fractions were assayed for concentration of Fab' fragments using the HPLC method described in section 2.2.

2.3.2.2 Micro-scale with PhyNexus microtips

The setup was aimed to utilize PhyNexus micro-tips in a traditional chromatography manner – downward unidirectional flow instead of aspirating and dispensing liquid from the micro-tips. Chromatography was performed with a PhyNexus microtip with 40 μL of resin dosed in a 1 mL pipette tip. The pipette tips are designed to be used with a liquid handling system such as Tecan® liquid handling system. By using a liquid handling system the flow direction of the

mobile phase in the column becomes bi-directional. The effects of adsorption of target protein on the stationary phase with bi-directional flow are unknown therefore a liquid handling system will not be used in this project.

Ultra scale-down involves the mimicking of a unit operation running under the same conditions at larger scale. To deliver a uni-directional flow into the micro-tip a Harvard PHD 44/4400 programmable (Harvard apparatus, Kent) syringe pump and a 50 mL stainless steel syringe (Harvard apparatus, Kent) were used to run all experiments. The setup of the experimental hardware is shown in figure 2.3.

Prior to the experiments, the micro-tips were first rinsed with 2 mL of ultra-pure water to displace all glycerol in the void space of the resin. Breakthrough of Fab' was determined at 0.259 mL min^{-1}, 0.192 mL min^{-1} and 0.129 mL min^{-1}. These running flowrates were determined by keeping the linear velocity the same when scaling down from a 1 mL HiTrap column to a 40 μL PhyNexus micro-tip. New micro tips were used for each experiment. All columns were equilibrated with 10 CV equilibration buffer composed of 20 mM sodium acetate at pH 5.2. Feedstock preparation method is the same as the millilitre scale experiments and was described in the previous section.

The experiment follows a traditional operation of a chromatography column – equilibration, load, wash, elute and re-equilibration. Samples were collected from the effluent during loading at time intervals determined by the flowrate (refer to table 2.1 for calculated times). The effluent is collected into a 2 mL deep 96 well-plate (Fischer Scientific, Leicestershire). The fractions were assayed for concentration of Fab' fragments using the HPLC method described in section 2.2.

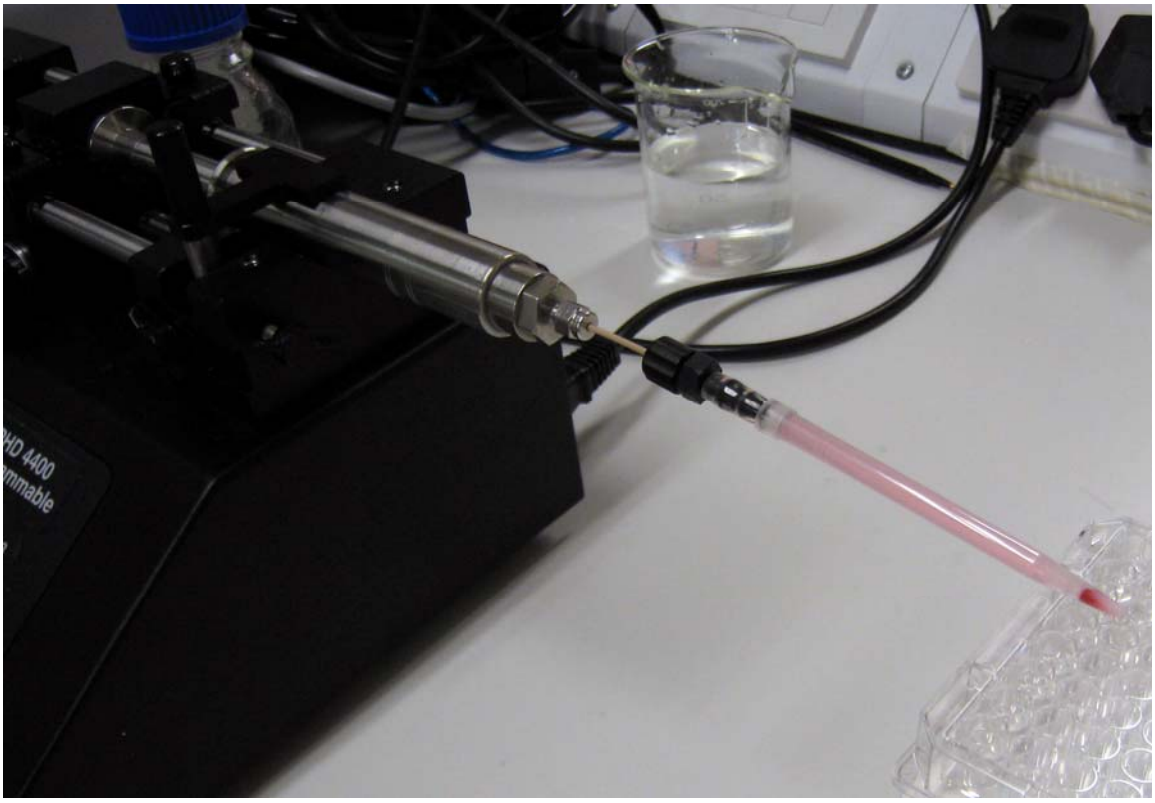

Figure 2.3 A photo shoot of the setup of the micro-scale experiment. In the image, a 50 mL syringe is set onto the pump device and the syringe is connected to a 40 µL pipette tip.

Table 2.1 Experimental and sample collection time for micro-scale breakthrough curves using a 40 µL micro-tip at different flowrates.

Linear velocity ($cm\ h^{-1}$)	Flowrate from Syringe pump ($mL\ min^{-1}$)	Total time (min) 35 mL loading volume	time between fractions (min) 500 µL samples
310	0.259	135	1.90
232	0.192	182	2.60
155	0.129	271	3.85

2.4 Chapter Summary

- The necessary experiments have been identified to optimize the adsorption system to obtain breakthrough curves for modelling purposes. These include:
    - Determination of adsorption isotherms to compare binding conditions of Fab' fragments onto SP Sepharose FF resin.
    - Method to Analyse the precipitation formed during pH adjustment of the clarified lysate containing Fab' fragments

- A method to obtain breakthrough curves at three different flowrates has been presented at:
    - 1 mL scale using a HiTrap column
    - 40 μL scale using PhyNexus micro tips scaling down from HiTrap using constant linear velocity

In the next chapter the theory behind the isotherm and the method of data handling will be described. The general rate model for analyzing the breakthrough curves will be presented and explained. In addition, the correlations for estimating the transport parameters for the general rate model will be described.

3. Theoretical considerations

In this chapter the theories and assumptions behind the adsorption isotherm, general rate model are presented. In addition the calculation of a theoretical diameter used for modelling a PhyNexus tip is also presented.

3.1 Isotherm

An adsorption isotherm is defined as the function which connects the amount of adsorbate on the adsorbant with its concentration. These isotherms are derived from a proposed kinetic mechanism with assumptions.

1. the adsorbent is uniform, that is the binding sites are equal and identical
2. the adsorbed molecules are inert and will not interact with other particles.
3. all adsorptions occur by the same mechanism.
4. at maximum adsorption a monolayer is formed, meaning that the adsorbate does not deposit on other adsorbed molecules. There is no interaction between molecules that are attached to resin ligands.

An example of an isotherm:

$$Q_{eq} = \frac{Q_{\max}(C_{eq})}{K_d + C_{eq}} \qquad (3.1)$$

The above isotherm is another form of the Michaelis-Menten equation and is commonly known as the Langmuir isotherm.

On the LHS of the equation is Q_{eq} - the amount of material bound to the adsorbant.

On the RHS of the equation, Q_{max} is the maximum binding capacity of the adsorbant, while K_d is the dissociation constant or Langmuir constant. C_{eq} is the concentration of adsorbate at equilibrium.

3.1.1 Calculations for experimental isotherm

The method to obtain an isotherm through batch adsorption is described in section 2.3.1.2 however to obtain a high resolution isotherm there are a few considerations. To obtain the Langmuir isotherm terms experimentally equation 3.2 is used.

$$Q_{eq} = (C_0 - C_{eq})(\frac{V_l}{V_m}) \quad (3.2)$$

Where for the Fab' *E.coli* lysate system we have:

Q_{eq} is the amount of materials bound to the adsorbant.
C_0 is the Fab' fragment concentration in the feed
C_{eq} is the concentration of Fab' at equilibrium of each batch system
V_l is the volume of Fab' *E.coli* lysate in each batch system
V_m is the volume of matrix in each batch system

Each batch experiment will yield at the end a liquid phase Fab' fragment concentration C_{eq}. Using this value, Q_{eq} can be calculated. A set of batch adsorption experiments will give an idea of the adsorption power of the adsorbant expressed as speed (K_{ads} or K_d) and point of saturation (Q_{max}). This is done by using a least square based fit of equation 3.1 for experimental values of Q_{eq} vs C_{eq} .

Concentration of the heat lysate used for obtaining the adsorption isotherm is crucial to the resolution of the experimental results. It is necessary to obtain points on the adsorption isotherm especially at the lower end of the curve; this region explains the efficiency of the adsorption system, in other words it is an indication of how likely the Fab' fragments adsorb onto the resin upon contact.

To obtain data points at the lower region of the isotherm a small Fab' lysate volume to matrix volume ratio is required, conversely the upper region of the isotherm requires a large Fab' lysate to matrix volume ratio. While designing the experiment, the matrix volume should be as small as possible, this minimises the amount of Fab' lysate required to complete a full set of experiment. It is also important to note that the volume of matrix should be large enough to allow the absorbate size distribution to be close to normal. In addition the volume of matrix should always be smaller than the volume of liquid to ensure there is sufficient mixing during the batch incubation. Because of this reason, the concentration of the target protein in the solution cannot be too high. A good balance between the Fab' concentration of the lysate and the matrix volume is key to obtain a high resolution isotherm.

3.1.2 Isotherm for a complex protein system

The Langmuir isotherm in equation 3.1 is a single component Langmuir isotherm. In other words there are no representations the protein influences of other proteins on the adsorption of the Fab'. Although a multi-component Langmuir isotherm does exist, this isotherm states that the adsorption of the target protein is a function of the sum of all the adsorbed species in the system. Not only is it generally not possible to characterize fully the different proteins in the adsorption system it is also not practical to isolate and obtain adsorption isotherms of each of these proteins. The difficulty can be caused by the use of a complex feedstock; separating a large number of impurities from the feedstock might not be an easy task. For the above reason, identifying the multi-component Langmuir isotherm was not a practical approach for the purposes of this project.

Apart from the difficulty in identifying the individual protein isotherm, the assumptions of the Langmuir isotherm also cause major uncertainties. For instance within a finite batch system, the mobile and stationary phases are confined in a container, the mobile phase composition changes rapidly as contact time increases. However when the feedstock is passing through a conventional chromatography column, fresh feedstock is constantly loaded into the column; the resin inside the column is always experiencing a constant mobile phase condition.

The accuracy of the isotherm depends on the amount of resin dosed into each batch system. Because each batch system is a discreet experiment, there are errors between each isotherm data point. Another source of error arises when trying to identify the actual amount of resin used; the equation calls for volume of matrices phase used; however, the volume dosed into each batch system is not the actual volume of resin that is due to the resin and the void space. The combined effect of the two sources of error explained above affects the volume of mobile phase to volume of stationary phase ratio which will greatly affect the value of Q_{eq} calculated.

For the above reasons, the values obtained from the finite batch isotherm might not necessarily represent a dynamic system under complex protein conditions; however, using isotherms, the adsorption of the target protein onto the stationary phase can be compared. This is particularly useful to determine the right conditions for chromatography.

3.2 General Rate Model

3.2.1 Predicting events within a column

In reality, column conditions are not ideal; it is necessary to take into account a lot of variables to model a real column. However, a larger number of variables will increase the complexity of the modelling to describe events within a chromatography column. To simplify the complexity of the model for more ready analysis, the column is assumed to be ideal. Therefore several assumptions are applied (Gu, Tsai et al. 1993).

The assumptions are as follows:

1. the column is isothermal and the physical and chemical conditions at any point of the chromatography column are the same.
2. the mobile phase velocity is constant and is independent of concentration.
3. the mobile phase compression is negligible.
4. the column bed is homogenous, with resin particles packed evenly in the column.
5. the packaging material is spherical and uniform; i.e. every resin particle has same adsorption properties.
6. the radial concentration gradient is negligible.
7. there is local equilibrium of each component between the pore surface and the stagnant fluid in the macropores; in other words, no convective flow within the particle pores.
8. mass transfer only occurs in an axial direction by convection and by axial dispersion.

With these assumptions stated above, the general rate model was derived to model the chromatographic separation. This model is believed to be the most comprehensive one available.

3.2.1.1 Continuity Equation in the flowing mobile phase

Equation of mass balance between chromatography column and the external film around the resin bead particle:

$$-D_{ax}\frac{\partial^2 C_{bi}}{\partial Z^2}+v\frac{\partial C_{bi}}{\partial Z}+\frac{\partial C_{bi}}{\partial t}+\frac{3K_i(1-\varepsilon_b)}{\varepsilon_b R_p}(C_{bi}-C_{pi,R=Rp})=0 \qquad (3.3)$$

The first term on the LHS of the equation indicates the transport by axial dispersion in the mobile phase. This term explains the diffusion of materials along the column with arbitrary dimension defined as Z. The effect of this term is negligible if the flow rate is high.

The second term takes into account the convective transport in the mobile phase along the column in the axial direction, which is the movement of the mobile phase driven by force/flow hence the term is a function of interstitial velocity *v*.

The third term defines the accumulation in the mobile phase. Change of concentration of protein in the bulk fluid occurs over time, i.e. as material progresses through the column.

The last term of the equation represents the accumulation in the stationary phase, which is the rate of mass transfer through the external film relating the bulk fluid concentration to the concentration at the surface of the resin particles.

3.2.1.2 Continuity Equation inside the Macropores

The equation describing the mass balance between the bulk fluid and the individual resin bead particle is:

$$(1-\varepsilon_p)\frac{\partial C^*_{pi}}{\partial t}+\varepsilon_p\frac{\partial C_{pi}}{\partial t}-\varepsilon_p D_{bi}[\frac{1}{R^2}\frac{\partial}{\partial R}(R^2\frac{\partial C_{pi}}{\partial R})]=0 \qquad (3.4)$$

The first term on the LHS of the equation defines the accumulation on the surface of the stationary phase. This term represents the protein concentration outside the stagnant film of a resin bead particle.

The second term represents the accumulation around the stagnant fluid in the macropores. This describes the diffusion of the protein product across the stagnant fluid phase.

Finally the last term describes the radial diffusion inside the porous particle. This term accounts for the diffusion of the protein product into the binding sites of the resin particles, with D_b being the speed proteins travel into the intra-particle space of a resin particle.

3.2.1.3 Boundary conditions

Solving the partial differential equations will give the relationship between the variables. Boundary conditions are used to complete the simulation of an ideal column by providing a finite solution.

Initial and boundary conditions are:

$$t = 0;\ C_{bi} = C_{bi}(0,Z)\ ;\ C_{pi} = C_{pi}(0,R,Z) \qquad (3.5)$$

Initially there is no material fed into the column, therefore the concentration at any point of the column and the resin bead is defined as zero. These conditions limit the calculated solutions for concentration to be positive values.

When Z=0:

$$\frac{\partial C_{bi}}{\partial Z} = \frac{v}{D_{bi}}(C_{bi} - C_{fi}(t)) \qquad (3.6)$$

This assumes no accumulation at the beginning of the column where flux to the entrance equals flux from the entrance to the exit of the column. In other words protein is not accumulated at the top of the column initially during loading when t=0; this is mathematically achieved by stating that concentration of bulk liquid minus the concentration of feed protein concentration profile as a function of time. So for frontal adsorption $(C_{bi} - (C_{fi}(t)/C_0)) = 1$.

When Z=L:

$$\frac{\partial C_{bi}}{\partial Z} = 0 \qquad (3.7)$$

Assumes that by the column end, no adsorption will occur.

When R = 0:

$$\frac{\partial C_{pi}}{\partial R} = 0 \tag{3.8}$$

The diffusion into the beads occurs uniformly from the bead surface into the particle.

When $R=R_p$:

$$\frac{\partial C_{pi}}{\partial R} = \frac{k}{\varepsilon_p D_{pi}}(C_{bi} - C_{pi,R=Rp}) \tag{3.9}$$

This assumption describes the maximum amount of protein product that can be diffused into the bead particle pores and at what speed protein diffuses into the particles.

3.2.2 Application of the general rate model

In this project, the general rate (GR) model (explained in sections 3.2.1) will be used in two different ways. The first way is to use the GR model to simulate a breakthrough curve; this is a traditional use. Users input the necessary parameters to complete the general rate model. These parameters can either be estimated from experimental data or from empirical correlations. Methods to estimate the parameters will be presented in chapter 3.2.6. A diagram listing all the input parameters is shown in figure 3.1.

The second way is to use the general rate model in an iterative manner. This method involves the use of the least square method to estimate the general rate parameters best representing the performance of chromatography. The performance of the chromatography is judged by the shape of a breakthrough curve. In figure 3.2, the input and output of the method is presented.

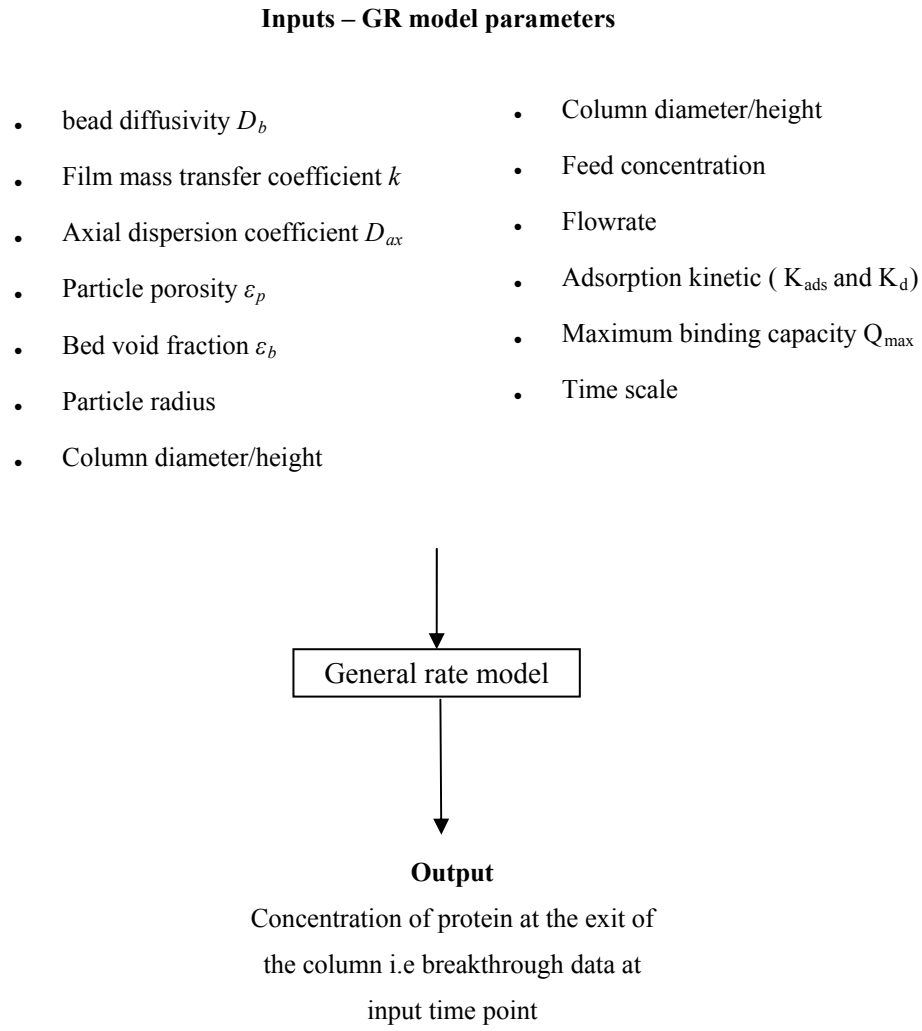

Figure 3.1 Inputs required to be identified to simulate a breakthrough curve with the general rate model.

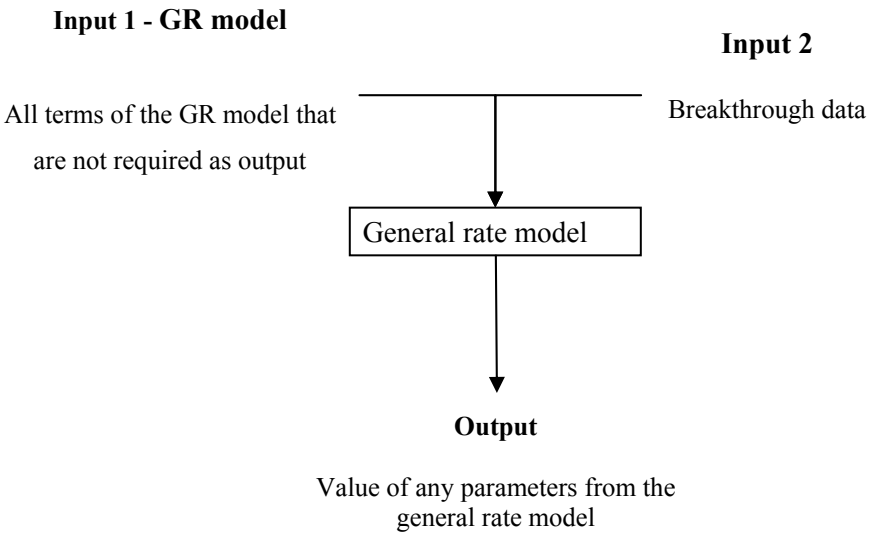

Figure 3.2 Inputs that are required to be entered into the general rate model to initiate a solving routine to calculate general rate parameters and adsorption kinetics. Input 1 are the general rate parameters that are known for the system whereas input 2 is the breakthrough curve obtained experimentally.

3.2.3 Adsorption kinetics

The adsorption kinetic equation is required to be used with the general model to describe the speed of adsorption of target protein onto the resin binding sites; hence the rate of change of target protein concentration in the bulk fluid phase can be calculated by the model. Typically a Langmuir isotherm is used for describing the adsorption of Fab' fragments to the matrix particles. For a product capture step feed materials will contain multiple contaminants including several proteins which can adsorb to the column matrix. A competitive Langmuir isotherm is ideally required to describe the complex adsorption.

For a complex feed material, the precise determination of all contaminants which may adsorb onto the column matrix and the associated isotherm constants would be impractical. Given this degree of complexity and the fact that only breakthrough of Fab' fragments from the column is specifically assayed; the breakthrough curve obtained using this method included the effect of other contaminant proteins on the binding of our target protein. A simple reaction equation (equation 3.10) can explain the binding of the target protein (S) onto matrix particles (K).

$$\mathrm{K} + \mathrm{S} \underset{K_d}{\overset{K_{ads}}{\longleftrightarrow}} \mathrm{KS}\ (Q_{max}) \qquad (3.10)$$

The rate of adsorption of Fab' onto the resin is represented by K_{ads} while the desorption constant is K_d the adsorption reaches equilibrium when Q_{max} is reached. These three parameters were obtained by curve fitting instead of a traditional experimental method utilising the single component Langmuir isotherm.

3.2.4 Transport parameters

Parameters required in the GR model include known parameter, such as column height and diameter, particle radius, molecular weight of product and flowrate. Other parameters, such as void fraction, particle porosity and pore diameter can be estimated based on values reported in the literature. Transport parameters such as film mass transfer coefficient (k), the axial dispersion coefficient and the effective intra-particle diffusivity, can be estimated using established correlations. The effective intra-particle diffusivity, D_b, was calculated using the correlation (Wallace W. Yau 1979).

$$D_b = \frac{D_m}{\tau}(1 - 2.104\lambda + 2.09\lambda^3 - 0.95\lambda^5), \tag{3.11}$$

Where, D_m is the molecular diffusivity, τ is the particle tortuosity and λ is the ratio of the molecular diameter, d_m, of the component to the pore diameter of the particles. The values of d_m and D_m were estimated from the molecular weight (MW) of the component (Marshall 1978).

$$d_m(A) = 1.44MW^{\frac{1}{3}} \tag{3.12}$$

$$D_m = 2.74x10^{-7}MW^{-\frac{1}{3}} \tag{3.13}$$

The film mass transfer coefficient, k, was calculated using the correlation (Wilson and Geankoplis 1966):

$$k = 0.687v^{1/3}\left(\frac{\varepsilon_b R_p}{D_m}\right)^{-\frac{2}{3}} \tag{3.14}$$

where v is the interstitial velocity , R_p is the particle radius and ε_b is the bed void fraction.

The axial dispersion, D_{ax}, coefficient was estimated by initially calculating the value of the Peclet number valid for flowrates of low Reynolds number (Chung and Wen 1968; Ting 1995)

$$Pe = \frac{0.1L}{R_p \varepsilon_b} \tag{3.15}$$

where L is the column length. The value of D_{ax}, was then calculated from the definition of Peclet number of axial dispersion $Pe = \frac{vL}{D_{ax}}$, giving D_{ax} = 1.95 x 10 $^{-7}$ m^2s^{-1}, which is of the same order of magnitude as values used in other modelling studies. For simulations of breakthrough carried out at different flowrates D_{ax} was assumed to be directly proportional to the linear flow rate since eddy diffusivity is the dominant mechanism of axial dispersion, and hence the Peclet number remains constant with changing flowrate over this range.

Values of ε_b reported in the literature for columns packed with SP Sepharose range from 0.29 – 0.42 (DePhillips and Lenhoff 2000). A value of 0.35 was assumed for simulations in this work. Values of ε_p for uptake of proteins in SP Sepharose matrix beads are also reported in the literature; however, because this is the accessible particle porosity, the value will depend on size of the binding protein. A value of ε_p = 0.65 was used based on diffusion of lysozyme in SP Sepharose FF matrix (Dziennik, Belcher et al. 2005). The value for particle tortuosity was derived based on the relation $\tau = \frac{(2-\varepsilon_p)^2}{\varepsilon_p}$ (Kramarczyk, Kelley et al. 2008) giving τ = 2.8. The value τ is used in the determination of D_b, giving D_b = 1.6 x 10^{-11} m^2s^{-1}. Allowing for differences in protein size, this value agrees well with the measured value of D_b of approximately 4 x 10^{-11} m^2s^{-1} which was obtained for uptake of lysozyme into SP Sepharose FF matrix particles from solutions of low ionic strength and low protein concentration (Chang and Lenhoff 1998). A median value for matrix particle diameter of 90 μm was used in all simulations.

3.3 Breakthrough curve

In order to obtain a full breakthrough curve assumptions need to be made to calculate the amount of *E.coli* lysate required to saturate a 1 mL Hitrap column.

Assuming SP Sepharose FF resin has a saturation binding capacity of 120 mg $_{\text{Fab' fragments}}$ mL^{-1} $_{\text{matrix}}$ and the *E.coli* lysate feed stock contains 0.15 mg mL^{-1} of Fab' fragments. The saturation binding capacity is assumed to be three times the dynamic binding capacity (40 mg $_{\text{Fab' fragments}}$ mL^{-1} $_{\text{matrix}}$). The amount of Fab' lysate required to saturate the column, bringing the breakthrough curve up to 100% requires 800 mL of feedstock.

The resolution of the breakthrough curve depends on the number and volume of fractions collected during the experiment.

3.4 Calculations for HiTrap column and PhyNexus microtips

To mimic the performance of a HiTrap column with a PhyNexus tip, the column attributes need to be calculated. The following calculations show the scale down strategies used for a PhyNexus tip.

A PhyNexus micro-tip is in the shape of a frustum of a cone. The mid cross sectional area is used to calculate the running linear velocity and to transform the frustum into a cylindrical shape using the mid point of the frustum as the average point. The length of the resin bed of a 40 µL and the top and bottom radius of the bed is 3 mm and 2 mm respectively. The radius at the 4.5 mm point of the frustum is calculated to be 0.125 cm. The calculation is shown in figure 3.4. This value can be used to calculate the cross sectional area of cylinder and the corresponding volumetric flowrate (equation 3.16) running at the same linear velocity as used at the 1 mL scale.

A typical linear velocity for adsorption is around 100 cm h^{-1}. The cross sectional area of a 1 mL HiTrap column is 0.385 cm^2. This makes the corresponding volumetric flowrate 0.88 mL min^{-1}. A flowrate of 1 mL min^{-1} was used for all the experiments to simplify subsequent experiments when changing volumetric flowrates. The calculation of volumetric flowrate from linear velocity is shown in equation 3.16. The corresponding volumetric flowrates at different linear velocities and scale are shown in table 3.2.

Linear velocity x cross sectional area = volumetric flowrate (3.16)
($cm\ h^{-1}$) (cm^2) ($mL\ h^{-1}$)

The volume of the frustum of a cone is given by:

$$V = \frac{\pi h}{3}(r_1^2 + r_2^2 + (r_1\ r_2)) \quad (3.17)$$

The volume of the frustum = volume of frustum (A) and volume of frustum (B)

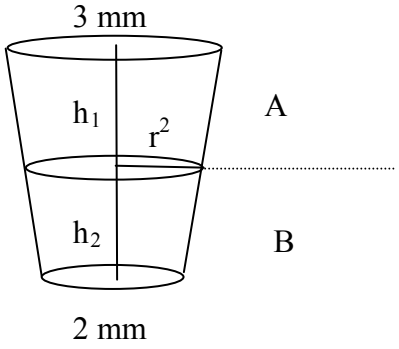

Because the intersection point is in the middle of the frustum, therefore

$$h_1 = h_2 = 4.5 \text{ mm} \quad (3.18)$$

$$\frac{9\pi}{3}(1.5^2 + 1^2 + (1 \times 1.5)) = \frac{4.5\pi}{3}(1^2 + r_2^2 + (r_2)) + \frac{4.5\pi}{3}(1.5^2 + r_2^2 + (1.5r_2)) \quad (3.19)$$

Using equation 3.18, the value for r_2 was calculated to be 1.25 mm.

Figure 3.3 calculations for the mid sectional radius of a conic frustum

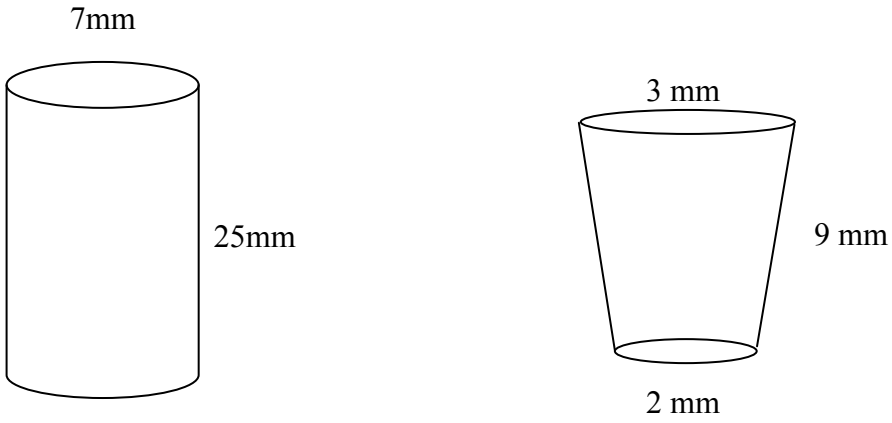

Figure 3.4 Geometry of a 1mL HiTrap column (left) and the resin bed of a 40 µL PhyNexus microtip (right). (drawing not to scale)

Table 3.1 Volumetric flowrates for operating PhyTip and HiTrap columns at specific linear velocities.

Linear velocity ($cm\ h^{-1}$)	Flowrate into PhyTip ($mL\ min^{-1}$)	Flowrate on HiTrap column ($mL\ min^{-1}$)
310	0.259	2.0
232	0.192	1.5
155	0.129	1.0

3.5 Chapter summary

In this chapter:

- The assumptions behind the general rate model are explained.
- The reasons behind a multi-component isotherm not being a reasonable tool to represent a complex feedstock are explained.
- The application of the general rate model in the project is presented
- The method of estimating parameters required to complete the general rate model for individual adsorption system is presented.
- Assumptions made for the PhyNexus tips to correct for its shape – a truncated cone are detailed.

Experimental data will be presented in Chapter 4 while the modelling results will be shown in Chapter 5.

4. Experimental Results

4.1 Introduction

The main purpose of the works presented in this chapter is to optimise the adsorption system of Fab' fragments onto a generic cation exchange resin by identifying a condition (pH and conductivity) where Fab' fragments readily bind to the resin upon contact. By using an optimised system to obtain breakthrough curves the results can fully represent a system running at its full potential.

Firstly, an assay technique was developed to quantify the amount of Fab' fragments in a sample. Secondly, batch adsorption method was used to obtain isotherms to visualise the adsorption efficiency at different feedstock conditions. Last but not least, using the optimised feedstock condition to obtain breakthrough curves and at the same time evaluating the system serving as a primary capture step.

4.2 Assay technique

The purpose of the assay is to quantify the amount of Fab' in a sample. A good assay technique should be able to detect the target protein at a low concentration while maintaining accuracy. In addition the assay should not be affected by other non-target protein species.

In this section, a calibration curve will be presented. The calibration curve obtained will be used for determining the concentration of Fab' fragments throughout the project. The calibration curve was repeated three times using the pure Fab' standard solution prepared from the same purification run.

Pure Fab' fragment samples were analysed using the method described in section 2.2.1. Samples were diluted to concentrations of 20 $\mu g\ mL^{-1}$, 50 $\mu g\ mL^{-1}$, 100 $\mu g\ mL^{-1}$, 200 $\mu g\ mL^{-1}$, 300 $\mu g\ mL^{-1}$, 400 $\mu g\ mL^{-1}$ and 500 $\mu g\ mL^{-1}$. The peak areas integrated were

plotted against concentration and are shown in figure 4.1. The R^2 value of the linear trend is 0.995 while the slope is 24.2

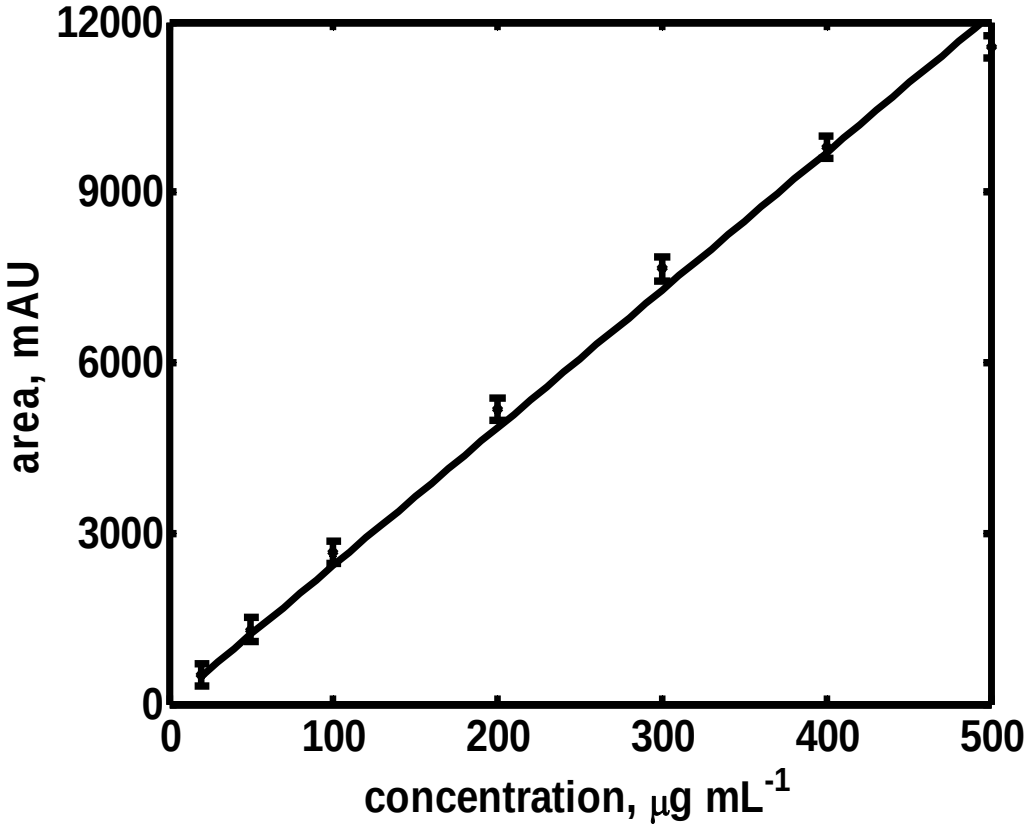

Figure 4.1 Standard curve of pure Fab' fragments with area (mAU*t) plotted against concentration (μg mL^{-1}). A linear trend line was fitted across the average of two sets of experimental data. The R^2 value of the trend line is 0.998. The error bars represents the standard deviation of the two sets of data.

4.1.2. Lysate

The sensitivity and effectiveness of the assay with a complex protein matrix were confirmed by testing the method using *E.coli* lysate. The initial concentration of the lysate was determined to be 510 μg mL^{-1} using the method described in section 2.2.1 and the calibration curve obtained in section 4.1. The lysate was diluted to 1/10, 1/15, 1/30, 1/100 and 1/200 of its original concentration. The result is shown in figure 4.3. The R^2 value of the linear trend is 0.967 and the slope is 26.3 $\frac{m * Au}{\mu g m L^{-1}}$.

From both of the calibration curves obtained using pure Fab' and lysate, the slopes are 24.2 and 26.3 respectively. In figure 4.2, a set of calculations to convert signal from the HPLC to Fab' fragment concentration were shown.

From pure Fab' standard curve:

$$Concentration = \frac{peakarea}{24.2} = peakarea \times 0.0413$$

From *E.coli* lysate standard curve:

$$Concentration = \frac{peakarea}{26.3} = peakarea \times 0.038$$

Figure 4.2 Calculation of concentration of Fab' fragment containing samples using standard curves obtained from using pure and *E.coli* lysate samples

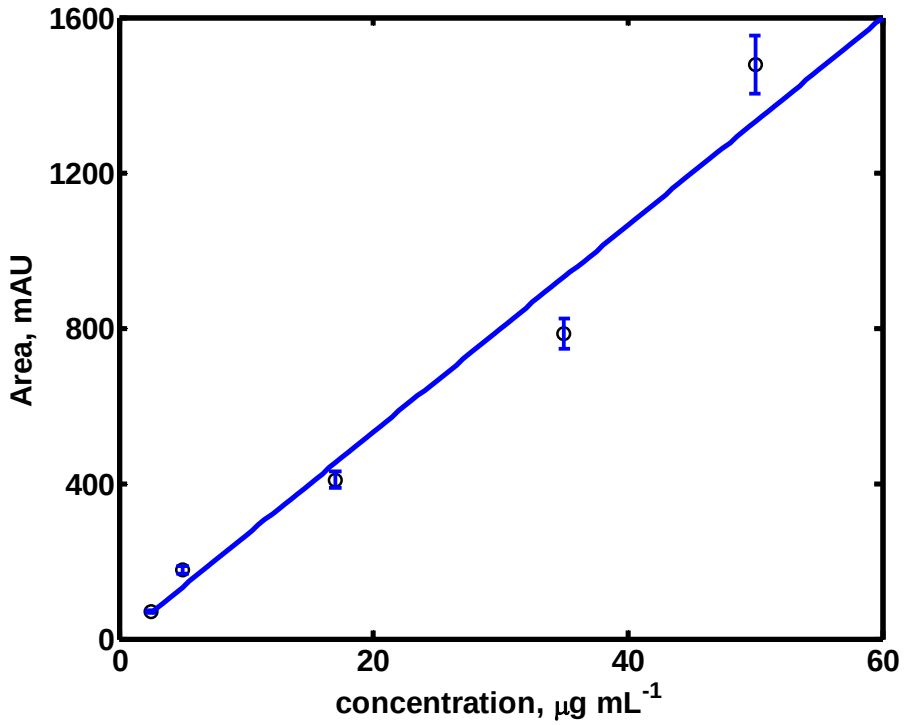

Figure 4.3 Standard curve (area (mAU*t) vs concentration (μg mL^{-1})) of *E.coli* lysate at 50 μg mL^{-1}, 35 μg mL^{-1}, 17 μg mL^{-1}, 5 μg mL^{-1} and 2.5 μg mL^{-1}. A linear trend line passing through origin was fitted across the average of three sets of data points. The R^2 value of the trend line is 0.968. Error bars represents standard deviation of three sets of data.

4.2. Batch adsorption

The aim of this section is to determine the right condition for adsorption of Fab' fragments in *E.coli* lysate onto SP Sepharose FF resin. This was done by obtaining isotherms, comparing the shapes and estimating the adsorption rate from them. Dry resin weight was also investigated to ensure the batch adsorption experiments were conducted accurately.

4.2.1. Dry resin weight

The method described in section 2.4.1.1 was used to conduct experiments using 50% (v/v ethanol) and 25% (v/v ethanol) resin. For 50 % (v/v ethanol) resin, due to the high viscosity of the suspension, the resin beads were difficult to aspirate accurately even with a wide bore pipette tip. If resin was aspirated equally and accurately, the percentage of liquid to resin should be maintained, but liquid phase of the emulsion reduced during the course of the experiment, this suggests that 50% (v/v water) resin is too challenging to dose accurately by hand. To reduce the viscosity, a higher ratio of liquid to resin volume was used. The experiment was repeated using 25 % (v/v ethanol) resin, because liquid to resin ratio is increased, dosing is less challenging and the percentage of liquid to resin remains unchanged throughout the experiment.

The dry resin weight was measured at different dosed volume. The results are summarised in table 4.1 and figure 4.4. The R^2 value of the trend line is >0.99; this shows that at 25% (v/v water) resin can be dosed accurately by hand especially at smaller volumes. It is also observed that at low viscosity, resin particles are less likely to stick to the sides of pipette tips causing major experimental error especially at small volumes.

Table 4.1 Summary of dry resin weight experiment. The table shows the pipetted volume of resin emulsion, its corresponding matrix volume at 25% (v/v), the dry resin weight and mass of matrix per volume of matrix pipetted.

Pipetted volume (μL)	matrix volume (μL)	Dry matrix mass, average of 4 repeats (±s.d.) (mg)	Matrix mass / Volume pipetted (mg μL^{-1})
40	10	1.40 ± 0.245	0.035
50	12.5	1.50 ± 0.245	0.0300
60	15	1.73 ± 0.222	0.0288
100	25	3.68 ± 0.450	0.0368
200	50	6.48 ± 1.27	0.0324
400	100	13.8 ± 0.891	0.0345
600	150	19.5 ± 2.67	0.0325
		Average	0.0329

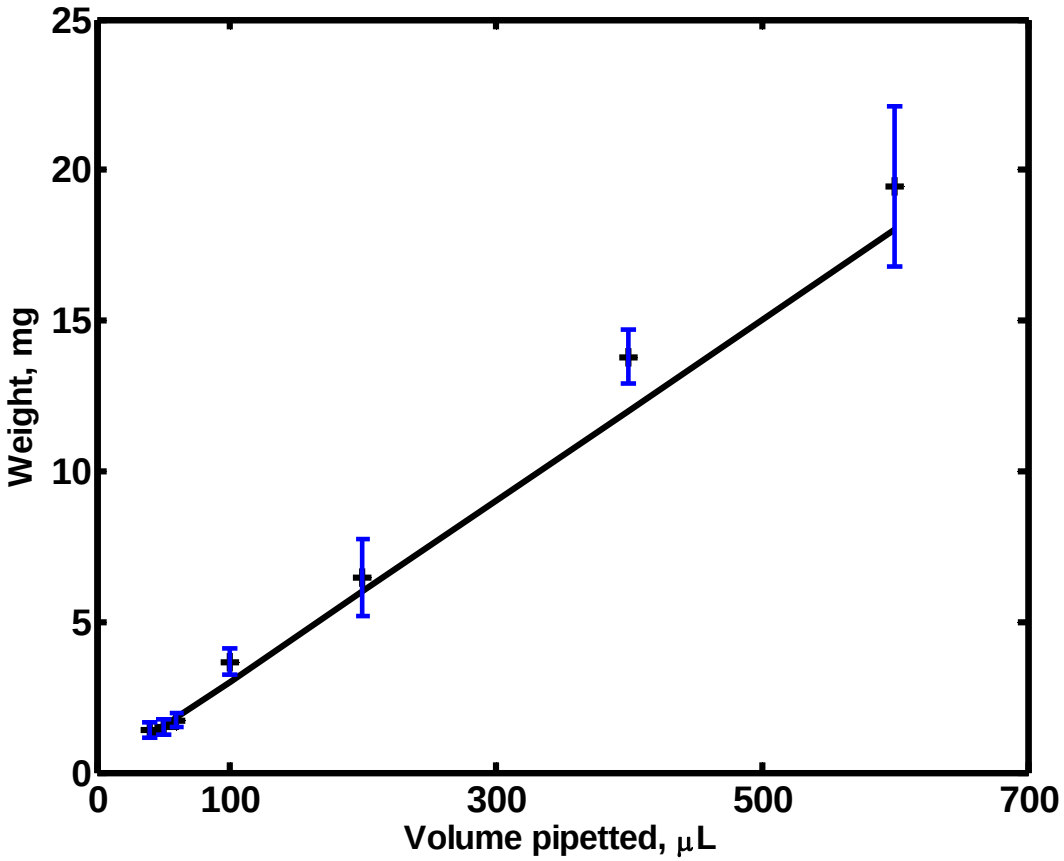

Figure 4.4 Graph showing the dry resin weight against the volume of 25% resin emulsion dosed. A trend line was drawn across the average of each data set. The R^2 value of the linear trend line passing through origin is 0.998. Error bars are standard deviation of the four repeats.

4.2.2. Isotherm

Based on the result from section 4.2.1., 20 μL of resin was used, that is dosing 80 μL of resin suspension. Because SP Sepharose FF resin size ranges from 45 – 165 μm, assuming that the resin size is normally distributed, choosing a larger sample size in this case pipetted volume, the size distribution of resin will be closer to normal compared to smaller volumes; hence the number of binding sites available in a batch system is proportional to a packed bed column.

Isotherms were obtained with *E.coli* lysate conditioned to pH 5 and pH 7 using the method describe in section 2.4.1.2. The result from the isotherms can be used to compare the pH effect on adsorption of Fab' fragments onto SP Sepharose FF resin. The results were shown in figure 4.5. The isotherm obtained using *E.coli* lysate at pH 7 was wider than pH 5; this showed that at pH 5 adsorption is faster and more efficient. In other words Fab' fragments are more likely to adsorb to the resin particles upon contact.

Focusing on the isotherm obtained at pH 7 (figure 4.5), the maximum binding capacity is when the graph reaches a stationary point, this point is observed to be at around 40 mg mL^{-1}, however when fitting the Langmuir isotherm through the data points, the maximum binding capacity is 186 μg mL^{-1}, which is far from normal. This binding capacity cannot be true because the binding capacity of a pure model protein such as lysozyme and BSA is around 110 mg mL^{-1}. It is impossible for a complex feedstock to achieve a binding capacity higher than 110 mg mL^{-1}.

Because of the nature of the isotherm, a different equation (refer to equation 4.1) was used to fit the data points. This equation is another form of the Langmuir isotherm with a correction factor *n*, giving a sigmoidal shape. The maximum binding capacity of Fab' fragments reduced to a more reasonable value of 43 μg mL^{-1}.

The equation used to fit the isotherm data:

$$Q_{eq} = \frac{(Q_{\max})C_{eq}{}^{n}}{K_d{}^{n} + C_{eq}{}^{n}} \text{ in the form of } y = \frac{ax^n}{b^n + x^n} \quad (4.1)$$

For the isotherm at pH 5 (figure.4.6) the Langmuir trend is sufficient to fit the data points. The Q_{max} value was fitted to be 56.3 mg mL^{-1}.

From the results above, not only the maximum binding capacity (Q_{max}) varies according to pH, the adsorption rate varies greatly with feed pH. Judging by the K_a value, the rate of initial adsorption of pH 5 almost 100 fold higher than pH 7 meaning that at pH 5, Fab' fragments are more readily adsorbed onto resin particles; hence pH 5 is a better binding condition for Fab' onto SP Sepharose FF strong cation exchange resin; this decisions was further reinforced by the fact that at pH 7 the value of K_d was 100 fold higher than at pH 5 meaning that at pH 7 the force of the adsorption is not strong enough to sustain the binding causing the bound materials to "leach" from the resin. As the liquid pH reduces the Fab' fragment becomes more positively charged. The trend obtained from the isotherms proved that the net charge of Fab' fragments is an important factor to allow effective adsorption onto SP Sepharose FF resin. A study was performed to confirm that pH 5 is the lowest possible pH to operate at without serious loss of yield. The study will be presented in the next section.

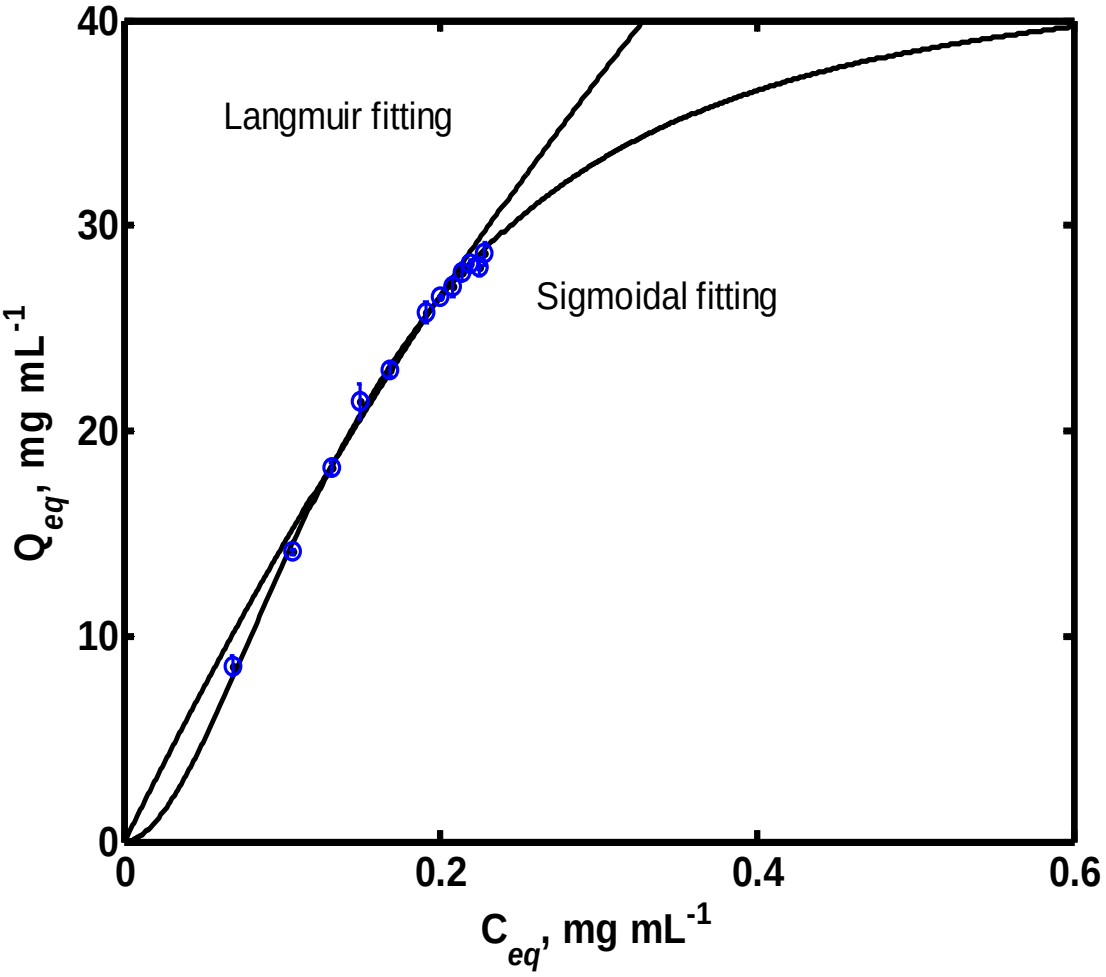

Figure 4.5 Isotherms of *E.coli* lysate at (+) pH 7 fitted using Langmuir isotherm and sigmoidal trends. Data points are average of two set of data while the error bars are standard deviation of the two set of data. (Some of the error bars are smaller than the data point marker)

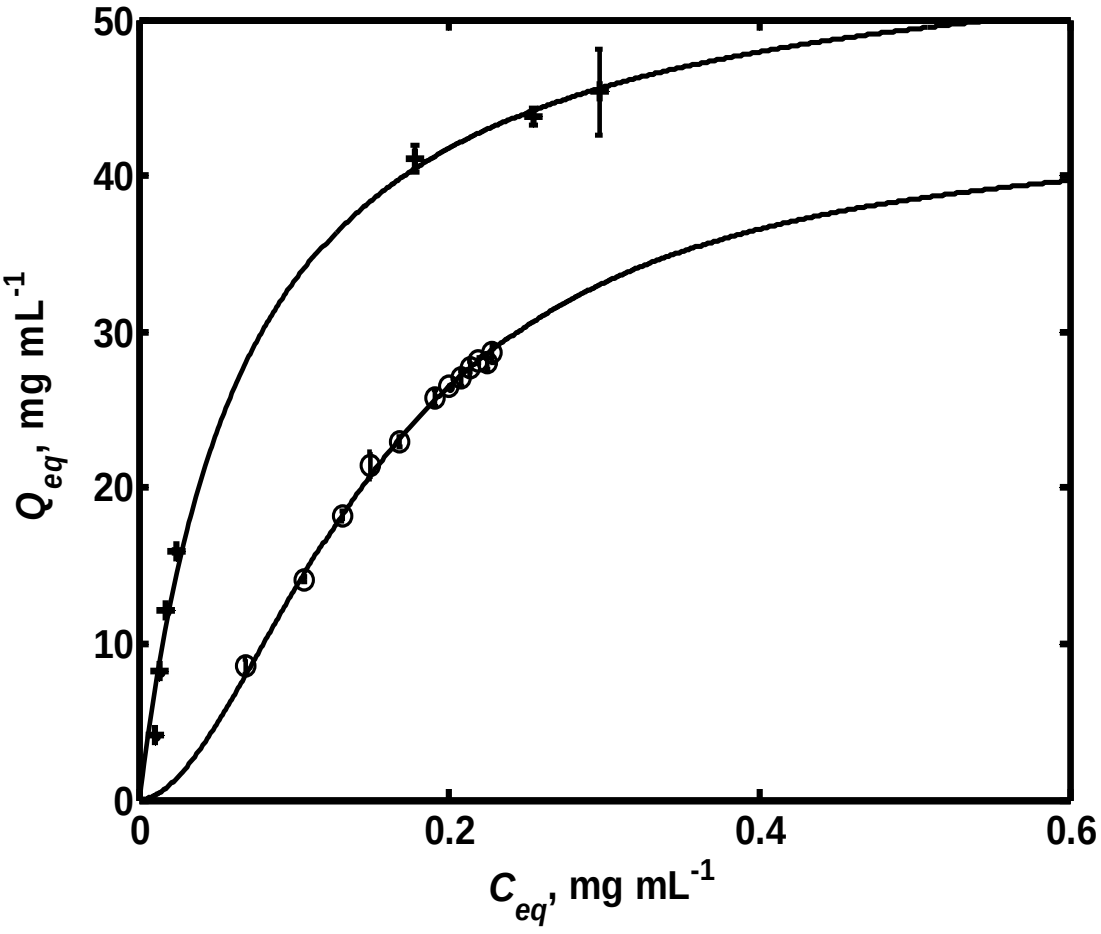

Figure 4.6 Isotherms of *E.coli* lysate on SP Sepharose FF at (+) pH 5 and (○) 7. The pH 5 isotherm was fitted using Langmuir isotherm while the pH 7 isotherm was fitted with a sigmoidal trend. Both trend lines are passing through the average of the two sets of experimental data. The error bars are standard deviation of the two set of experimental data. (Some of the error bars are smaller than the data markers)

Table 4.2 Summary of isotherm parameters (Q_{max}, K_d, K_a and n) obtained through curve fitting of experimental isotherms.

	pH 5	pH 7
Q_{max} ($mg\ mL^{-1}$)	56.3	43.0
K_d ($mL\ mg^{-1}$)	0.0671	6.47
K_{ads} (K_d^{-1}) ($mg\ mL^{-1}$)	14.3	0.155
n		1.83

4.4. Characterisation of *E.coli* lysate

As pH reduces, proteins from the *E.coli* lysate precipitate. SDS page and affinity HPLC were performed to confirm the composition of the particulates and the supernatant phases. An analysis was done using the method described in section 2.3.1.

In the reducing SDS-page gel images (figure 4.7) the supernatant and the particulates were analysed at different pH values. At pH 5 the majority of the Fab' fragments remain in the supernatant phase. However when pH is reduced below 5, the Fab' lysate becomes more turbid due to rapid protein precipitation. SDS Page and affinity HPLC both confirmed that Fab' fragments were present in the particulates at low pH (figure 4.7). In addition, at low conductivity, Fab' fragments are more prone to precipitate, as shown in figure 4.8. Fab' fragment concentration in liquid phase significantly decreases at pH lower than 5 (2 mS cm^{-1}) while at 15 mS cm^{-1} the Fab' fragment concentration did not drop significantly until pH is lower than 2.

Binding of the target protein on a cation-exchange resin requires the feedstock pH to be lower than the isoelectric point (pI). The Fab' fragments (A33) used in this project has a pI of ~8.3, at a pH lower than the pI, the net charge of Fab' fragments is positive. Binding of Fab' fragments on a cation-exchange resin will be stronger when the net charge is stronger. From the studies described above, the lowest pH achievable is 5, in other words pH 5 is the operating edge of the system, beyond this pH, significant Fab' fragments will be loss due to precipitation.

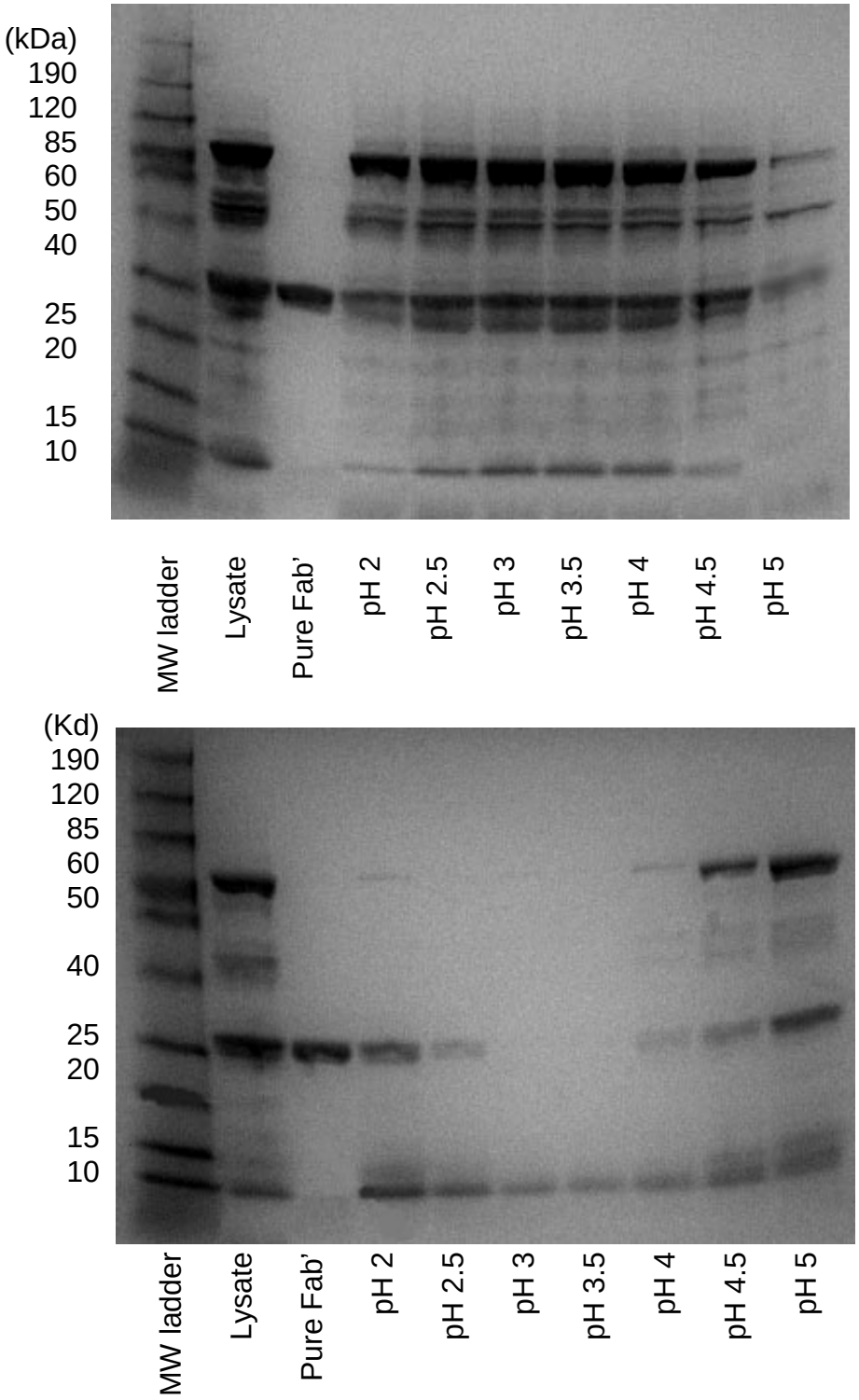

Figure 4.7 Comparison of the composition of *E.coli* lysate at different pH values using reducing SDS page. The top image shows the composition of dissolved particulates and the bottom image shows the liquid phases composition at various pH values.

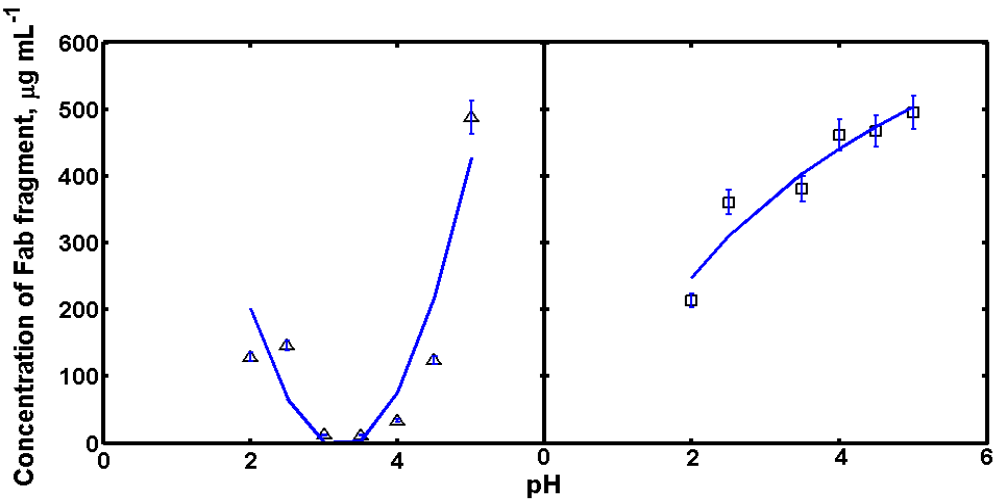

Figure 4.8 Concentration of Fab' fragments in supernatant phase of clarified *E.coli* lysate at (▲) 2 mS cm^{-1} and (■) 15 mS cm^{-1} at different pH. The original concentration of the clarified *E.coli* lysate was 495 µg mL^{-1} before pH adjustments. The error bars are assuming 5% error from the assay. Some of the error bars are smaller than the data point markers. The trend lines drawn across the data points are used to guide the eyes (trend line not model fit).

4.5. Breakthrough curves

In this section, breakthrough curves are presented at 1 mL millilitre-scale and 40 μL micro-scale. At millilitre-scale, breakthrough curves were obtained at 310 cm h^{-1}, 232 cm h^{-1}, and 155 cm h^{-1}. In addition, breakthrough curves obtained under weak isotherm conditions are shown. At micro-scale, a set of breakthrough curves were obtained under the same linear velocities as for the millilitre-scale. A method to alleviate assay artefact was developed to define a baseline for the breakthrough curves.

4.4.1 Millilitre-Scale

The conditioned *E.coli* lysate for breakthrough experiments contains 150 μg mL^{-1} of Fab' fragments; the solution pH was 5.2 and the conductivity was 2.0 mS cm^{-1}. These conditions were shown to be optimal for binding to a strong cation exchange in previous sections (refer to section 4.3).

Breakthrough experiments were performed using the method described in chapter 2.4.2. *E.coli* lysate was loaded into a 1 mL Hitrap column until the column was almost saturated. The effluent was collected in fractions and analysed using affinity HPLC. The Fab'antibody fragment peaks from the HPLC chromatograms were integrated. The peak areas of the fractions were divided by the peak area of Fab' antibody present in the raw feedstock. The resulting values were plotted against volume of feed loaded into the column, resulting in a normalised breakthrough curve of Fab' antibody fragment.

To demonstrate the importance of pH on the adsorption of Fab' fragments onto SP Sepharose FF strong cation resin, breakthrough curves for feed solutions adjusted to both pH 7.0 (figure 4.9) and pH 5.2 (figure 4.10) were obtained.

From the pH 7.0 breakthrough curves, no distinct baselines were observed, breakthrough occurs as soon as feed material passes through the column even at linear velocity lower than 100 cm h^{-1} (0.5 mL min^{-1}) this suggests that adsorption is very slow, in other words, the isotherm is weak. Moreover, the rate of rise of the breakthrough curves is flowrate

dependent; this further suggests that the binding condition is unfavourable. The poor adsorption is caused by the weak net charge of Fab' fragments at pH 7, which leads to a weak driving force for Fab' fragments to enter the stagnant film of the resin particles, and hence slow diffusion of Fab' fragments into the infrastructure of the resin particles. To increase the surface net charge of Fab' fragments, the lysate was reduced to pH 5.2. Although according to section 4.3 the operating edge is pH 5, using a slightly higher pH give a leeway to counter error from the pH probe and at the same time preventing major Fab' fragment loss during feedstock preparation.

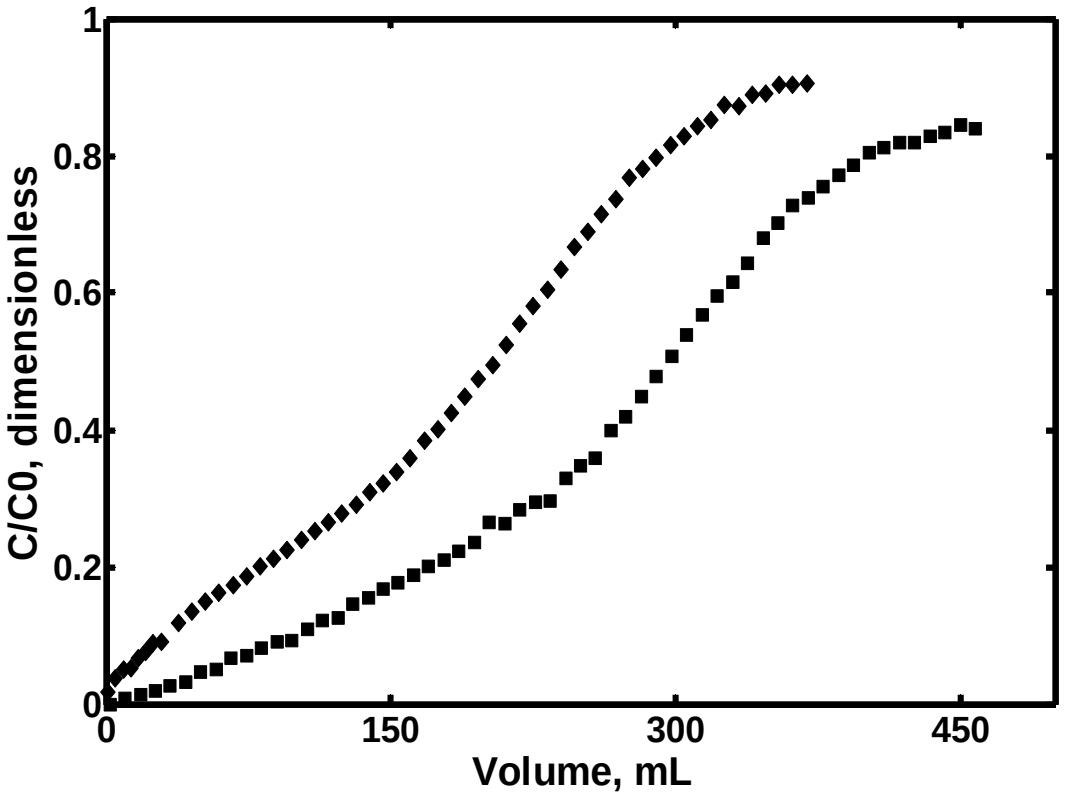

Figure 4.9 Breakthrough curves of Fab' antibody in *E.coli* lysate at pH 7.0 running through a HiTrap 1mL SP Sepharose FF column at (■) 72.5 cm h^{-1} (0.5 mL min^{-1}) and (♦) 155 cm h^{-1} (1 mL min^{-1}).

For the breakthrough curves obtained using lysate at pH 5.2 (refer to figure 4.10), distinct baselines can be observed, however, the baselines are elevated. The extent of elevation is the same across all linear velocities; this suggests that the phenomenon is not an adsorption problem but rather, is an assay artefact. To confirm this speculation, eluate from the protein G HPLC was collected and analysed using SDS-PAGE. From figure 4.11, four distinct bands can be seen, apart from the 54 kDa band representing Fab' fragments; there are also bands at 150 kDa and two bands at around 25 kDa. The SDS-PAGE showed that not only Fab' fragments can bind to protein G ligands, but also other proteins. Judging by the sizes, the smaller molecular weight ~25 kDa bands can be fragments of the Fab' fragments and the larger molecular weight can be caused be aggregates or truncated (aggregated fragments of Fab' fragments) versions of Fab' fragments.

The protein G assay quantifies Fab' fragments by absorbance measurements of the eluate from the affinity column. All non-functional Fab' fragments bound onto the protein G column will affect the result of the assay and hence potentially overestimate the amount of Fab' fragments in a sample. The other non Fab' fragment bands from the SDS-PAGE image (refer to figure 4.11) can be due to the presence of truncated versions of Fab' that were either expressed by the cells or formed by degradation or could be due to aggregation.

The elevated breakthrough can be caused by the presence of these proteins in the effluent of the ion-exchange column. In other words these truncated versions of Fab' fragments cannot bind effectively to a strong cation exchanger but have the ability to bind to a protein G ligand thus "corrupting" the raw breakthrough curve data.

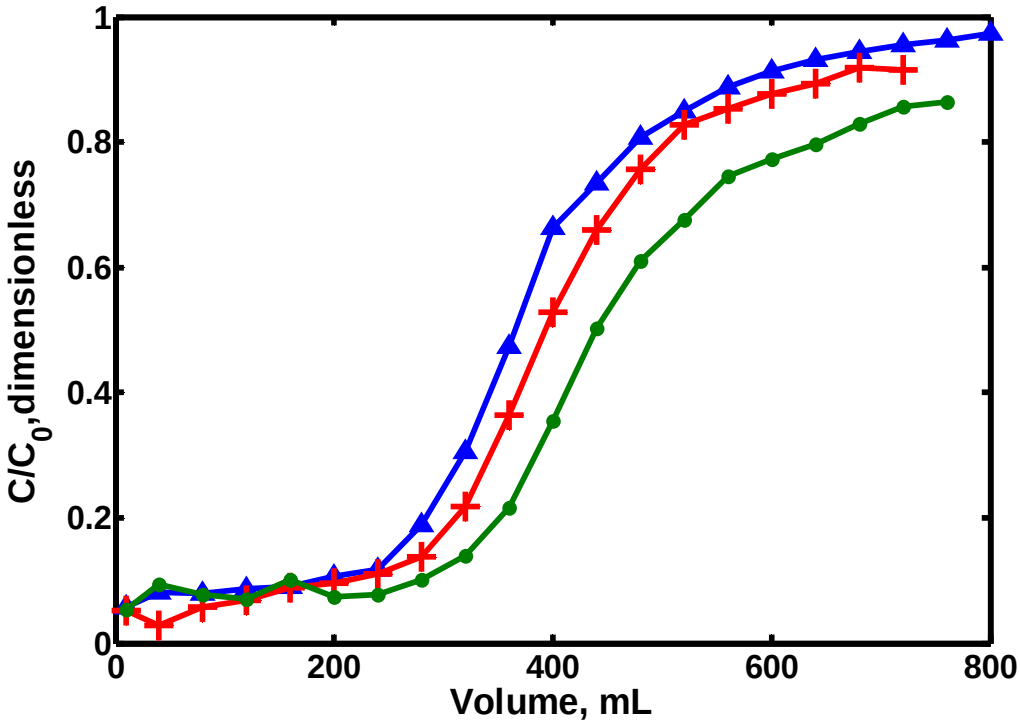

Figure 4.10 Breakthrough curves of Fab' antibody in *E.coli* lysate at pH 5.0 running through a HiTrap 1mL SP Sepharose FF column at (●) 155 cm h^{-1} (1 mL min^{-1}), (+) 232 cm h^{-1} (1.5 mL min^{-1}) and (▲) 300 cm h^{-1} (2 mL min^{-1}).

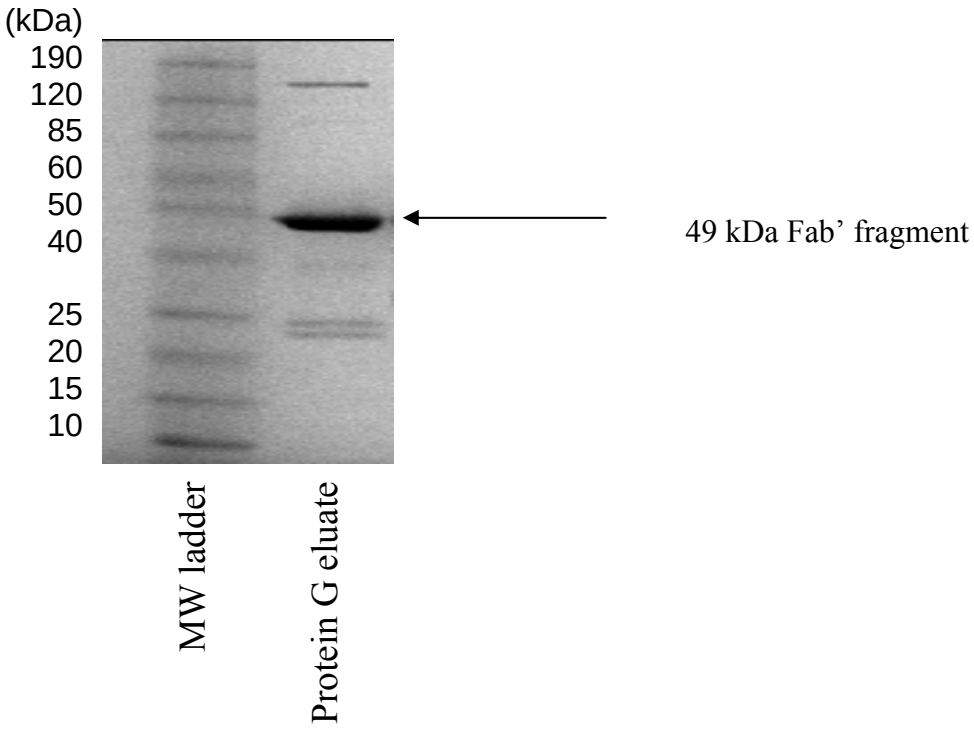

Figure 4.11 SDS-PAGE image illustrating the composition of eluate from a protein G column loaded with *E.coli* Fab' lysate. Lane 1 is the protein molecular weight ladder while lane 2 is the eluate from the protein G column.

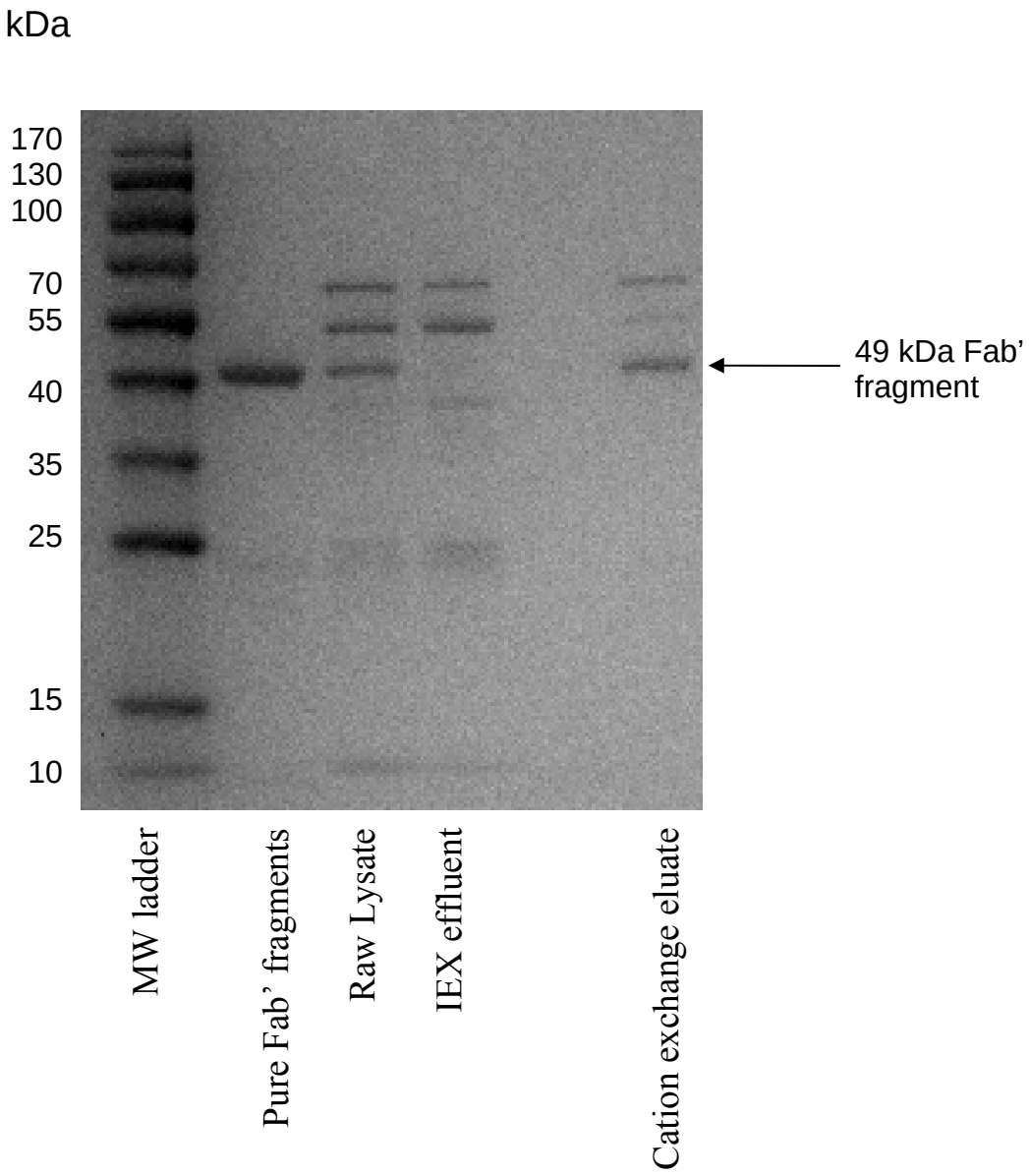

Figure 4.12 SDS-PAGE study of Fab' separation from *E.coli* lysate using with SP Sepharose FF strong cation exchange resin.

From the SDS-Page in fig.4.12 the Fab' fragment band represented by the 49 kDa band is absent from the cation exchange effluent. The only explanation for this is Fab' fragments were adsorbed by the cation exchange resin. If Fab' fragments were absent from the initial flow through materials from the column, the detected peak from the protein G assay can be due to the presence of truncated Fab' fragments, since Fab' fragments are the only IgG components expressed by the strain of *E.coli* used. This is proved by figure 4.11, showing the species of protein that the protein G assay can detect in *E.coli* lysate. For the above reason, it is suggested that the elevated breakthrough obtained using protein G assay method is an artefact. There are seven main species of protein present in the *E.coli* lysate (figure 4.12. lane 3) and only three species of proteins present in the eluate. Cation exchange chromatography not only serves as a primary capture step in this system, but also has the ability to remove truncated versions of Fab' fragments of a smaller molecular weight and some contaminant proteins of a higher molecular weight.

Because the breakthrough curves shown in figure 4.10 include the breakthrough of another species of protein, a strategy to eliminate the assay artefact from the experimental data needs to be developed to bring the baseline down to zero.

To bring the baseline of the breakthrough curves to zero, the following logic was used:

Assume that $\frac{C}{C_0}$ is the breakthrough of Fab' fragments and truncated/aggregated version of Fab' fragments measured from the protein G assay.

Let $\frac{P}{P_0}$ be the actual Fab' fragment breakthrough at any given time.

P is the concentration of Fab' fragment flowing through the column and

P_0 is the total Fab' in the sample.

The actual breakthrough of Fab' fragments (P) is the difference between the measured amount of Fab' fragments and the amount of truncated/aggregated Fab' fragments (a);

$P = C-a$; $P_0 = C_0 - a$

Combining the equations;

$$\frac{P}{P_0} = \frac{C-a}{C_0-a} \tag{5}$$

or writing in terms of the breakthrough curve

$$\frac{P}{P_0} = \frac{1}{1-a}\left(\frac{C}{C_0} - a\right) \tag{6}$$

For the system used in this project there were 10 % impurities in the sample therefore $a = 0.1\ C_0$

$$\frac{P}{P_0} = \frac{1}{0.9}\left(\frac{C}{C_0} - 0.1\right) \tag{7}$$

The strategy described above was applied and the results are shown in figure 4.13. Breakthrough occurs after 200 mL, 240 mL and 280 mL of feed was being loaded into the column at 2 mLmin^{-1}, 1.5 mL min^{-1} and 1 mL min^{-1} respectively. The corresponding linear velocities are 310 cm h^{-1}, 232 cm h^{-1} and 155 cm h^{-1} respectively. Unlike breakthrough curves of pure proteins, the binding capacities are not the same at different flowrates, in other words the area above curves are not identical across different flowrates.

From the breakthrough curves, binding capacities increase when linear velocity decreases. In addition, as resin-feedstock contact time (loading time) increases, the binding capacities increases. For the same amount of *E.coli* lysate loaded into the column, more Fab' fragments were adsorbed at a slower flowrate compared to a faster flowrate.

The reason behind this phenomenon requires further investigation. The investigation was done in the next chapter with the aid of modelling.

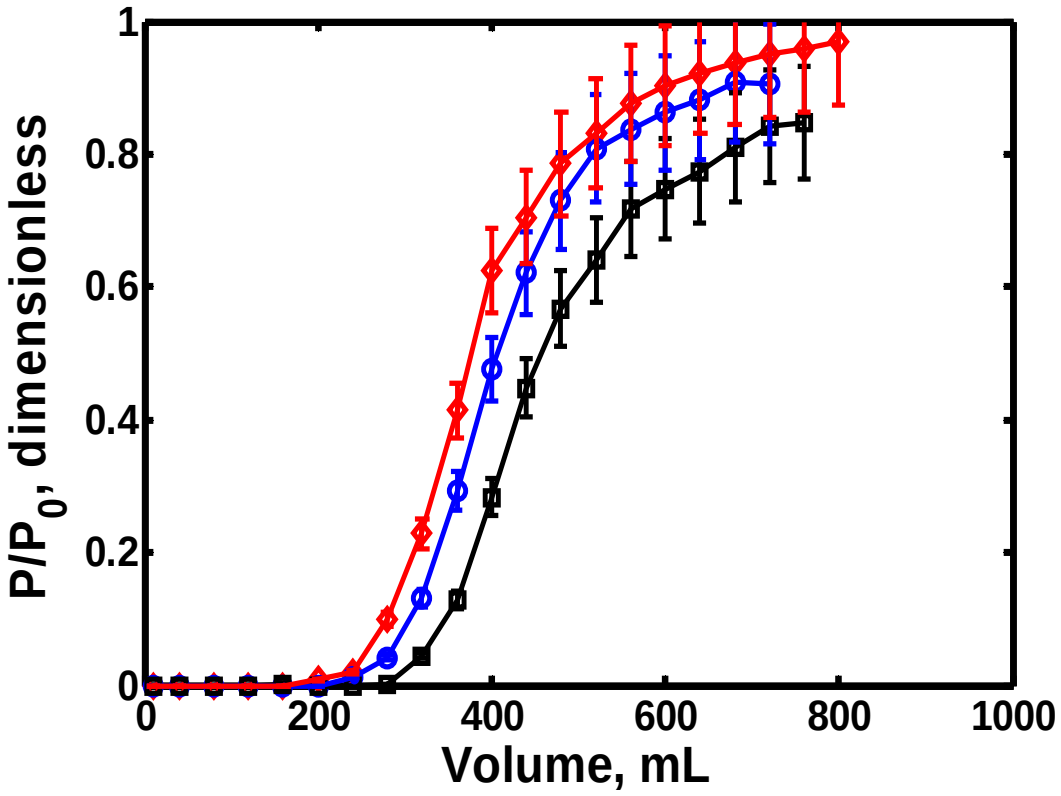

Figure 4.13 Breakthrough curves of Fab' antibody in *E.coli* lysate at pH 5 running through a HiTrap 1mL SP Sepharose FF column at (□) 155 cm h^{-1}, (○) 232 cm h^{-1} and (◊) 310 cm h^{-1}. The breakthrough curves were adjusted to define a baseline, eliminating the assay artefact caused by Fab' like contaminants with the equation 1.7. A line was drawn across the data points to visualise the trend. The error bars are representing a 10% error for all data points obtained.

4.4.2 Micro-scale

In this section, the breakthrough curves obtained using micro tips (PhyNexus Inc, San Jose, USA) will be presented.

The breakthrough curves were obtained using the method described in section 2.5 each set of experiments were repeated three times. In figures 4.14, 4.15 and 4.16, the raw data and the corrected version of the breakthrough curves obtained at 310 cm h^{-1}, 232 cm h^{-1} and 155 cm h^{-1} were shown respectively. The mean values for three repeats of each set of data were calculated and are shown in figure 4.17.

Constant linear flowrate was chosen as the scale-up strategy. With the liquid flowing speed around the beads remained unchanged, the adsorption of Fab' fragments on the resin particles can be compared at a different scale, in addition this strategy reduces the time required to obtain the experimental breakthrough curves. Whereas if the residence time is constant, the running flowrate will be slower for a shorter column, in this case below 100 cm h^{-1}, a flowrate that is slower than recommended for use with columns at industrial scale.

From figure 4.14, the breakthrough curves show similar trends compared to HiTrap breakthrough curves (refer to figure 4.13). This includes the elevated breakthrough baseline and the increased binding capacity when operating at lower flowrates.

To compare the millitre-scale and micro-scale breakthrough curves, instead of plotting concentration ratio against loading volume, the concentration ratio was plotted against column volume (figure 4.15). By plotting the breakthrough curves in such manner, column sizes are taken into account as it not only it nullifies the effects of scale difference in both sets of experimental data it also allows the comparison between adsorption of Fab' fragments onto the columns with different geometries.

From figure 4.15, the breakthrough curves obtained using micro-scale tips are less sharp compared to millilitre-scale column experimental data, in other words the dynamic binding capacities are different across different scales for identical linear velocities. This

trend is observed when feed residence time in the column decreases, in this case at 155 cm h^{-1} the feed residence times for a 1 mL HiTrap and 40 µL PhyNexus tip are 60 seconds and 19 seconds respectively. Although the shapes of the breakthrough curves at both scales are different, the maximum binding capacity should remain the same at the same linear velocities for this system and the experimental results are supporting this theory. A more detailed analysis of the maximum binding capacities will be presented in the next chapter.

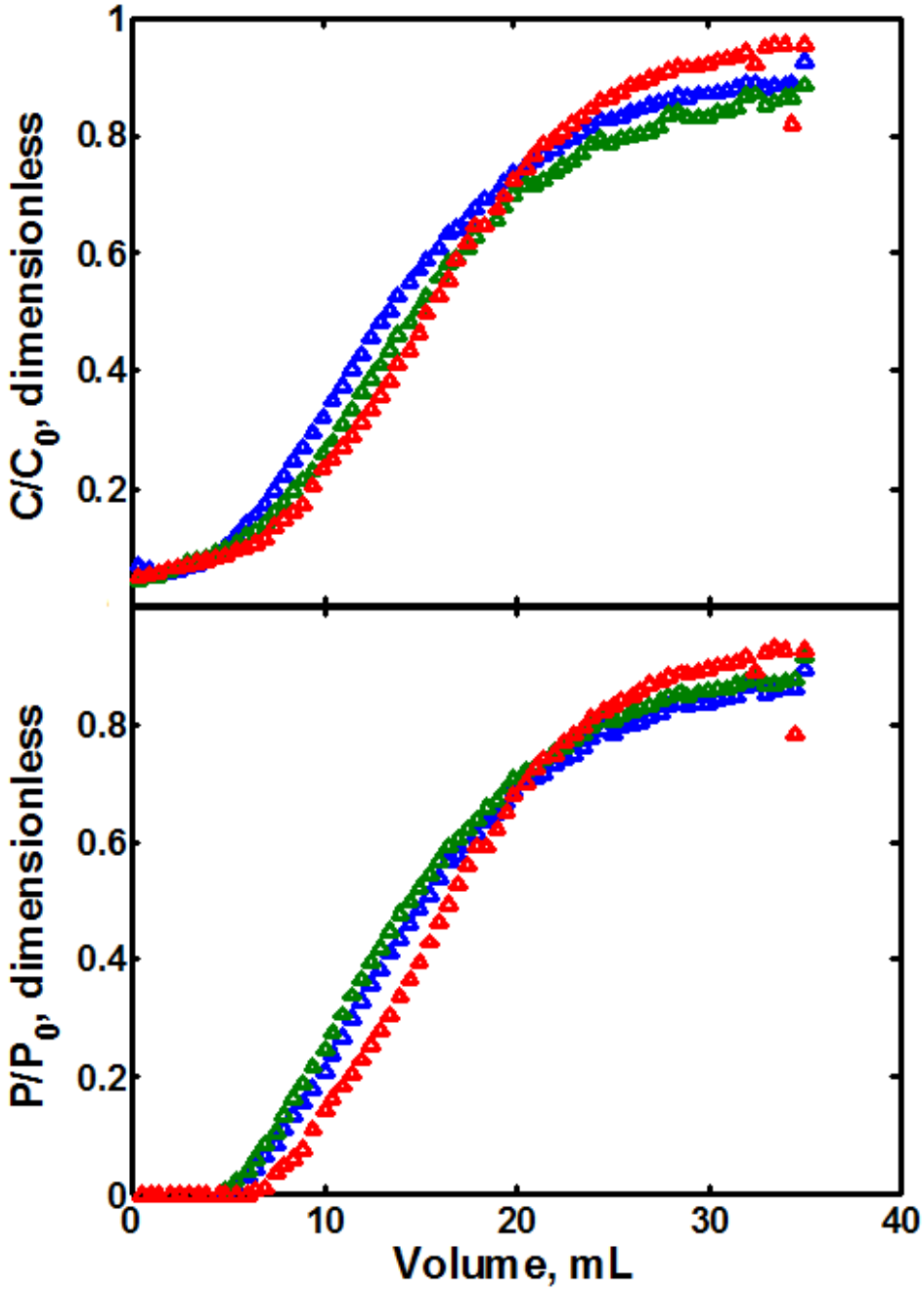

Figure 4.14 Breakthrough curves of Fab' antibody in *E.coli* lysate at pH 5 running through a 40 µL PhyNexus microtip at 310 cm h^{-1}. The raw data is shown in the top graph (a) while the adjusted breakthrough curves are shown in the bottom graph (b). The breakthrough curves were adjusted to define a baseline, eliminating the assay artefact caused by Fab' like contaminants with the equation 1.7.

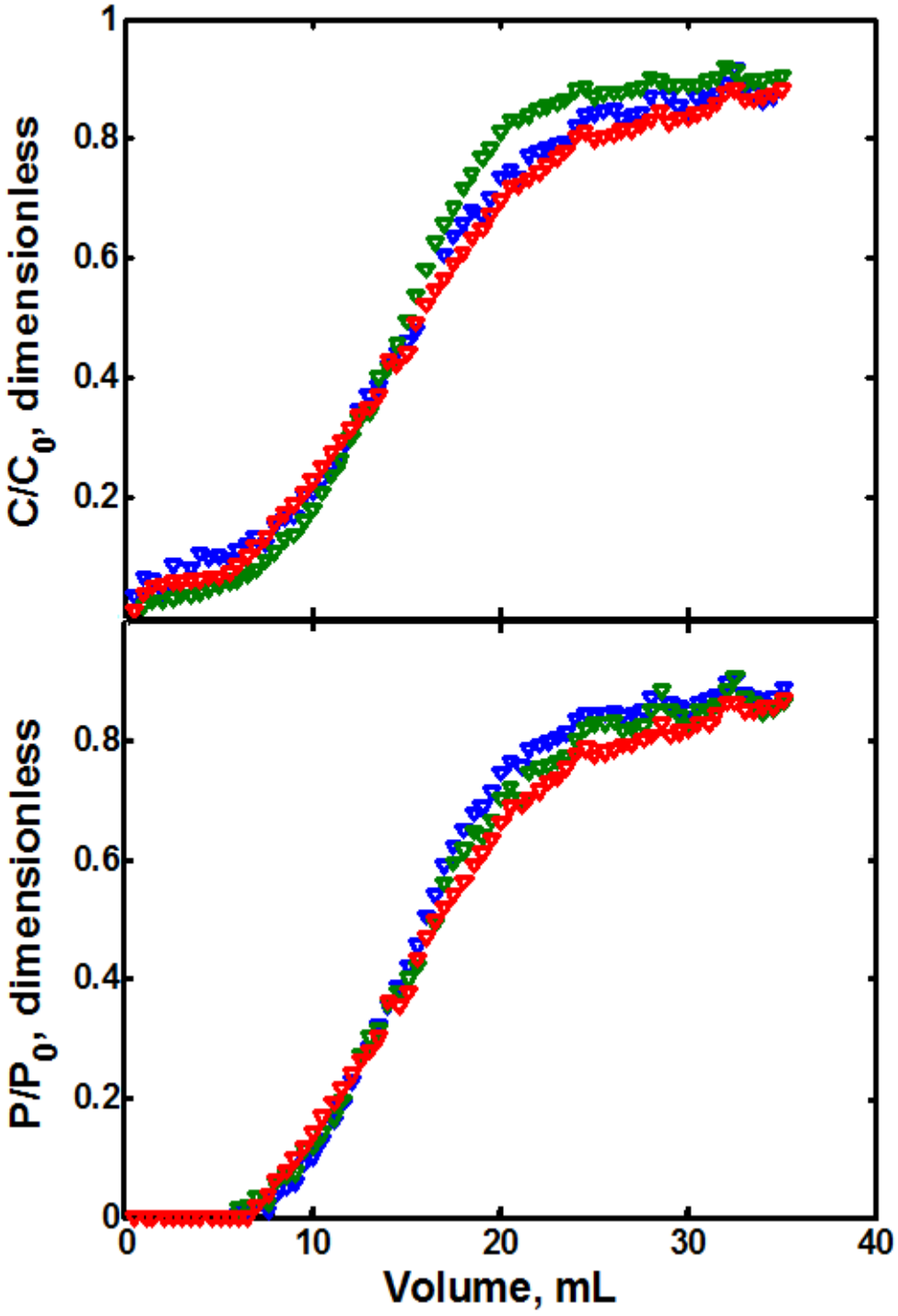

Figure 4.15 Breakthrough curves of Fab' antibody in *E.coli* lysate at pH 5 running through a 40 µL PhyNexus microtip at 232 cm h^{-1}. The raw data is shown in the top graph while the adjusted breakthrough curves are shown in the bottom graph (b). The breakthrough curves were adjusted to define a baseline, eliminating the assay artefact caused by Fab' like contaminants with the equation 1.7.

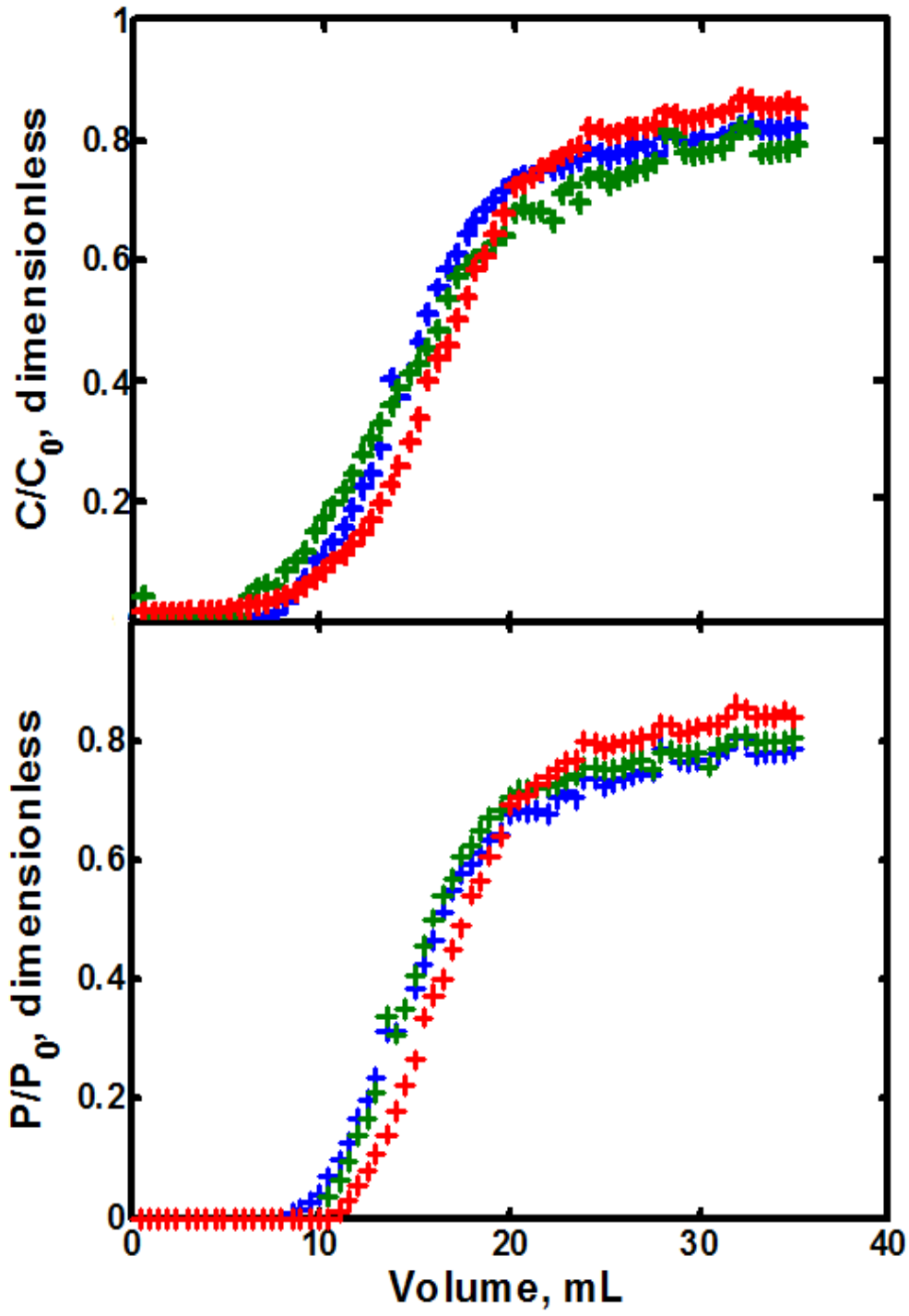

Figure 4.16 Breakthrough curves of Fab' antibody in *E.coli* lysate at pH 5 running through a 40µL PhyNexus microtip at 155 cmh^{-1}. The raw data is shown in the top graph while the adjusted breakthrough curves are shown in the bottom graph (b). The breakthrough curves were adjusted to define a baseline, eliminating the assay artefact caused by Fab' like contaminants with the equation 1.7.

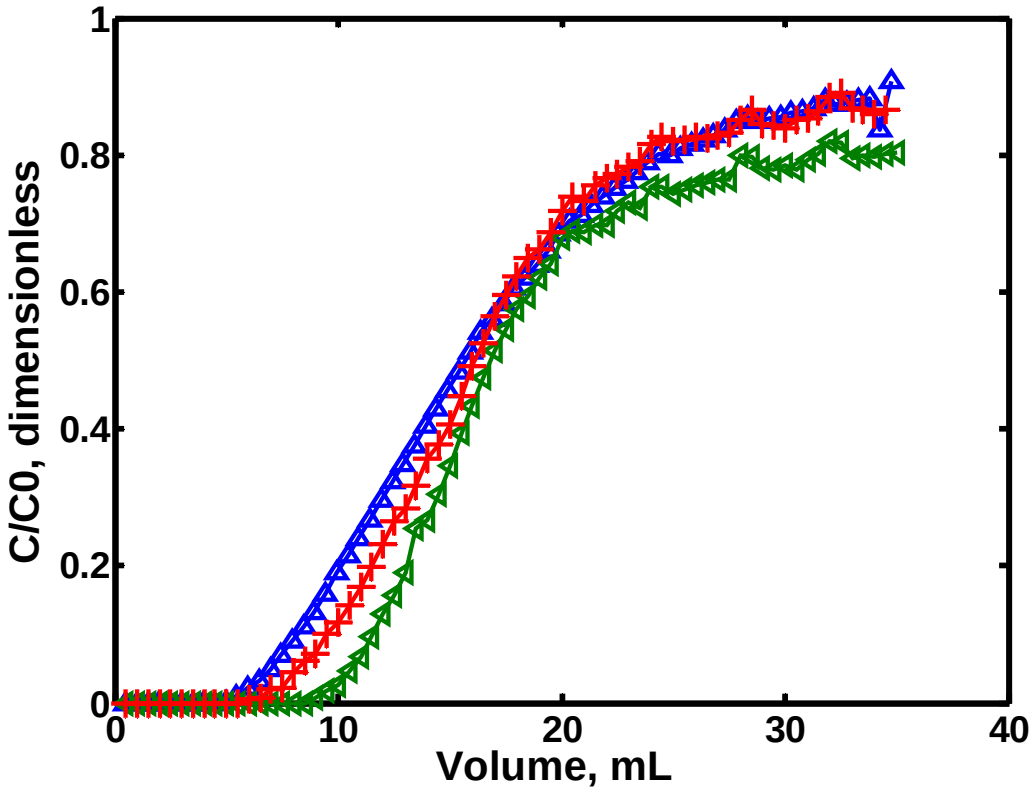

Figure 4.17 Breakthrough curves of Fab' antibody in *E.coli* lysate at pH 5 running through a 40 µL PhyNexus microtip with SP Sepharose FF resin at (△) 310 cm h^{-1}, (+) 232 cm h^{-1} and (◁) 310 cm h^{1}. The data points represent the mean value of data points of three repeats.

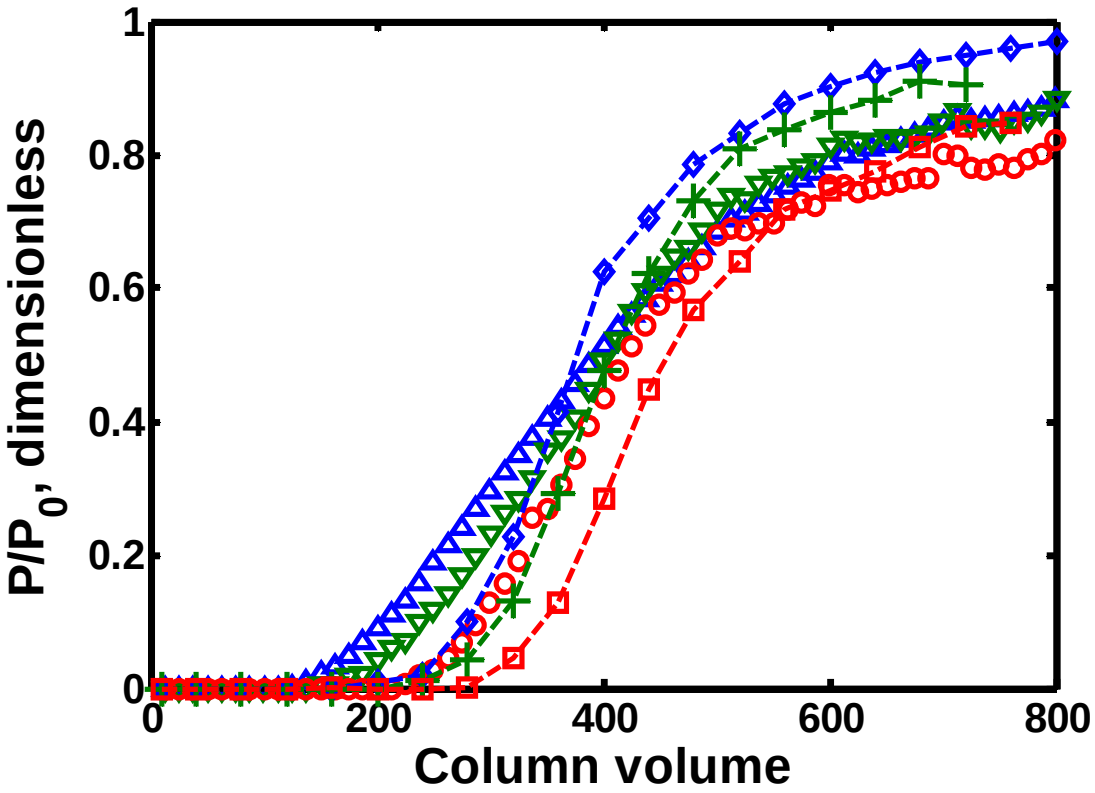

Figure 4.18 Comparison between breakthrough curves of Fab' antibody in *E.coli* lysate at pH 5 running through a 40 µL PhyNexus microtip and 1 mL HiTrap column with SP Sepharose FF resin. The breakthrough curves were obtained at 310 cm h^{-1}(blue), 232 cm h^{-1}(green) and 155 cm h^{-1}(red). Millilitre scale are represented by (□) (+) and (◊) while micro-scale data are shown as (○) (▽) and (△).

4.6 Conclusion – Experimental results

An assay technique was developed and the error of the assessed as around 5%. The feedstock conditions were examined and the operating edge was identified. The adsorption of Fab' fragments onto SP Sepharose FF strong cation exchange resin is strongest at pH 5, below pH 5 a significant amount of Fab' in the feedstock will be precipitated. Although at a lower pH value the net charge of the Fab' fragments in the feedstock is stronger, the major loss of Fab' fragments below pH 5 suggested that pH 5 is the lowest achievable pH for this system.

The condition identified was used to obtain breakthrough curves at millilitre-scale using 1 mL HiTrap columns and at micro-scale using 40 μL PhyNexus micro-tips. A strategy was developed to bring the elevated baseline of the breakthrough curves down to zero. The elevation of the breakthrough curves were caused by the assay over-estimating the amount of Fab' fragments due to the presence of truncated/aggregated versions of Fab' fragments; it appears that 10% of the detected Fab' fragments from the assay are truncated/aggregate Fab' fragments.

The ability of the system to serve as a primary capture step was also investigated. Not only does the system have the ability to capture Fab' fragments efficiently, it also has the ability to separate some of the truncated versions of Fab' fragments. This capability is observed through the SDS page image (Figure 4.12) obtained; in the analysis two protein species of a smaller molecular weight (around 25 kDa) are absent from the eluate (lane 5); the same proteins species were observed from Protein A eluate (Figure 4.11) meaning that these small molecular weight proteins are in fact truncated versions of Fab' fragments.

In the next chapter, the breakthrough curves at millilitre-scale and micro-scale will be used to gain a further understanding of chromatography; translating the description of the adsorption system into mathematical relationships by considering the physical processes in the column in terms of the diffusion and mass transfer constants.

5. Results II - Modelling

5.1. Introduction

In this chapter attempts will be made to translate chromatographic performance into mathematical terms using the general rate model both at 1 mL scale and at 40 μL scale. The breakthrough curves obtained from chapter 4 were used throughout the chapter.

At 1 mL scale, one experimental breakthrough curve will be used to calculate parameters best representing the chromatographic system. The calculated parameters will then be used to predict breakthrough curves of a different flow rate. The accuracy of the model will be determined by the agreement between the prediction and the experimental data. A strategy was created to modify the general rate model to include theoretical assumptions.

At 40 μL scale, the modified general rate model was tested to confirm the accuracy of the model moreover to establish a link between the micro-scale and millilitre –scale. The ultimate aim of the activity is to allow the model to predict breakthrough curves at different flowrates and at different scales.

A guide is provided in the next section to summarise the findings of all the modelling activities. This summary seeks to draw out the most important findings with reference to their location in the main text of the chapter. This is provided because some of the stages of the model development, which necessarily to be abandoned, still provided key insights into the physical effects of the adsorption system.

5.1.1 Reading guide

The aim of this reading guide is to summarise the findings explained in the main text of this chapter in simpler terms. The guide lists out the steps of the development of the model cross references the corresponding sections in the main text where a more detailed explanation is provided together with clues and reasoning behind all the changes made to implement all the findings made into the final developed version of the general rate model.

The breakthrough curve obtained at 310 cm h^{-1} at millilitre-scale was fitted using the general rate model using the isotherm parameters (Q_{max}, K_d and K_{ads}) as the variables. The result of the fitting was unsatisfactory (pg 122-123).

A sensitivity analysis was completed by manually changing the values of mass transfer coefficient (K), bead diffusivity (D_b) and axial diffusivity (D_{ax}). The analysis suggested that mass transfer coefficient and bead diffusivity have the largest impact on the shape of the predicted breakthrough curve (pg 124).

The number of fitted parameters was increased from three to five to also include D_b and k. However the result was still unsatisfactory (pg 128).

The sensitivity analysis was revisited and it was identified that the bead diffusivity could be a function of time. An exponential decay equation as a function of time was added to the general rate model to describe the rate of change of bead diffusivity. The addition of this equation allowed a good fit of breakthrough curves at one flowrate but could not predict breakthrough curves at slower flowrates (pg 130-132).

This equation did not take into account the influence of flowrate on diffusivity. The exponential decay equation was modified to be a function of flowrate and time, in other words of the amount of material loaded onto the column. This version of general rate model can successfully fit and predict breakthrough curves at millilitre-scale (pg 133-

135). Hence the fouling of resin which affects the diffusivity of the Fab' fragments is governed by the total amount of contaminants entering the resin. It seems that this is a rapid process that is controlled by the actual amount loaded onto the column rather than time of exposure.

The model developed was used to fit and predict breakthrough curves at micro-scale. However, while the model can fit and predict breakthrough curves at micro-scale the fitted parameters cannot be transferred to the millilitre-scale. Tests were conducted to examine the effects of bed voidage and bead diffusivity trend to help establish a link between both scales (pg 136 – 144).

The bead diffusivity decay equation was modified to be a function of saturation of beads in the column. The newer version of the model was used to fit and predict millilitre-scale breakthrough curves to verify the model (pg 144-145). This version of the model can fit and predict millilitre-scale. But at micro-scale bed voidage changes as flowrate changes (pg 145-154).

The equation describing bead diffusivity decay was modified to be a function of saturation per layer of resin. This version of the general rate model has the ability to fit and predict breakthrough curves at both scales; in addition it has the ability to predict breakthrough curves at millilitre scale using parameters obtained from micro-scale (pg 155-167).

5.2. Modelling of 1 mL scale data

The modelling uses the breakthrough curves described in chapter 4.4.1obtained using a 1 mL HiTrap column. To translate a breakthrough curve into mathematical terms, the general rate model (refer to chapter 3.2.1 for the model) was used to back calculate the values of the parameters which gave a least square best fit to the experimental breakthrough curve. The fitting of the experimental breakthrough curves was carried out using COMSOL - MATLAB finite element solver. The model iteratively solves for the parameters which best fits the breakthrough data input in a least square sense. The limits of the solving routine were set from 0 to 1000, allowing the model to search freely for a

solution between these limits. The wide limit range was given to test the ability of the model. If the model truly is capable of representing a system in terms of all the physical parameters, the constraints will not affect the output.

The data was first fitted with three parameters, maximum binding capacity Q_{max}, adsorption coefficient K_{ads} and the dissociation constant K_d as solving variables while the rest of the parameters were set to literature values or calculated using empirical correlations (refer to chapter 3.2.4 and 3.2.5 for the parameters). The experimental breakthrough curve obtained at a flow rate of 2 mL min^{-1} experimental data was chosen as the fitted breakthrough curve due to the fact that it is obtained under the fastest flowrate out of the set of data. It is believed that at a faster flowrate feedstock variability caused by prolonged loading is lower compared to the other two breakthrough curves obtained under slower flow rates.

The fitted values are presented in table 5.1. The result of the fitting is compared against the experimental result in figure 5.1. Figure 5.1 also showed that by obtaining the values of the adsorption kinetics alone is not enough to represent the system, it is speculated that other parameters contribute to the shape of the breakthrough curves.

From the results from the previous section (section 5.2), it is shown that the model based on adsorption kinetics is insufficient to represent a chromatography system under complex conditions. The general rate model needs to be modified to address the effects of a multi-component system. In the following sections a study will be carried out to search for the dominating parameters that determine the shape of the breakthrough curves; bead diffusivity, axial dispersion coefficient and mass transfer coefficient are investigated in these sections.

5.2.1. Preliminary test of Sensitive parameter sensitivities

Bead diffusivity, axial dispersion and mass transfer coefficient were investigated; these parameters were chosen because the values used in the previous sections were estimated from literature correlations by assuming the feedstock behaves in the same manner as model proteins or water and it is possible that the values are not applicable for complex

systems. These three parameters were chosen to be investigated because they are most likely to be affected by the binding competition between proteins on the resin particles. The investigation will be done by increasing and decreasing the parameters by two times of the literature values to observe their effects on the overall shape of a breakthrough curve. The adsorption parameters (Q_{max}, K_{ads} and K_d) from table 5.1 were used for all the tests.

Bead diffusivity is defined as the speed of protein travels within the infrastructure of the resin particles. The higher bead diffusivity the faster the adsorption hence delaying breakthrough of Fab' fragments. From figure 5.2a a better match at the lower region of the breakthrough curve is observed. Conversely when bead diffusivity is lowered, Fab' fragments cannot enter the pores of the resin particles efficiently, causing a wider breakthrough curve. From figure 5.2 b, when the bead diffusivity is reduced to half ($3.5e^{-11}$ ms^{-1}) of its original value, a better match can be observed at the upper region of the breakthrough curve but the match is worse at the lower region.

Axial dispersion is defined as fluid movement caused by diffusion and turbulence/convection. In chromatography terms, the higher the axial diffusivity, the greater the zone spreading along the fluid flow direction. This parameter was used to evaluate if flow regime has an effect on the breakthrough curves. From figure 5.2 c, axial dispersion has little effect on the overall shape of the breakthrough curve, and therefore fluid flow pattern is not a dominating factor in this system.

Mass transfer coefficient (k) is defined as the speed of protein travelling from bulk fluid phase to the stagnant film around resin particles. The speed of mass transfer is higher at slower flowrate and lower at faster flowrates. Mass transfer coefficient has slight effect at the lower end of the breakthrough curve (figure 5.2 d) but no observable effect towards the upper end; this suggests that mass transfer of Fab' fragment is fast, the Fab' fragments are congested in the stagnant film of the resin particles waiting to enter the pore.

To conclude the analysis above, bead diffusivity and mass transfer coefficients have the most influence on the shape of the breakthrough curves.

Table 5.1 Adsorption kinetic parameters fitted from the general rate model using the HiTrap experimental breakthrough curve obtained at 2 mL min^{-1}

Q_{max} (mol m^{-3} $_{matrix\ skeleton}$)	K_{ads} (m^3 mol^{-1} s^{-1})	K_d (s^{-1}) (10)$^{-3}$
1.94	4.69	2.78

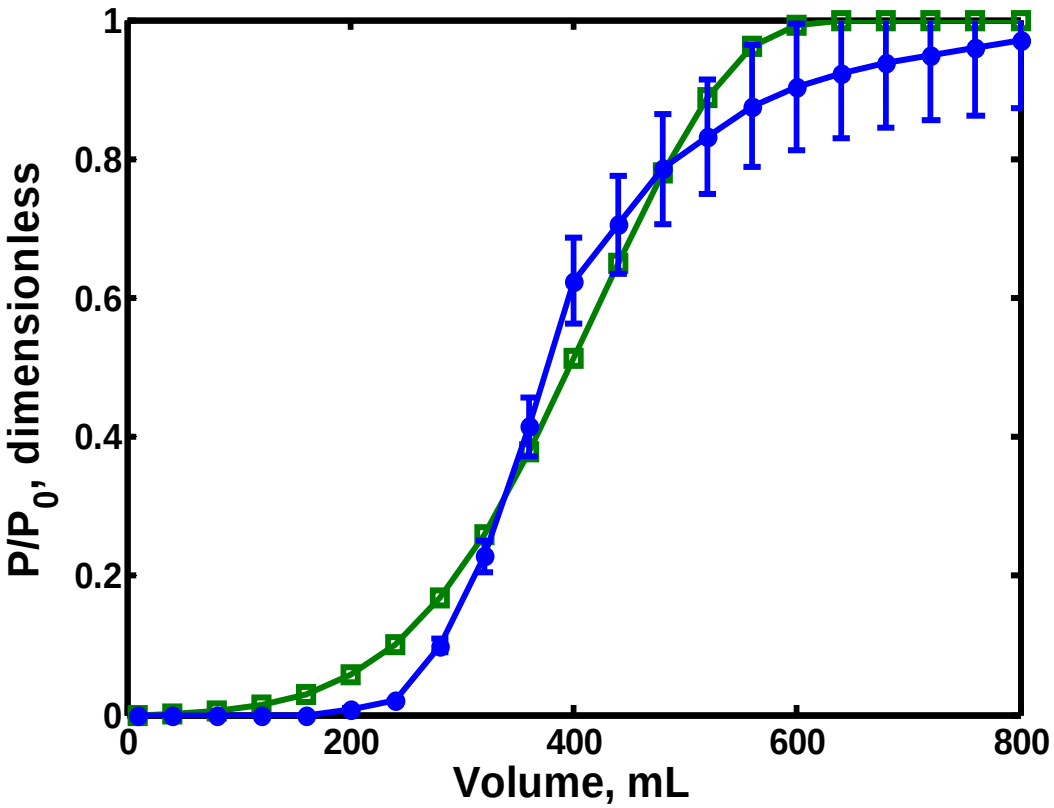

Figure 5.1 Comparison of model fit of the breakthrough curve using three fitted parameters. Q_{max}, K_{ads} and K_{dis} – see table 5.1 and experimental data (-●-) obtained using load rate of 2 mL min^{-1} on a 1 mL HiTrap column. The error bars are based on 10% error of experimental data. A line is drawn across data points to guide the eyes. The R^2 of the fit is 0.987.

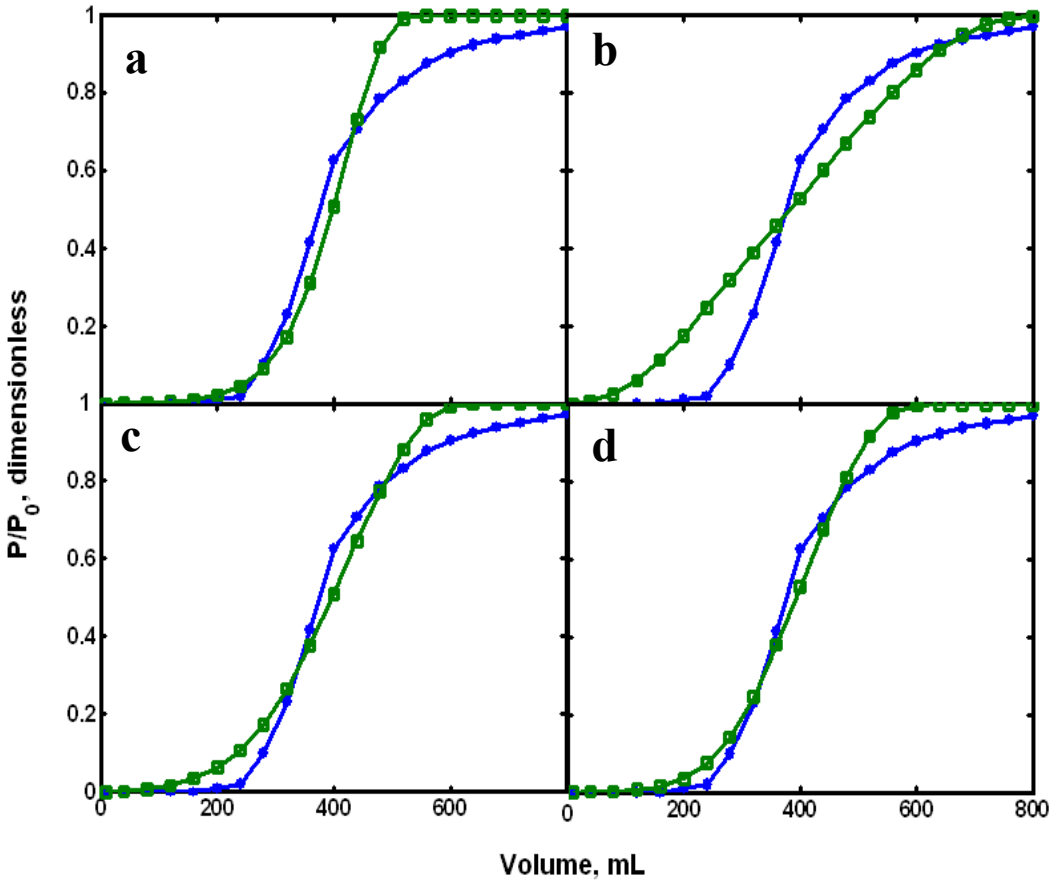

Figure 5.2 Graph showing the effects of bead diffusivity, axial dispersion and mass transfer coefficient on the shape of a breakthrough curve. Calculated (□) and experimental (●) data for 2 mL min^{-1} breakthrough curve with 5 fitted parameters with modifications to bead diffusivity, axial dispersion coefficient and mass transfer coefficient. (Q_{max}, K_{ads}, K_{dis}, D_b and K)

(a) Bead diffusivity value is multiplied by 2
(b) Bead diffusivity value is divided by 2.
(c) Axial dispersion coefficient multiplied by 2.
(d) Mass transfer coefficient is multiplied by 2.

5.2.2 Increasing fitted parameters

With the sensitive parameters identified, the next step is to increase the number of parameters to be fitted by the general rate model. The additional fitted parameters are bead diffusivity (D_b) and mass transfer coefficient (k) and on top of that adsorption kinetic parameters. Bead diffusivity appraises the speed with which Fab' fragments travel within the pores of the resin and also the effect of competition of Fab' fragments with other species of proteins that have similar charges. The mass transfer coefficient accounts for the rate of Fab' fragments enter the film around resin particles.

The fitted parameters are shown in table 5.2 and figure 5.3. The result shows the fitting of the breakthrough curve using five different variables calculated by the model. Comparing figures 5.1 and 5.3, the fitting using five parameters showed a slight improvement but still not significant enough to give a satisfactory fitting. From figures 5.2 (b) and 5.2 (c), a smaller value of bead diffusivity will lead to a better fitting at the top part of the breakthrough curve, while bigger value will lead to a better fitting at the lower end of the breakthrough. This suggests that there is a possibility that bead diffusivity changes as more material was being loaded into the column. Because the data of a full breakthrough curve is being fitted and parameters calculated are fixed values; the progressive loading effect is not included. A solution to solve this problem is to modify the general rate model to include as expression for the bead diffusivity change as the feedstock contact time with the resin increases.

Table 5.2 Parameters fitted from the general rate model using the millilitre-scale experimental breakthrough curve obtained at 2 mL min^{-1}. The five fitted parameters are Q_{max}, K_{ads}, K_d, D_b and K.

Q_{max} (mol m^{-3} $_{matrix\ skeleton}$)	K_{ads} (m^3 mol^{-1} s^{-1})	K_d (s^{-1}) $(10)^{-3}$	D_b (10^{-11})	k (m s^{-1}) (10^{-4})
3.87	0.939	3.88	18.7	15.8

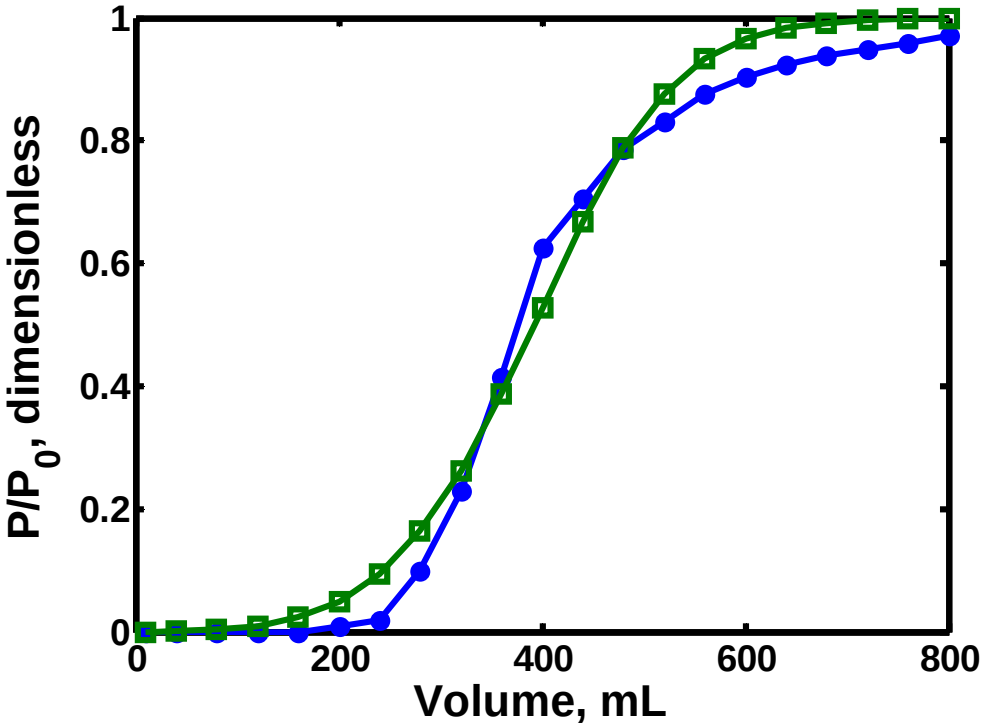

Figure 5.3 Model fitting of experimental breakthrough curve using five fitted parameters (Q_{max}, K_{ads}, K_{dis}, D_b and K). The breakthrough curves were obtained at a loading rate of 2 mL min^{-1} on a 1 mL HiTrap column. Graph showing the (□) fitting and (●) experimental data for the 2 mL min^{-1} breakthrough curve. The R^2 of the fit is 0.987.

5.2.3 Including effects on adsorption during loading

To account for the fact that bead diffusivity decreases as more proteins were being loaded into the column, the bead diffusivity term is expressed as a decay equation (equation 5.1), instead of a fixed value of $7e^{-11}$ ms^{-1} obtained from literature assuming Fab' fragments behave similarly as water.

$$\mathbf{D_b = 7 \times 10^{-11}(e^{-at})} \qquad \mathbf{(5.1)}$$

The equation will account for the bead diffusivity drop as contact time increases; the rate of decrease is determined by variable 'a' - a function of loading time. With this equation added to the general rate model and the number of fitted parameters increased to five - bead diffusivity constant and mass transfer coefficient, (Q_{max}, K_{ads}, K_{dis}, a and K) the fitting of the experimental data greatly improved (refer to table 5.3 for fitted values and fitting from figure 5.4). This suggests that bead diffusivity changes as more material is being loaded into the column. This effect is most likely caused by protein species with charges similar to Fab' fragments; as the beads are more saturated by Fab' fragments and other contaminants, the repulsion force increases hence hindering movement of Fab' fragments into the resin particles and this leads to slower binding.

Table 5.3 Five parameters fitted from the general rate model using the 1 mL scale experimental breakthrough curve obtained at 2 mL min^{-1}. The general rate model has been modified to include bead diffusivity decay over time equation (5.1). The five fitted parameters are Q_{max}, K_{ads}, K_d, a and K.

Q_{max} (mol m^{-3} $_{matrix\ skeleton}$)	K_{ads} (m^3 mol^{-1} s^{-1})	K_d (s^{-1}) (10)$^{-3}$	a (s^{-1}) (10^{-5})	k (m s^{-1}) (10^{-4})
1.81	5.06	0.839	6.54	6.59

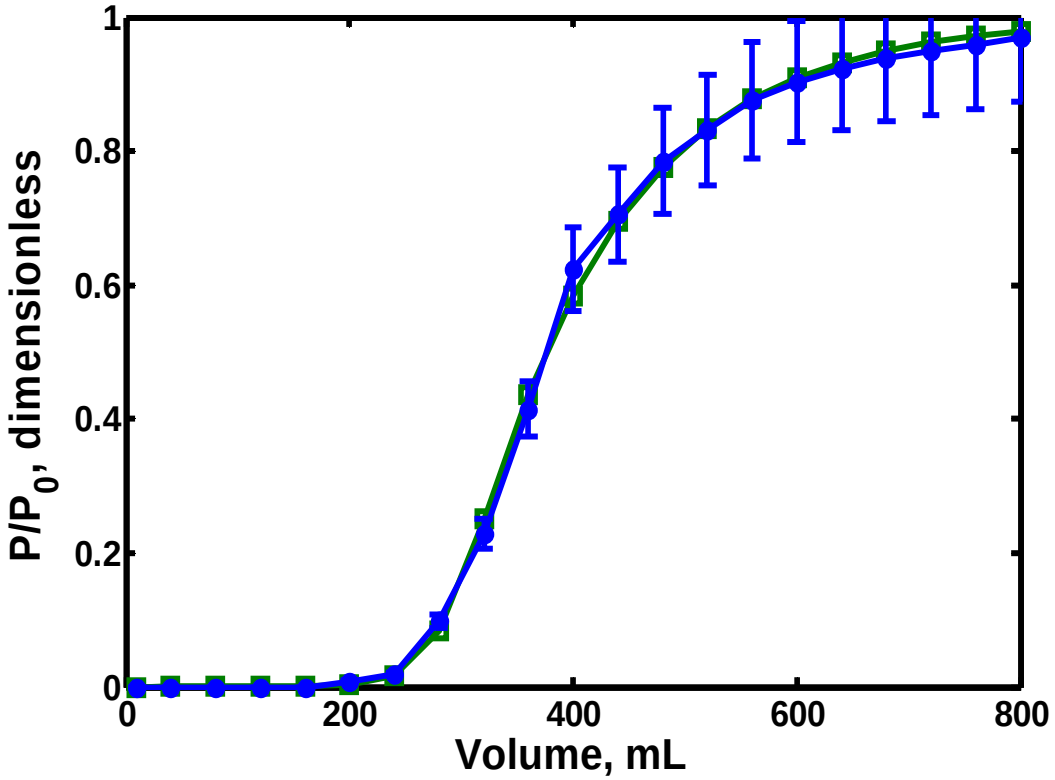

Figure 5.4 Model fitting of experimental breakthrough curve using five fitted parameters and equation 5.1 at 1 mL scale (Q_{max}, K_{ads}, K_{dis}, D_b and K). The experimental data was obtained using a loading rate of 2 mL min^{-1} on a 1 mL HiTrap column. Graph showing the (□) fitting and (●) experimental data for 2 mL min^{-1} breakthrough curve. The R^2 value of the fitting is 0.999.

5.2.4 Using modelling to predict chromatographic performance

A good fitting for a 2 mL min^{-1} (310 cm h^{-1}) breakthrough curve was achieved (refer to figure 5.4) using the diffusivity equation 5.1. The next step is to test the prediction ability of the model using the parameters calculated by the model using one breakthrough curve (refer to table 5.3). Mass transfer coefficient and axial dispersion coefficient change as linear velocity changes, these two parameters were calculated using literature correlations (refer to chapter 3.2.4 and 3.2.5 for the equations). The prediction of 1.5 mL min^{-1} (232 cm h^{-1}) and 1 mL min^{-1} (310 cm h^{-1}) were compared against the experimental data in figures 5.5a and 5.5b respectively.

From figures 5.5a and 5.5b, the predictions of the breakthrough curves are not matching the experimental results. The predicted breakthrough curves deviate from the experimental curves as linear velocity increases, this suggested that flowrate influence is absent in one of the fitted parameters. Assumptions need to be made to improve the prediction ability of the model.

The shape of the breakthrough curve can be altered by changing the adsorption isotherm parameters (Q_{max}, K_d and K_{ads}), but adsorption of protein onto a resin particle is independent of flowrate; by doing so implies that the properties of the resin changes. Changing adsorption kinetic parameters to improve the prediction is far from sensible and will turn the activity into a curve fitting game.

From the previous section (section 5.2.3), we concluded that bead diffusivity decreases as more materials are being loaded into the column. In equation 5.1, bead diffusivity is correlated to time only. If linear velocity changes, the bead diffusivity decay rate will also change because different amount of feedstock will be loaded into the column at a given time. To account for the change of loaded volume, the bead diffusivity decay rate equation is changed to equation 5.2.

$$\mathbf{D_b = 7 \times 10^{-11}(e^{-aQt})} \qquad \mathbf{(5.2)}$$

Bead diffusivity is now a function of feedstock flowrate and time, in other words it is related to the amount of materials loaded into the column. The result of the fitting is shown in figure 5.6a and the fitted results are presented in table 5.4. Predictions of the 1.5 (232 cm h^{-1}) mL min^{-1} and 1 mL min^{-1} (155 cm h^{-1}) are shown in figures 5.6b and 5.6c respectively. The fitting of the 2 mL min^{-1} breakthrough curve is almost perfect while the predictions are showing very good match at the lower end of the breakthrough curves (<50% breakthrough) in both flowrate predictions.

The upper region of the breakthrough curve predictions showed a progressive disagreement when predicting slower flowrates, this might due to the fact that at slower flowrates, protein within the pores of the resin particles have time to rearrange to a more efficient alignment before more Fab' fragments enter the pores. This causes the resin appear to have a higher binding capacity compared to a faster linear velocity. However in the general rate model, this re-arrangement of bound material is not accounted.

The model has the ability to use one single breakthrough curve to obtain the necessary parameters to represent the system. This is done by using the model to calculate parameters for the adsorption system from a breakthrough curve. With the calculated parameters the breakthrough curve of other flowrates can be predicted.

Table 5.4 Five parameters fitted from the general rate model using the 1 mL scale experimental breakthrough curve obtained at 2 mL min^{-1}. The general rate model has been modified to include bead diffusivity decay over time equation (5.2). The five fitted parameters are Q_{max}, K_{ads}, K_d, a and K.

Q_{max} (mol m^{-3} $_{matrix\ skeleton}$)	K_{ads} (m^3 mol^{-1} s^{-1})	K_d (s^{-1}) $(10)^{-3}$	a (10^3) (mL^{-1})	k (m s^{-1}) (10^{-4})
4.84	4.46	0.844	7.12	1.22

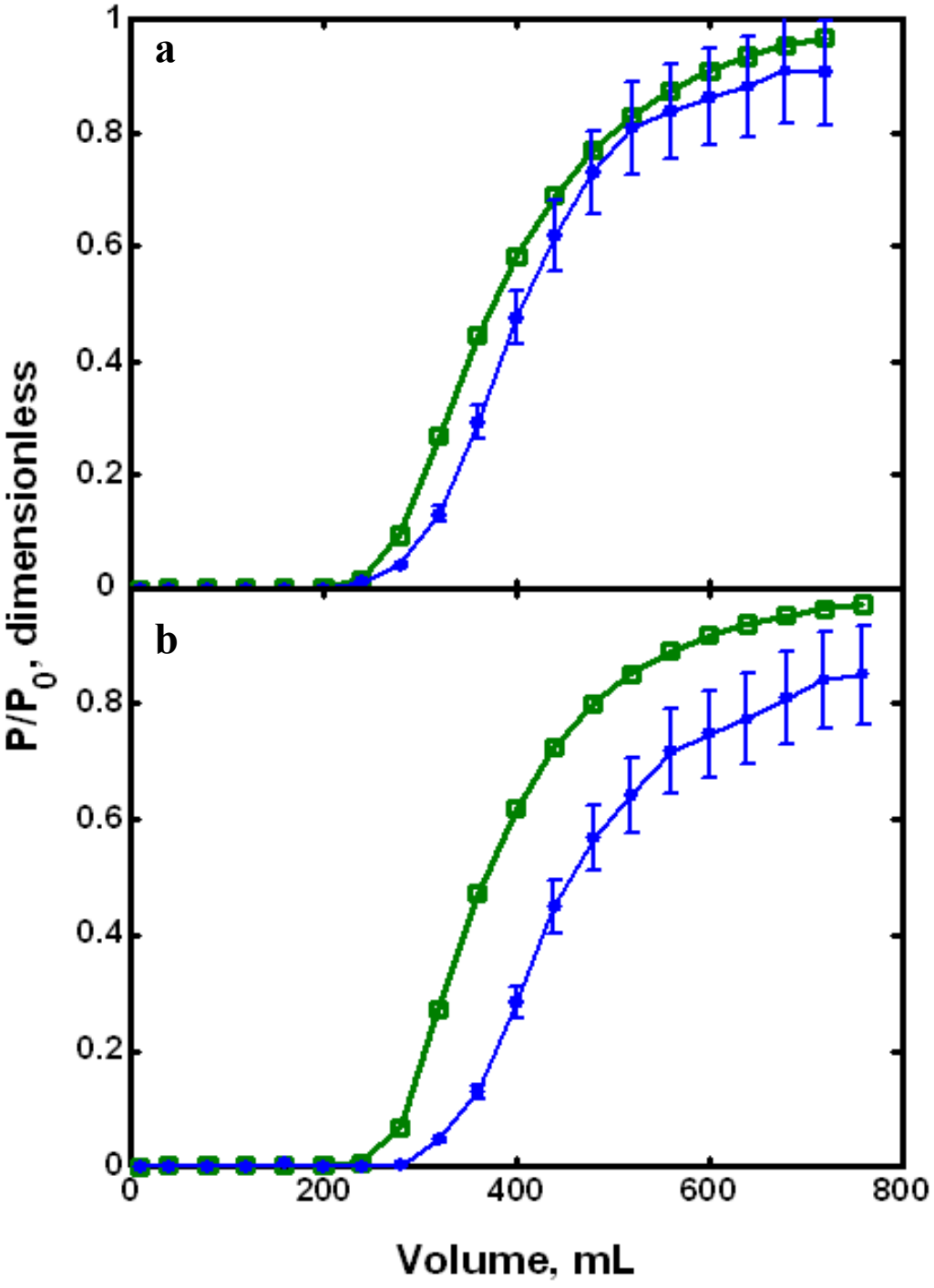

Figure 5.5 Predicted (-□-) breakthrough curves of 232 cm h^{-1} (a) and 155 cm h^{-1} (b) using equation 5.1 (see table 5.3 for values) compared against millilitre-scale experimental data (-●-). The prediction was done by using the parameters obtained by fitting a 310 cm h^{-1} breakthrough curve. The error bars are assuming 10% experimental error from a HiTrap column. The R^2 value for graph a and b are 0.974 and 0.607 respectively.

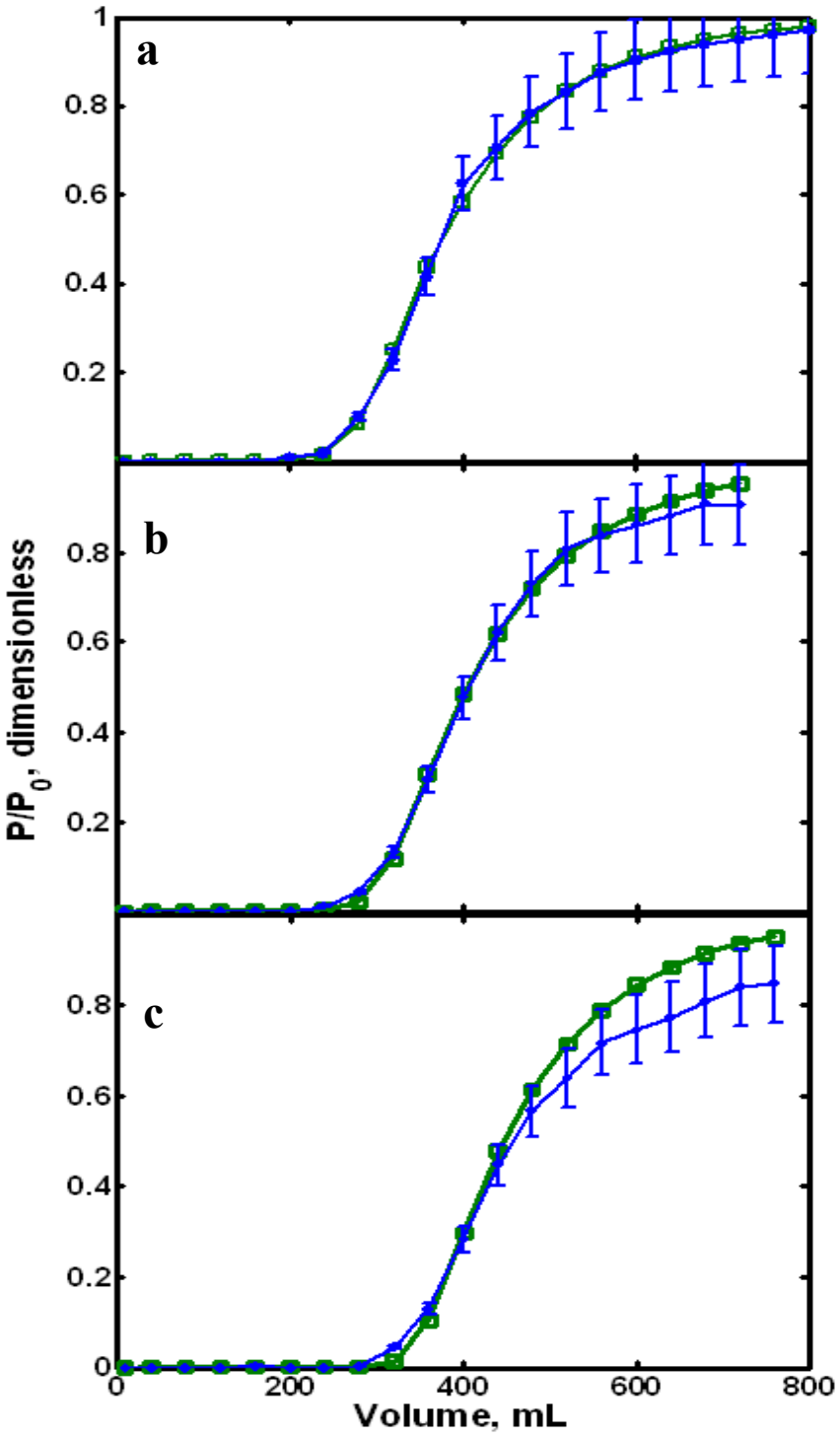

Figure 5.6 Model fitting of 310 cm h^{-1} (a) and predicted (-□-) breakthrough curves of 232 cm h^{-1} (b) and 155 cm h^{-1}(c) using equation 5.2 (see table 5.4 for values) compared against millilitre-scale experimental data (-●-). The prediction was done by using the parameters obtained by fitting a 310 cm h^{-1} breakthrough curve. The error bars are assuming 10% experimental error from a HiTrap column. The R^2 value for graph a, b and c are 0.999, 0.997 and 0.970 (0.983 at 55% breakthrough) respectively.

5.3 40 µL scale

A model that is capable of predicting breakthrough curves across different flowrates for a millilitre-scale column has been developed; the next step is to test the model's ability using 40 µL scale experimental data i.e. to calculate a set of parameters best representing the system and also the ability to predict breakthrough curves at different flowrates and scales.

In this section, the modified general rate model will be used to fit the breakthrough curves obtained at 40 µL scale using PhyNexus microtips. The effects of bed voidage on the adsorption kinetic parameters, the bead diffusivity decay rate will be investigated. The bead diffusivity trends at both scales were investigated to provide opportunities to predict 1 mL scale breakthrough curves using 40 µL scale experimental data.

5.3.1 Calculating parameters using general rate model

The breakthrough curve obtained using the fastest linear velocity (310 cm h^{-1}) was used to solve for adsorption parameters. The result of the calculation is shown in table. 5.5.

The simulations of the fitted parameters are shown in figure 5.7. Although the fittings are showing agreements with the experimental data, the values obtained are not agreeing with parameters calculated using 1 mL scale experimental data. Theoretically for the same feedstock Q_{max}, K_{ads} and K_d should be the same regardless of column size and linear velocity.

It is observed that the PhyNexus tips are less densely packed compared to a HiTrap column; increasing running flowrate will cause the bed to compress, therefore the effect of packing was investigated to determine if the adsorption parameters will agree with the 1 mL scale values.

In table 5.6, the calculated parameters were shown, however as the bed voidage increases, the fitting and predictions (figure 5.8) showed no improvements, more importantly the adsorption parameters were not agreeing with 1 mL scale data.

Bed voidage directly affects the fitted results of the adsorption parameters; because the void fraction represents the number of binding sites available for adsorption. Once the correct voidage is defined, the fitted adsorption parameters can be accurately determined. The adsorption parameters maximum binding capacity, adsorption rate and desorption rate (Q_{max}, K_{ads} and K_d) are expressed in terms of dry resin weight, in other words the set of parameters are resin specific and can be applied to different columns with different packing conditions. To further investigate the effect of packing on the breakthrough curves, the bed voidage was set to be one of the fitted parameters, increasing the number of fitted values to six (table 5.7).

From the simulations (figures 5.9) the fitting and the predictions of different breakthrough curves are showing good matches with the experimental data. As voidage decreases maximum binding capacity Q_{max} decreases, however, adsorption rate (K_{ads}) and desorption rate (K_d) values are changing, which should not be the case since these two values are resin specific and are also independent to number of binding sites available. The rate of protein adsorbed on to the matrix should be the same in any case, given that the resin and the feed conditions are the same.

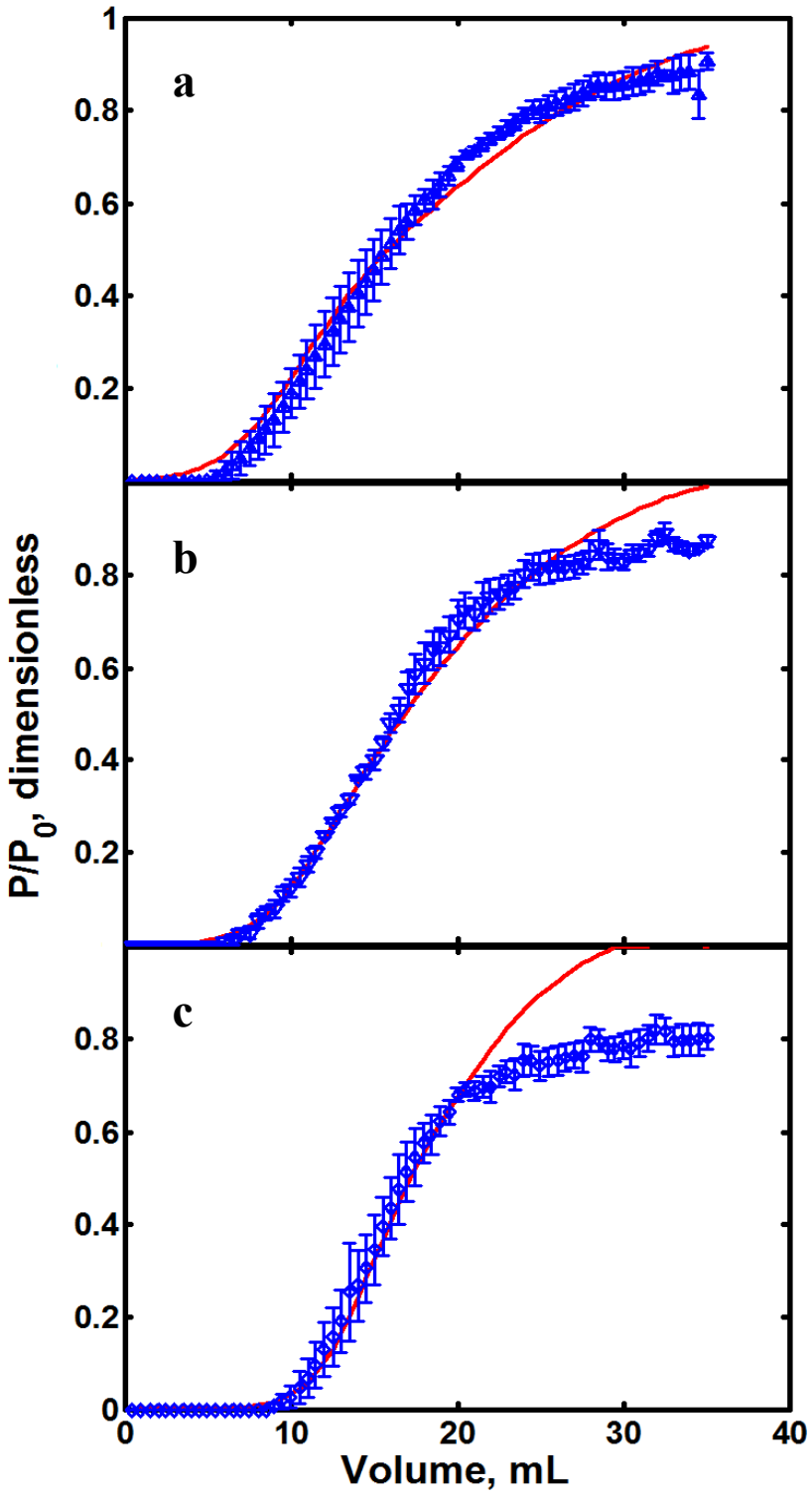

Figure 5.7 Model fitting (-)of 310 cm h^{-1} (a) breakthrough curves of 232 cm h^{-1} (b) and 155 cm h^{-1} (c) using equation 5.2 (see table 5.4 for values) compared against 40 µL scale experimental data (◊). The prediction was done by using the parameters obtained by fitting a 310 cm h^{-1} breakthrough curve. The error bars on the experimental data represent the standard deviation of three repeats. The R^2 value for graph a, b and c are 0.990, 0.979 and 0.900 respectively.

Table 5.5 Parameters iteratively calculated by the same general rate model used for the 1 mL scale experimental data and equation 5.2. Bed voidage was kept at 0.35.

Q_{max} (mol m^{-3} matrix skeleton)	K_{ads} (m^3 mol^{-1} s^{-1})	K_d (s^{-1}) $(10)^{-3}$	Constant a (10^3) (mL^{-1})	k (m s^{-1}) $(10)^{-4}$
1.48	4.66	0.036	14.075	6.91

Table 5.6 Parameters iteratively calculated by the same general rate model used for the millilitre-scale experimental data using equation 5.2, with the bed voidage set to 0.45.

Q_{max} (mol m^{-3} matrix skeleton)	K_{ads} (m^3 mol^{-1} s^{-1})	K_d (s^{-1}) $(10)^{-3}$	Constant a (10^3)	k (m s^{-1}) $(10)^{-4}$
1.75	7.75	0.19	4.92	10.9

Table 5.7 Parameters iteratively calculated by the modified general rate model fitting for six different parameters and equation 5.2. Bed voidage (ε_b), maximum binding capcity (Q_{max}), adsorption rate (K_{ads}), desorption rate (K_d), bead diffusivty constant (a) and mass transfer coefficient (k).

Voidage (ε_b)	Q_{max} (mol m^{-3} matrix skeleton)	K_{ads} (m^3 mol^{-1} s^{-1})	K_d (s^{-1}) $(10)^{-3}$	Constant a (10^3)	k (m s^{-1}) $(10)^{4}$
0.1	1.19	3.3	0.54	51	3.4

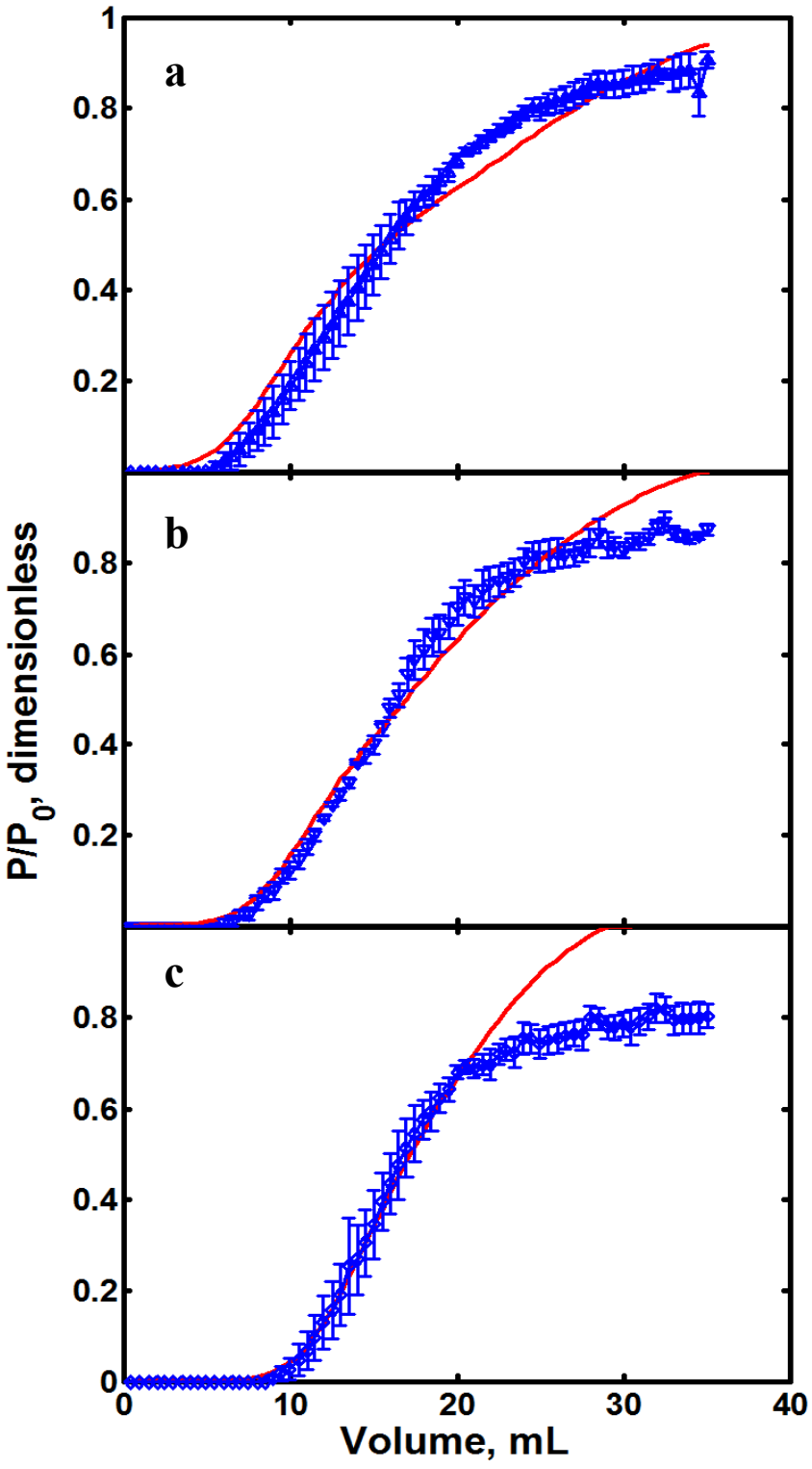

Figure 5.8 Model fitting (-) of 310 cm h^{-1} (a) breakthrough curves of 232 cm h^{-1} (b) and 155 cm h^{-1} (c) using equation 5.2 and with bed voidage set at 0.45 (see table 5.6 for values) compared against 40 µL scale experimental data (◊). The error bars on the experimental data represent the standard deviation of three repeats. The R^2 value for graph a, b and c are 0.990, 0.979 and 0.900 respectively

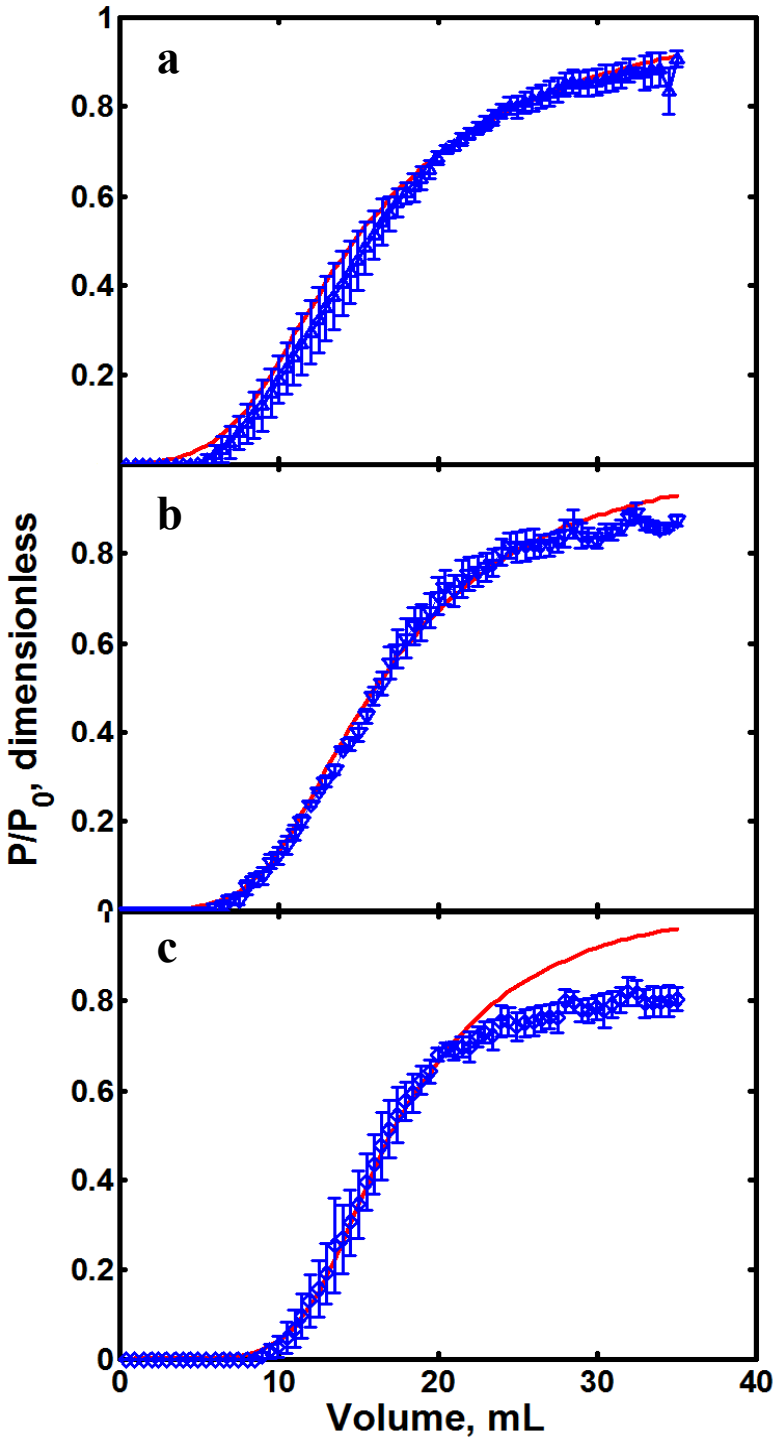

Figure 5.9 Model fitting of 310 cm h^{-1}(a) and predicted (-) breakthrough curves of 232 cm h^{-1} (b) and 155 cm h^{-1}(c) using equation 5.2 (see table 5.7 for values) compared against 40 µL scale experimental data (◊). The prediction was done by using the parameters obtained by fitting a 310 mL cm h^{-1} breakthrough curve with six variables. The error bars on the experimental data represent the standard deviation of three repeats. The R^2 value for graph a, b and c are 0.992, 0.994 and 0.953 respectively.

The ultimate goal of the model is to predict breakthrough curves across different scale; therefore its scale up ability needs to be investigated before we can conclude that the model is completed. Assuming the adsorption parameters (Q_{max}, K_{ads} and K_d), bead diffusivity profile and mass transfer coefficient remain unchanged for a larger chromatography column, the parameters obtained at a smaller-scale should be applicable to a larger scale and vice versa. However according to the prediction in figure 5.10, the parameters did not serve the purpose of representing the adsorption of Fab' fragments onto the matrix, hence there is a mismatch between predicted and experimental breakthrough curves at a different scale.

Judging by the C/C_0 vs column volume plot (Chapter 4.4.2 figure 4.15) the breakthrough curves are quite similar regardless of the fact that the 40 μL scale breakthrough curves are less sharp compared to the 1 mL scale; the breakthrough curves should give similar Q_{max} values, however from the fitting of the general rate model this was not the case. From the 1 mL scale experimental data, the fitted Q_{max} was 4.84 mol m^{-3}(56 $mg_{fab'}$ mL^{-1}) whereas using the same curve fitting routine the result for the 40 μL scale experimental data, the Q_{max} is 1.19 mol m^{-3} (13.7 $mg_{fab'}$ mL^{-1}). This suggests that the model does not have the ability to accurately relate adsorption to column size. Further investigation in the model needs to be done to improve the scalability of the model.

The first parameter investigated was the bead diffusivity-the decay equation introduced to relate bead diffusivity to volume of feedstock loaded. As the column size decreases, the amount of feed required to saturate the column decreases in other words the time required to bring the breakthrough curve up to full saturation will decrease. If the bead diffusivity constant 'a' remains the same at all scales, the different loading volume will alter the bead diffusivity profile due to the nature of the equation. Figure 5.11 the bead diffusivity trend at 1 mL and 40 μL scale is presented. In the graph it is assumed that the 40 μL scale breakthrough curve has the same bead diffusivity constant and adsorption parameters as the 1 mL scale breakthrough curve. The trend of the bead diffusivity at 40 μL scale is different from the 1 mL scale; this implies that the resin particles behave differently in micro- scale, but this cannot be true for an identical system running at the same linear velocity.

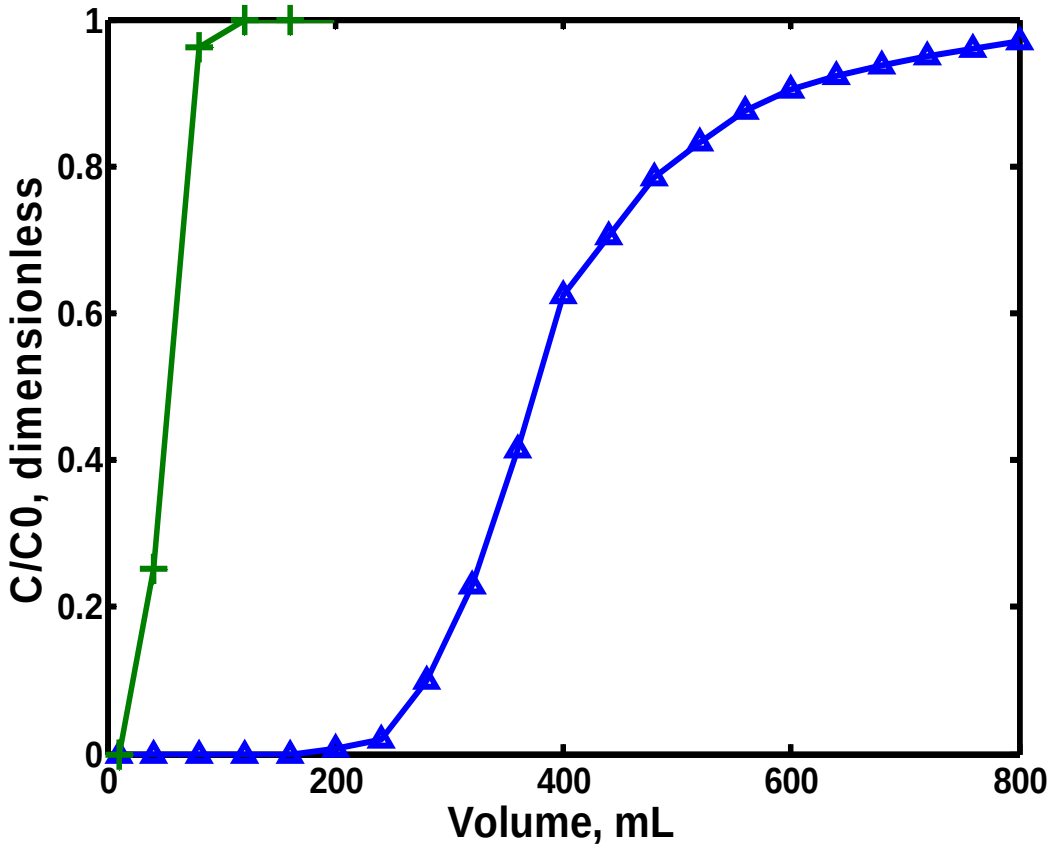

Figure 5.10 Scale up prediction of a 1 mL scale breakthrough curve running at 310 cm h^{-1} using parameters obtained from 40 µL scale running at the same linear velocity with equation 5.2. (+) is the predicted breakthrough curve and (▲) is the experimental breakthrough curve.

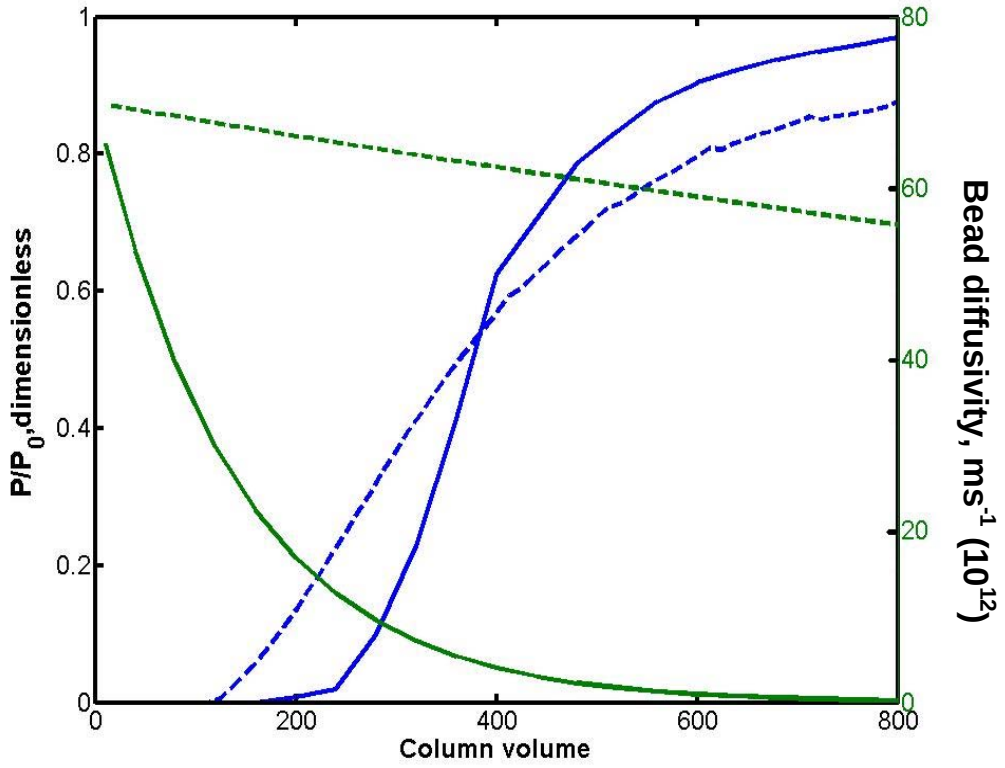

Figure 5.11 A comparison between breakthrough curves and bead diffusivity at 1 mL and 40 µL scale using the equation $D_b = 7x10^{-11} e^{(-aQT)}$. 40 µL scale breakthrough curve is compared against the bead diffusivity (---) and the same comparison method was used on the millilitre-scale data (-). The values for 'a (bead diffusivity constant)' were set at 7.12 x 10^3 at both scales.

5.4 Bead diffusivity as a function of bead saturation

To alleviate this problem the bead diffusivity equation was altered to correlate bead diffusivity to the amount of materials loaded per volume of resin beads, in other words the bead diffusivity is correlated to the saturation of the beads.

$$D_b = 7 x10^{-11} e^{\frac{-aQT}{(1-\varepsilon_b)(\pi r_c^2 h)}} \qquad (5.3)$$

Because the equation is altered, the 1 mL scale data was fitted again using this new correlation to ensure the assumptions made are still valid. The fitted results are shown in table 5.8. The simulations and predictions of the 1 mL scale breakthrough curves are presented in figures 5.12.

The predicted breakthrough curves agree with the experimental data. Apart from K_d and constant a, the values of the adsorption parameters Q_{max}, K_{ads} and k are almost identical (with less than 10% deviation) to the values calculated when using equation 5.2. The reason behind different calculated K_d and constant a are to be investigated.

Table 5.8 Parameters iteratively calculated by the general rate model with bead diffusivity equation 5.3 for a millilitre-scale column are shown in row 1. Row 2 parameters are copied from table 5.4 for comparison.

Voidage (ε_b)	Q_{max} (mol m^{-3} matrix skeleton)	K_{ads} (m^3 mol^{-1} s^{-1})	K_d (s^{-1}) $(10)^{-3}$	Constant a (10^{-3})	k (m s^{-1}) $(10)^{-4}$
0.35	4.82	4.40	0.541	4.604	1.94
0.35	4.84	4.46	0.844	7.12	1.22

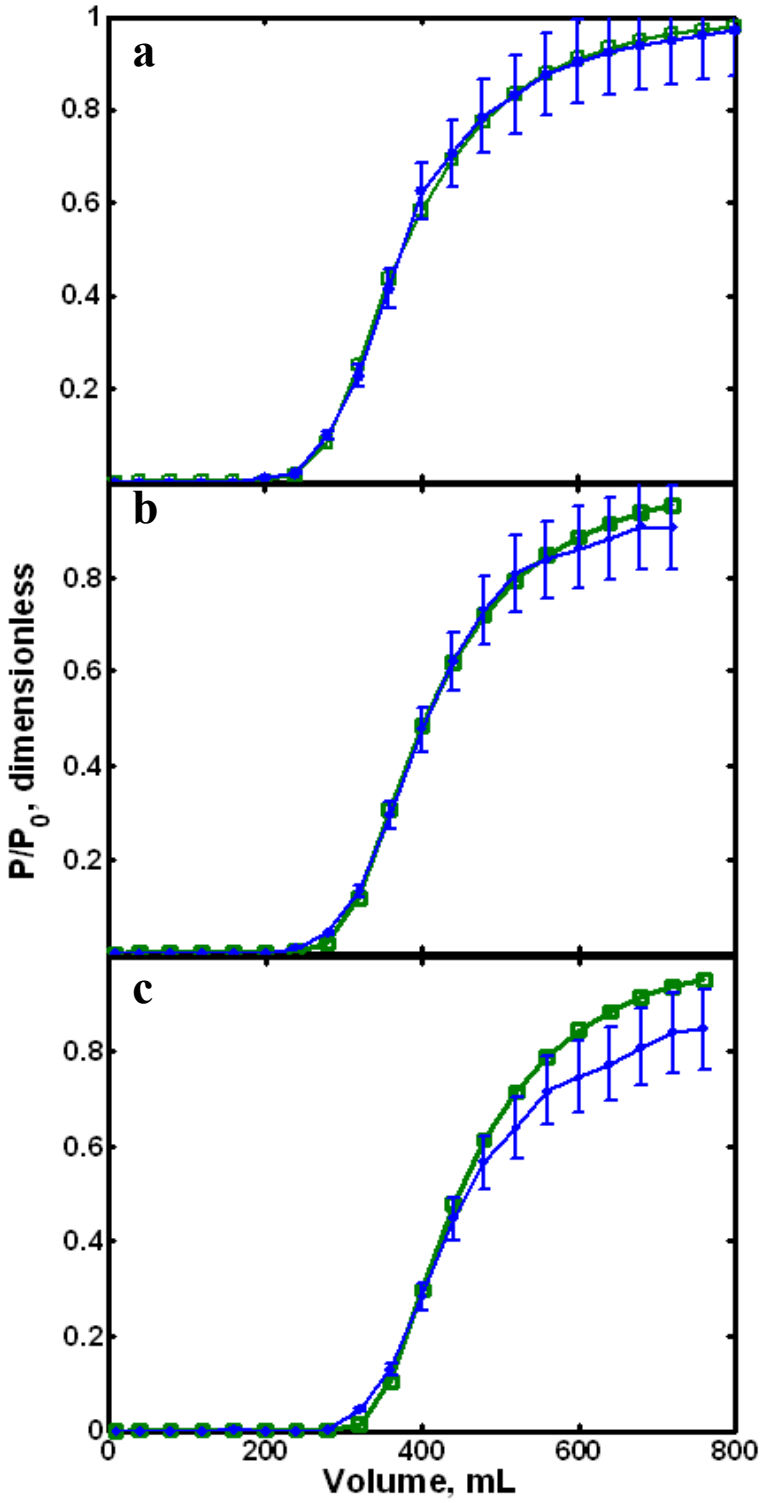

Figure 5.12 Use of model fitting of breakthrough data for 1 mL scale column to predict the effect of change of flowrate. Model based on equation 5.3 was used to obtain the adsorption parameters from an experimental breakthrough curve ran at 310 cm h^{-1}(a) (see table 5.8 for values). Trend lines are drawn by eye through experimental and predicted data points. Predicted (-□-) breakthrough curves of 232 cm h^{-1} (b) and 155 cm h^{-1}(c) were compared against 1 mL scale experimental data (-●-). The error bars are based on 10% experimental error. The R^2 value for the fit of experimental and modelled/predicted data graphs a, b and c are 0.999, 0.997 and 0.970 respectively.

Using equation 5.3 the 40 μL scale breakthrough curve was evaluated using different bed voidage values to investigate the influence of this parameter on the fitted solutions. The values are shown in table 5.9. As voidage increases the Q_{max} values increases. This is due to the fact that as more resin particles are present in a unit volume space, the maximum binding capacity needs to decrease to satisfy the breakthrough profile; whereas when the amount of resin decreases per unit volume, the value of the maximum binding capacity of the resin needs to be bigger to satisfy the adsorption profile. The adsorption and desorption rates (K_{ads} and K_d) and bead diffusivity (D_b) are approximately the same regardless of the voidage and Q_{max} values, which reflects the theory of resin specific parameters – the adsorption kinetics of resin under the same buffered conditions should remain unchanged. The deviation can also be caused by resin lot to lot variations; this variation can potentially affect the resin bead flow characteristics and binding capacities.

It is useful to compare the adsorption kinetic parameters obtained at 1 mL scale in table 5.8 with the fitted parameters derived for various bed voidage values in table 5.9; when the voidage is set at 50%, the adsorption kinetics (Q_{max}, K_{ads}, K_d) are in closest agreement to the 1 mL scale data. Because the matching adsorption kinetic parameters were obtained through trial and error of the voidage value, it is necessary to confirm if the model agrees with this value. This is done by setting the bed voidage value as one of the parameters to be fitted on top of the other five parameters, bringing the total number of fitted parameters to six. The results are also shown in the last line of table 5.9. From the fitted results, the bed voidage of the micro-tip is estimated at 0.54; the adsorption rate (K_{ads}) and desorption rate (K_d) calculated are very close to the rest of the simulations as shown in table 5.9, thus suggesting that the intra-particle adsorption is similar and independent of voidage.

After obtaining a set of parameters by fitting an experimental breakthrough curve, the ability of the model to predict breakthrough curves at different flowrates was investigated. The predictions were carried out by keeping the adsorption parameters, bead diffusivity constant and bed voidage (Q_{max}, K_{ads}, $K_{dis,}$ a, k and ε_b)the same as show in the last line of table 5.9 while changing the mass transfer coefficient according to literature correlation (refer to section 3.2.6 equation 3.14 for the correlation). The fitting and predictions are shown in figures 5.13.

Table 5.9 Fitted parameters for a breakthrough curve obtained at 0.258 mL min^{-1} in a 40 µL column using the general rate model with a bead diffusivity equation correlated to the amount of material loaded into the column. Maximum binding capacity, adsorption rate, desorption rate, bead diffusivity constant and mass transfer coefficient (Q_{max}, K_{ads}, K_{dis}, a and k) were fitted with the bed voidage set at 0.35, 0.45 and 0.5. The values presented in the last row of the table are obtained by having the model to fit for six variables- namely the maximum binding capacity, adsorption rate, desorption rate, bead diffusivity constant mass transfer coefficient and bed voidage (Q_{max}, K_{ads}, K_{dis}, a, k and ε_b)

Voidage (ε_b)	Q_{max} (mol m^{-3} $_{matrix\ skeleton}$)	K_{ads} (m^3 mol^{-1} s^{-1})	K_d (s^{-1}) $(10)^{-3}$	Constant a (10^{-3})	k (m s^{-1}) $(10)^{-4}$
0.35	2.95	4.05	0.729	2.08	7.60
0.45	4.00	4.00	0.609	1.97	3.09
0.5	4.88	4.34	0.729	1.82	1.91
0.54	5.33	4.27	0.450	1.66	3.30

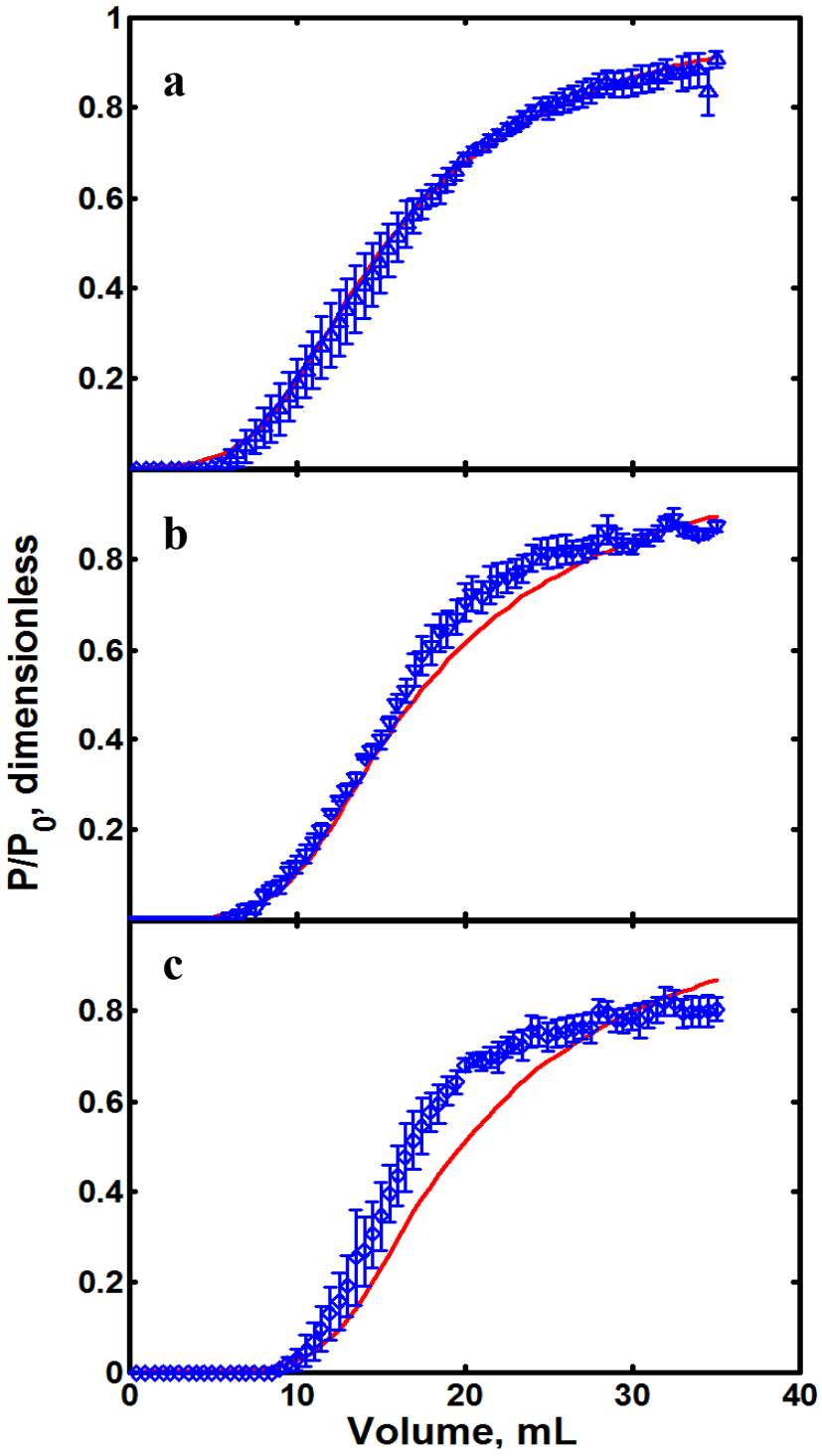

Figure 5.13 Use of model fitting of breakthrough data for a 40 µL scale column to predict the effect of change of flowrate. Model based on equation 5.3 was used to obtain the adsorption parameters (including bed voidage) from an experimental breakthrough curve obtained from a 40 µL column ran at 310 cm h^{-1}(a). The parameters (see table 5.9-row five for values) were then used to predict (-) breakthrough curves of 232 cm h^{-1} (b) and 155 cm h^{-1}(c) compared against 40 µL scale experimental data. The error bars on the experimental data represent the standard deviation of three repeats. The R^2 value for the fit of experimental and model predicted data for graphs a, b and c are 0.994, 0.991 and 0.961 respectively.

5.5 Understanding the physics of a microtip

From figure 5.13 the disagreement between the experimental and predicted breakthrough curves below 50% breakthrough gets bigger as the linear velocity decreases. However this trend was not observed when predicting the performance of 1 mL scale breakthrough curves (refer to figures 5.12); this suggests that there is a flowrate dependent variable in the 40 μL scale system and is reflected from the simulations in figure 5.13.

The disagreement between the predicted and experimental breakthrough curves only showed in 40 μL scale data and more importantly after introducing equation 5.3. This suggests that the change is caused by bead diffusivity being a function of volume of matrix in the column. To confirm this, the bead diffusivity constant was altered manually to investigate the effect of this parameter on the shape of the breakthrough curves at different flowrates. In figure 5.14 the predictions of 310 cm h^{-1} and 232 cm h^{-1} breakthrough curves obtained by changing the values of the bead diffusivity constant "a" are shown and the values are presented in table 5.10. The study is to test that the parameter that caused the disagreement between the experimental and predicted breakthrough curve is included in the bead diffusivity equation. In theory the value of bead diffusivity constant "a" will not change for an identical system, this is due to the fact that for an identical system the rate of protein entering the intra-particular space of the resin particles should be independent of the column size.

From the above study, it is suggested that a flowrate dependent variable is included in the bead diffusivity decay equation. Since the equation is a function of flowrate, loading time, bed voidage and bed dimensions therefore the flowrate dependent variable must be one of these parameters. Because flowrate and loading time are known variables; this suggests that bed voidage or bed height is the key element; a match between the experimental and the predicted breakthrough curve can be achieved by changing either or both of these two values. An explanation for this is the packing condition of the PhyNexus tips. The tips were manufactured to have a fixed amount of resin instead of in the form of a packed bed. As resin particles inside PhyNexus tips are not restricted by top and bottom frits, packing conditions within the tips change as flowrate changes, making bed voidage (ε_b) a function of flowrate. In addition as flowrate increases, the

extent of compression in the bed will also increase, causing bed voidage to decrease as flowrate increases. The reduced bed voidage reduces the ability of liquid to gain access to the binding sites of the resin particles; the reduction of liquid – resin contact also reduces protein – resin contact hence reduces adsorption. In figure 5.15 the bed voidage was altered and values of bed voidage (refer to table 5.11) were scouted until the R^2 value is as close to 1 as possible. It is observed that the bed height does not change as the flowrate increases. The values obtained in table 5.11 are obtained assuming that the bed height is constant.

Table 5.10 Fitted parameters of a 0.258 mL min^{-1} (310 cm h^{-1}) breakthrough curve and scouted values of constant a at 0.192 mL min^{-1} (232 cm h^{-1}) and 0.129 mL min^{-1} (155 cm h^{-1}) . The fitting was done by using the general rate model with a bead diffusivity equation correlated to the amount of material loaded into a 40 µL scale column. The bed voidage in all the fitting/predictions are kept at 0.54. (equation 5.3)

Linear velocity (cm h^{-1})	Q_{max} (mol m^{-3} $_{matrix\ skeleton}$)	K_{ads} (m^3 mol^{-1} s^{-1})	K_d (s^{-1}) $(10)^{-3}$	Constant a (10^{-3})	k (m s^{-1}) $(10)^{-4}$
310	5.33	4.27	0.450	1.66	3.30
232	5.33	4.27	0.450	1.89	3.30
155	5.33	4.27	0.450	2.00	3.30

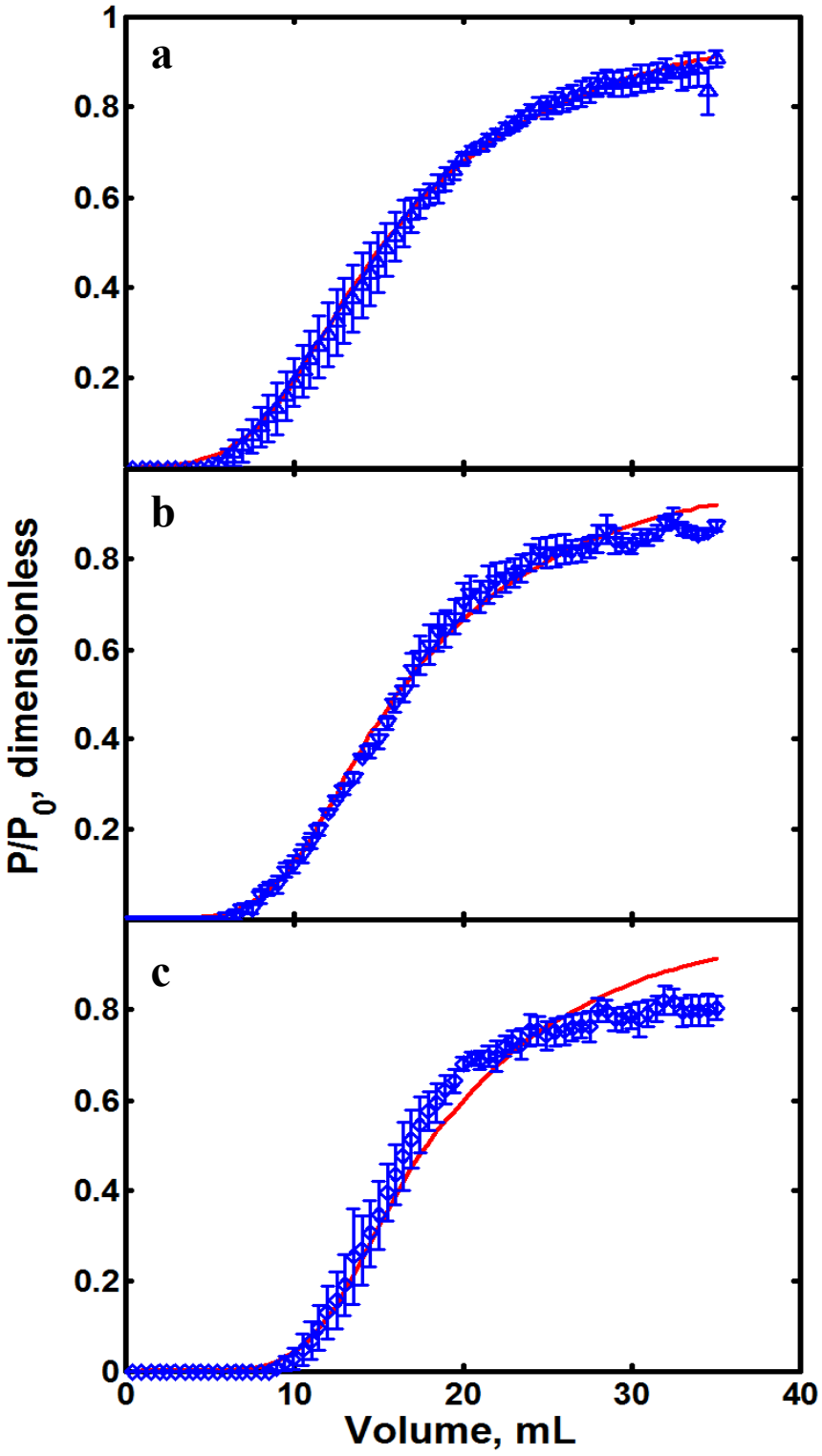

Figure 5.14 Effect of change of bead diffusivity relationship on model fitting of breakthrough data for 40 uL scale column to predict the effect of change of flowrate. Model based on equation 5.3 was used to obtain the adsorption parameters of an experimental breakthrough curve of a 40 uL column ran at 310 cm h^{-1}(a). The parameters were then used to predict breakthrough curves of 232 cm h^{-1} (b) and 155 cm h^{-1}(c) with bead diffusivity constant changing according to flowrate. The predictions are (see table 5.10 for values) compared against 40 uL scale experimental data. The error bars on the experimental data represent the standard deviation of 3 repeats. The R^2 values for graph a, b and c are 0.994, 0.993 and 0.980 respectively.

Table 5.11 Fitted parameters of a 0.258 mL min^{-1} (310 cm h^{-1}) breakthrough curve and scouted values of constant a at 0.192 mL min^{-1} (232 cm h^{-1}) and 0.129 mL min^{-1} (155 cm h^{-1}). The fitting was done by using the general rate model with a bead diffusivity equation correlated to the saturation of the column (equation 5.3).

Linear velocity (cm h^{-1})	voidage (ε_b)	Q_{max} (mol m^{-3} matrix skeleton)	K_{ads} (m^3 mol^{-1} s^{-1})	K_d (s^{-1}) $(10)^{-3}$	Constant a (10^{-3})	k (m s^{-1}) $(10)^{-4}$
310	0.54	5.33	4.27	0.450	1.66	3.3
232	0.56	5.33	4.27	0.450	1.66	3.3
155	0.58	5.33	4.27	0.450	1.66	3.3

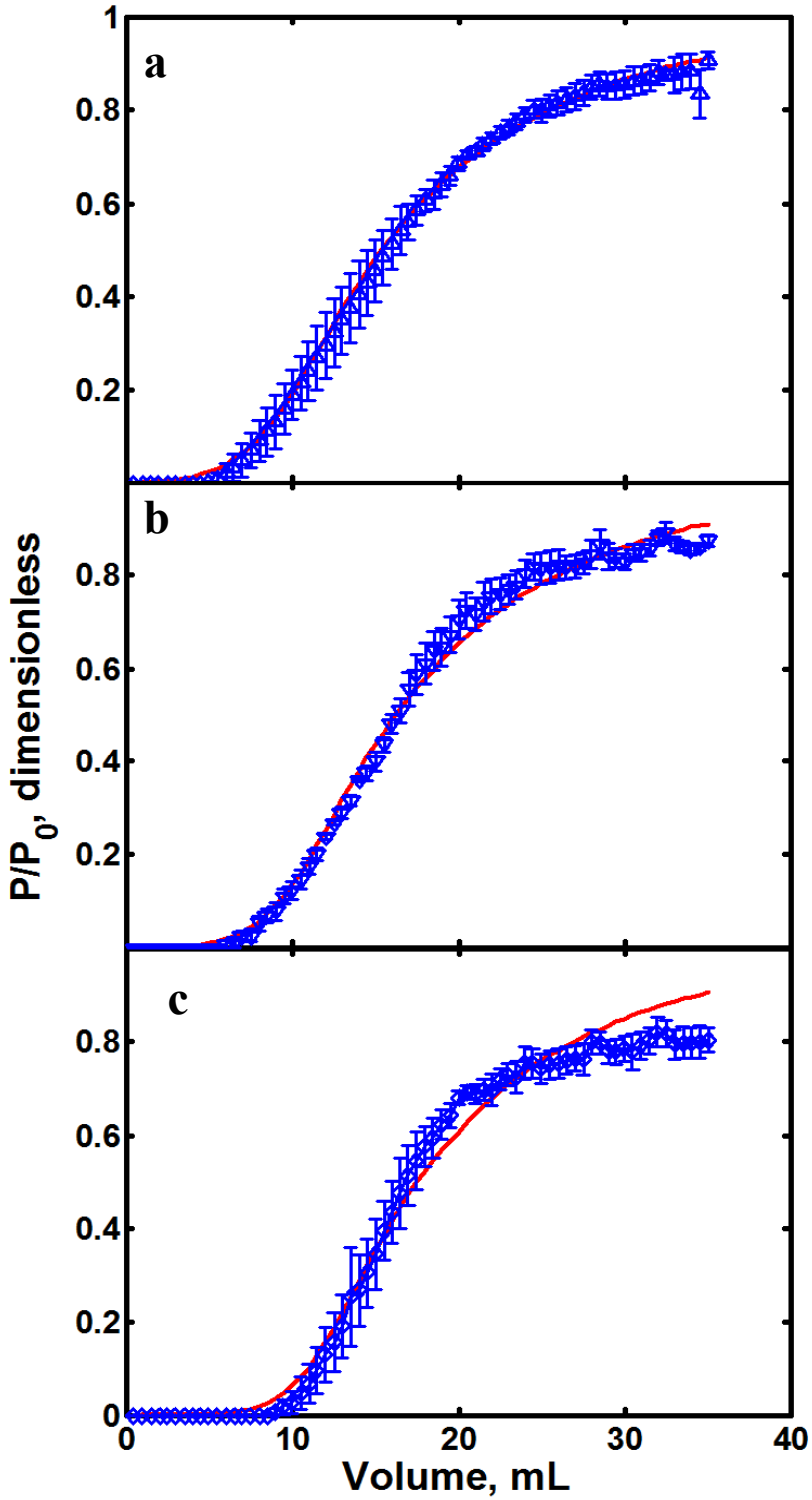

Figure 5.15 Effect of change of bed voidage relationship on model fitting of breakthrough data for 40 uL scale column to predict the effect of change of flowrate. Model based on equation 5.3 was used to obtain the adsorption parameters (including bed voidage) of an experimental breakthrough curve of a 40 uL column ran at 310 cm h^{-1}(a). The parameters were then used to predict breakthrough curves of 232 cm h^{-1} (b) and 155 cm h^{-1}(c). The predictions are (see table 5.10 for values) compared against 40 uL scale experimental data. The error bars on the experimental data represent the standard deviation of 3 repeats. The R^2 values for graph a, b and c are 0.998, 0.992 and 0.983 respectively.

5.6 Scale-up predictions

A model that has the ability to represent a chromatographic system at 1 mL scale and 40 µL scale has been developed. The next step is to test whether the calculated parameters from the 40 µL scale experimental data can be used to predict the performance of a 1 mL scale column. In figure 5.16 a prediction of the millilitre-scale breakthrough curve was obtained using the set of parameters calculated from a 40 µL scale experiment running at 310 cm h^{-1} and the prediction of the 1 mL scale is far from the experimental data.

Referring back to the calculated parameters of 1 mL scale and 40 µL scale in tables 5.8 and 5.9 row 5 respectively, the adsorption kinetics parameters (Q_{max}, K_{ads}, K_{dis}) are very similar, the only parameters that showed a significant difference is the bead diffusivity constant (a); as for mass transfer coefficient, it is proven in section 5.2.1.1.1 that twice the magnitude will not have any significant influence in the shape of the breakthrough curve. To test if bead diffusivity constant is the main cause of the bad predictions of the 1 mL scale breakthrough curves from parameters obtained from 40 µL experimental data, the value of "a" is altered to the value obtained from 1 mL scale and the results are shown in figure 5.17.

With the value of constant "a" altered, the predicted breakthrough curves of 1 mL scale from 40 µL scale parameters are improved; A summary of the values of the parameters used in all predictions is presented in table 5.12. It is necessary to investigate the reason behind the change of constant "a" while predicting breakthrough curves from 1 mL scale to 40 µL scale, hence gaining a better understanding of chromatography through the model and at the same time testing the ability of the model in predicting breakthrough curves across different scales.

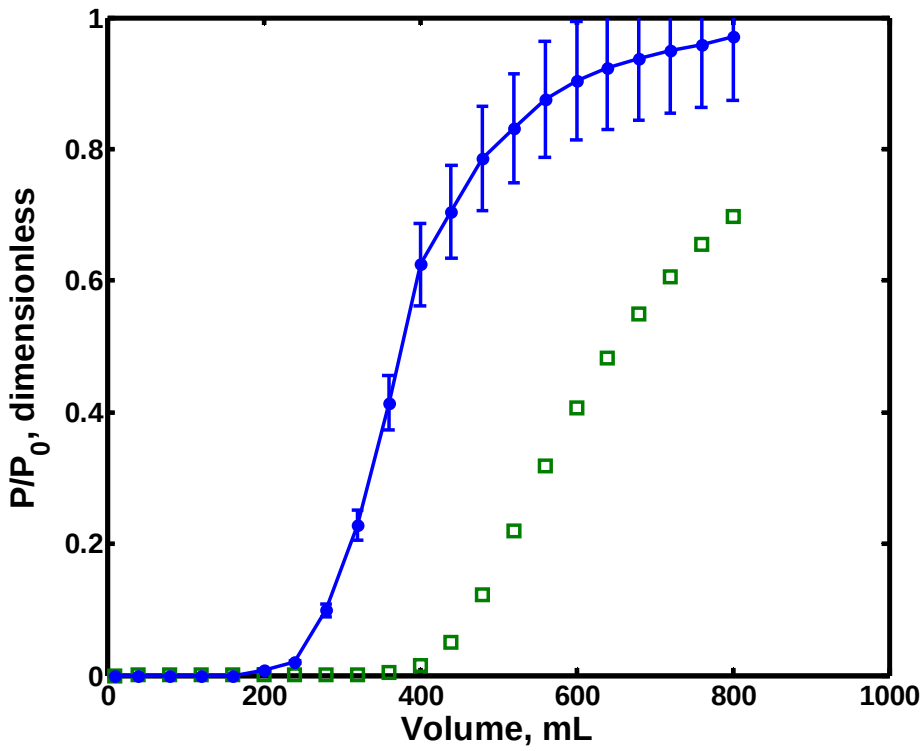

Figure 5.16 Prediction of a 1 mL column (□) breakthrough curve at 310 cm h^{-1} using parameters obtained from a 40 µL scale column at the same linear velocity (refer to table 5.1 for values). The prediction was done by using the parameters obtained by fitting a 310 cm h^{-1} 40 µL scale breakthrough curve with five variables. Trend lines are drawn by eye across experimental data points (●). The error bars on the experimental data assumes a 10% experimental error. The R^2 value for the prediction is 0.136.

Table 5.12 Values of the parameters for breakthrough curve predictions at 1 mL and 40 μL scale. The fitting was done by using the general rate model with a bead diffusivity equation (equation 5.3) correlated to the saturation of the column and 40 μL scale breakthrough curve running at 310 cm h^{-1}. The value of constant "a" at 1 mL scale is assumed to be the same as the fitted value presented in table 5.8.

Scale	Voidage (ε_b)	Linear velocity (cm h^{-1})	Q_{max} (mol m^{-3} matrix skeleton)	K_{ads} (m^3 mol^{-1} s^{-1})	K_d (s^{-1}) $(10)^{-3}$	Constant a (10^{-3})	k (m s^{-1}) $(10)^{-4}$
40μL	0.54	310	5.33	4.27	0.450	1.66	3.30
40μL	0.56	232	5.33	4.27	0.450	1.66	3.30
40μL	0.58	155	5.33	4.27	0.450	1.66	3.30
1 mL	0.35	310	5.33	4.27	0.450	4.69	3.40
1 mL	0.35	232	5.33	4.27	0.450	4.69	3.40
1 mL	0.35	155	5.33	4.27	0.450	4.69	3.40

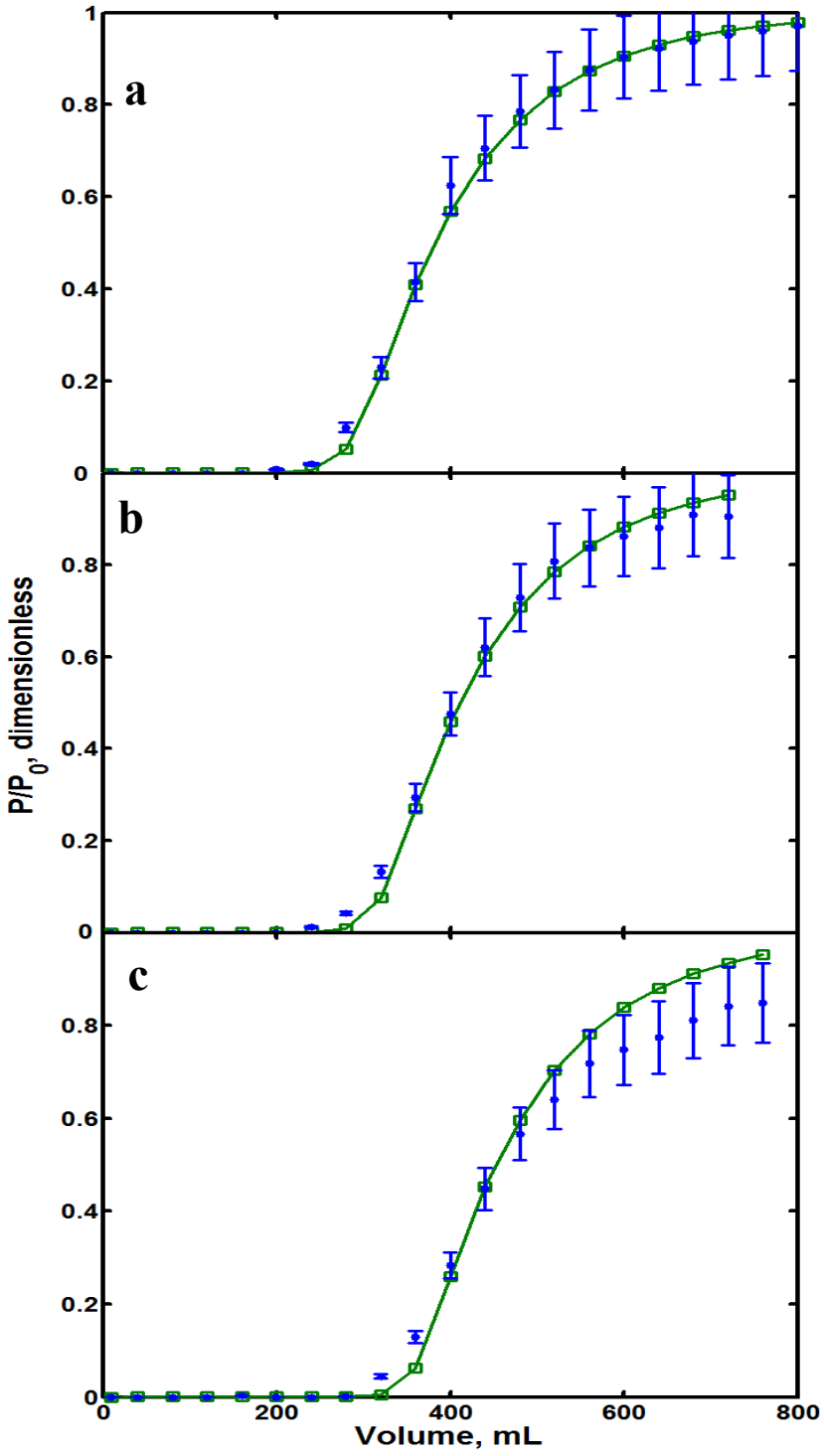

Figure 5.17 Predicted 1 mL column breakthrough curves (□) at 310 cm h^{-1}, 232 cm h^{-1} and 155 cm h^{-1} parameters obtained by fitting a 40 µL micro-tip experimental breakthrough curve (●) at 310 cm h^{-1} but changing values of bead diffusivity constant "a" from 1.66 to 4.69 x 10^{-3}. The predictions are assuming linear velocities of 310 cm h^{-1}(a) 232 cm h^{-1} (b) and 155 cm h^{-1}(c) and using equation 5.3. The error bars on the experimental data assumes a 10% experimental error. The R^2 values for graph a, b and c are 0.996, 0.995 and 0.972 respectively.

5.6.1 Bead diffusivity as a function of saturation of bead layer

It is observed that the predictions of the 1 mL scale breakthrough curves are slightly different from the experimental data (refer to figure 5.17) after changing the value of "a". The disagreement is very likely caused by error while solving for the adsorption kinetic parameters using experimental data obtained using 40 µL micro-tips. The differences in the calculated adsorption kinetics are likely caused by the dimension of the tip, i.e., the conic shape of the micro-tips and also the pressure difference within the column. The model assumes that the micro-tip is cylindrical instead of a frustum of a cone but for the model the radius of the cylinder is set at the middle of the frustum of the cone. Because of the above assumption, the actual linear velocity at the entry point of the column is slower than the calculated value; however the extent of the effect of this assumption is unknown.

The reason behind the differences between the values of constant "a" at both 40 µL and 1 mL scale requires further investigation. In figures 5.18 and 5.19, the bead diffusivity profiles calculated using different values of constant "a" are shown. From figure 5.18 when bead diffusivity is a function of bead saturation, the rate of change of the profile is very similar. However when constant "a" for 1 mL scale was altered to match the breakthrough curves (in section 5.6), the bead diffusivity profiles are very different at both scales (Refer to figure 5.19a). The differences between the bead diffusivity profile is because bead diffusivity was ploted against column volume. The time taken to load one column volume of feedstock into a 1 mL column is longer than a 40 µL micro-tip; in other words the resin in a 1 mL column will be in contact with the feedstock for a longer period of time compared to a 40 µL micro-tip. If the bead diffusivity profile is plotted against time (contact time) then the rate of change of bead diffusivity will be similar (see figure 5.19 b).

Looking at the magnitude of constant "a", the values of this parameter seems to be correlated to the bed height of the columns. The height ratio between a 1 mL HiTrap column to a 40 µL microtip is 2.78 (Refer to chapter 3.4 for dimensions). From table 5.12 the value of "a" for 1 mL scale and 40 µL scale is 1.69×10^{-3} and 4.69×10^{-3} respectively and the ratio between the constant "a" for 40 µL to 1 mL is 2.775, this

suggests that there is possibility that there is a height influence in equation 5.3. To confirm the height influence, the height term was taken out from equation 5.3; the bead diffusivity will be correlated to the volume of feedstock loaded per layer of resin. This new equation (equation 5.5) provides the model with the saturation profile of a layer of resin instead of the column as a whole.

If a_1 x h is the new value for bead diffusivity constant

$$D_b = 7x10^{-11} e^{\frac{-(a_1 h)QT}{(1-\varepsilon_b)(\pi r_c^2 h)}} \quad (5.4)$$

$$D_b = 7x10^{-11} e^{\frac{-a_1 QT}{(1-\varepsilon_b)(\pi r_c^2)}} \quad (5.5)$$

The value of constant "a" was re-calculated using equation 5.5 by maintaining the bead diffusivity profile obtained when fitting the experimental breakthrough curve at 40 µL (310 cm h^{-1}) using equation 5.3, this is based on the assumption that the bead diffusivity profile will not change when the equation changes; the re-calculation of constant "a" will keep the trend identical when using either equation 5.3 or 5.5. The re-calculated value for constant "a" is 1.86 x 10^{-1}.

If the bead diffusivity equation 5.3 is genuinely affecting the predictions because it is a function of column height; then the re-calculated value of constant "a" using equation 5.5 should remain unchanged in order to calculate the correct bead diffusivity profile for 1 mL scale. In figure 5.22 are the simulations of the 1 mL-scale breakthrough curves using the calculated constant "a" and the adsorption parameters. The calculated values of constant "a" using equation 5.5 for both scales are shown in table 5.13.

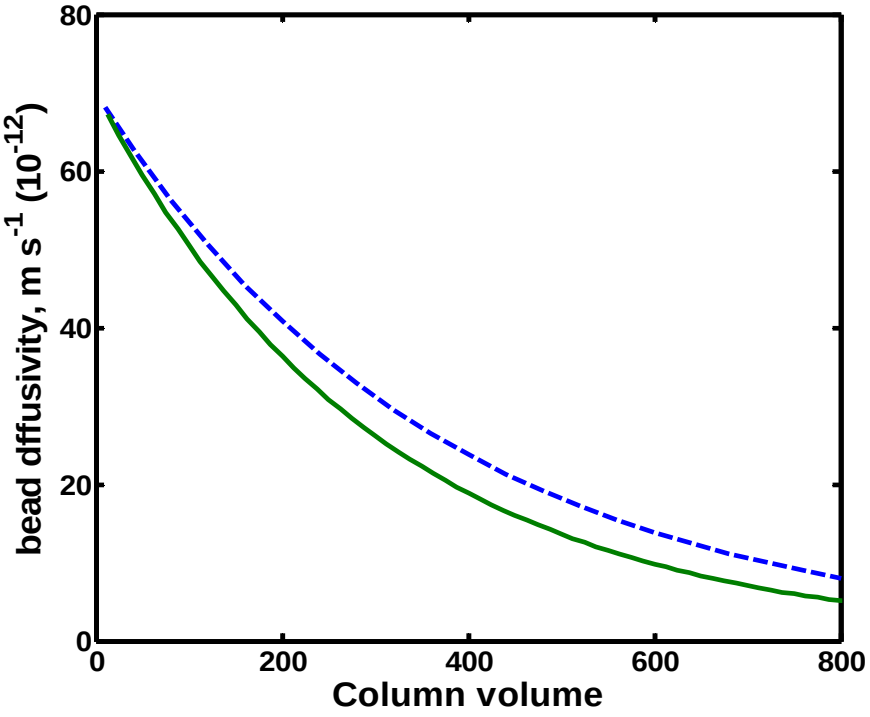

Figure 5.18 Bead diffusivity profile calculated with equation 5.3 at 1 mL and 40 µL scale with no correction to the value of constant "a". The value of constant "a" was calculated by fitting the 40 µL scale breakthrough curve (310 cm h^{-1}) using equation 5.3 as the bead diffusivity decay equation. The value of constant "a" was kept the same 1.66 x 10^{-3} at 1 mL scale (- - -) and 40 µL scale (-).

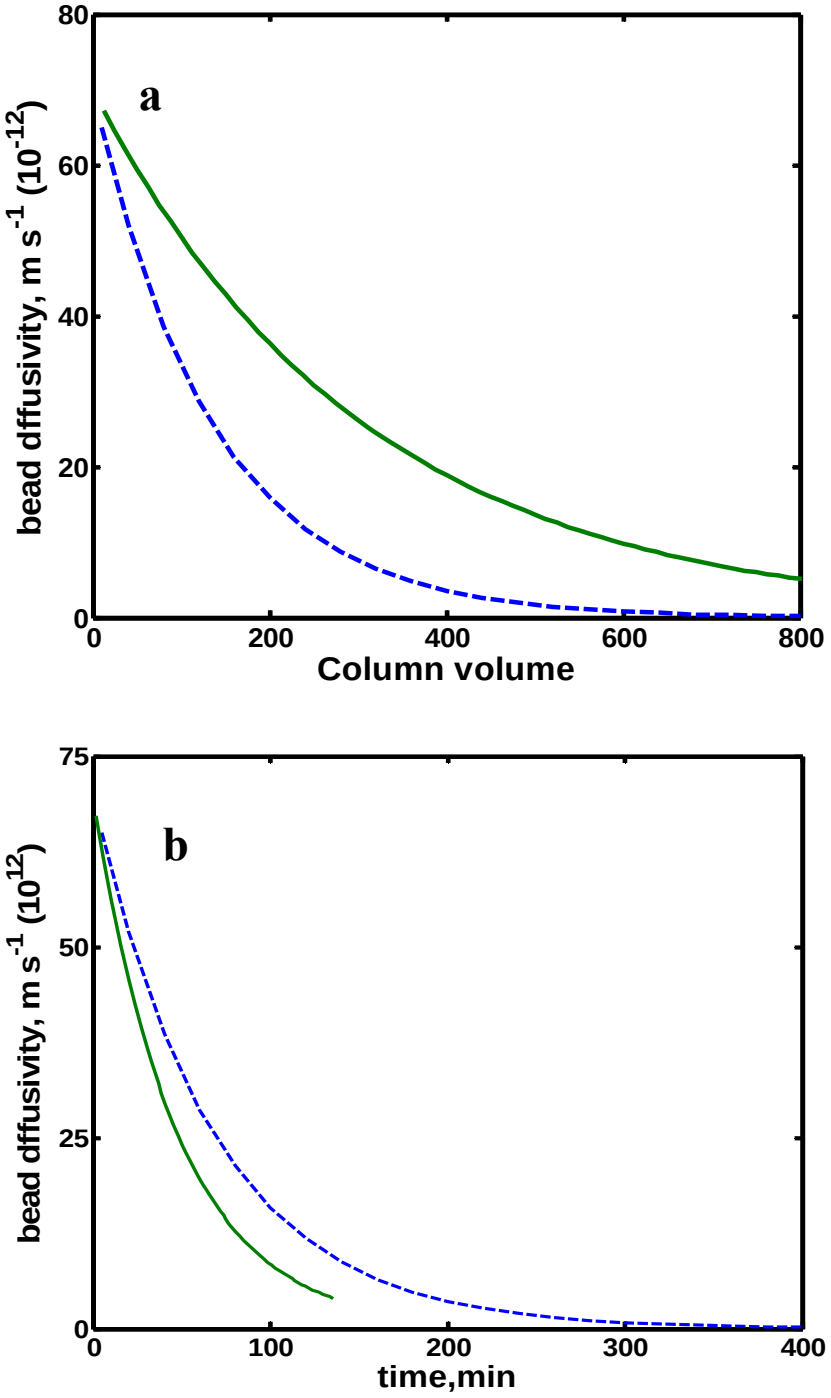

Figure 5.19 Bead diffusivity profile calculated with equation 5.3 at 1 mL and 40 µLscale with corrections to the value of constant "a". The value of constant "a" was kept the same 1.66 x 10 $^{-3}$ at 1 mL scale (- - -) and 4.69 x 10^{-3} at 40 µL scale (-).

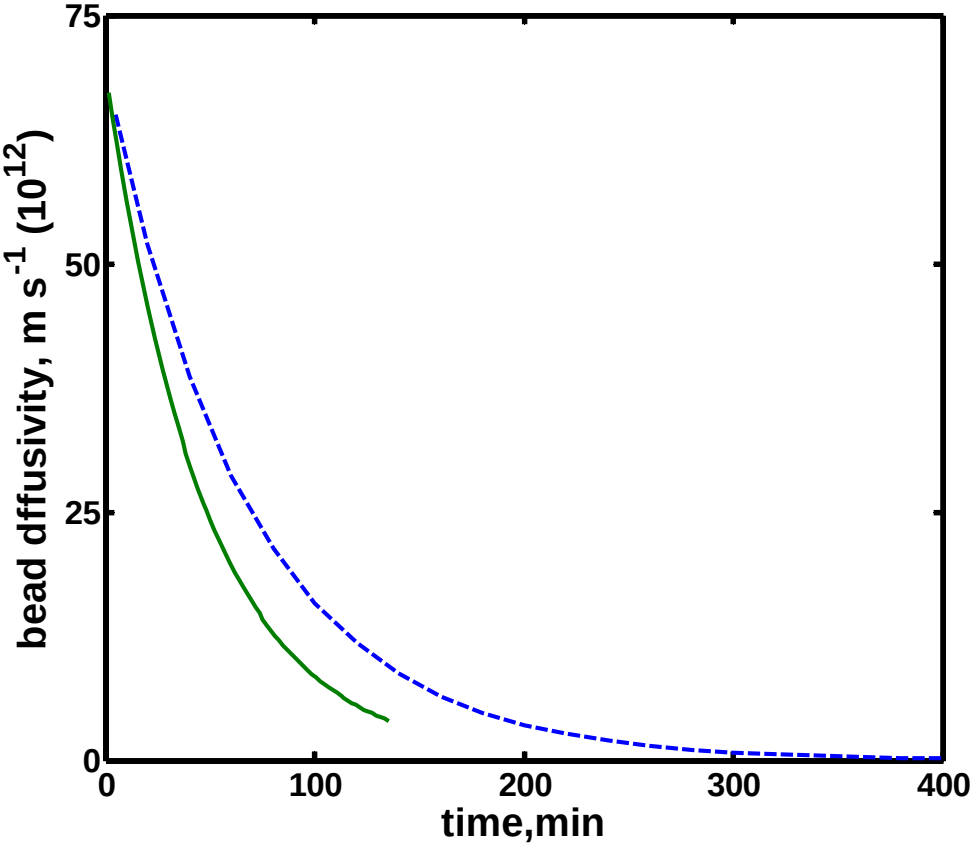

Figure 5.20 Bead diffusivity profile calculated with equation 5.5 at 1 mL and 40 µL scale both scale shares the same value for constant "a". The value of constant "a" was calculated by fitting the 40 µL scale breakthrough curve using equation 5.5 as the bead diffusivity decay equation. The value of constant "a" was kept the same (1.86×10^{-1}) at 1 mL scale (- - -) and 40 µL scale (-).

Table 5.13. Re-calculated value of constant "a" at 40 μL and predicted parameters at 1 mL scale using equation 5.5. The set of values are based on the fitted parameters shown in table 5.11. The fitting was done by using the general rate model with a bead diffusivity equation correlated to the amount of material loaded into the column. (equation 5.3)

Scale	Linear velocity ($cm\ h^{-1}$)	Q_{max} ($mol\ m^{-3}_{matrix\ skeleton}$)	K_{ads} ($m^3\ mol^{-1}\ s^{-1}$)	K_d (s^{-1}) $(10)^{-3}$	Constant a (10^{-1})	k $(m\ s^{-1})\ (10)^{-4}$
40μL	310	5.33	4.27	0.450	1.86	3.30
1 mL	310	5.33	4.27	0.450	1.86	3.40

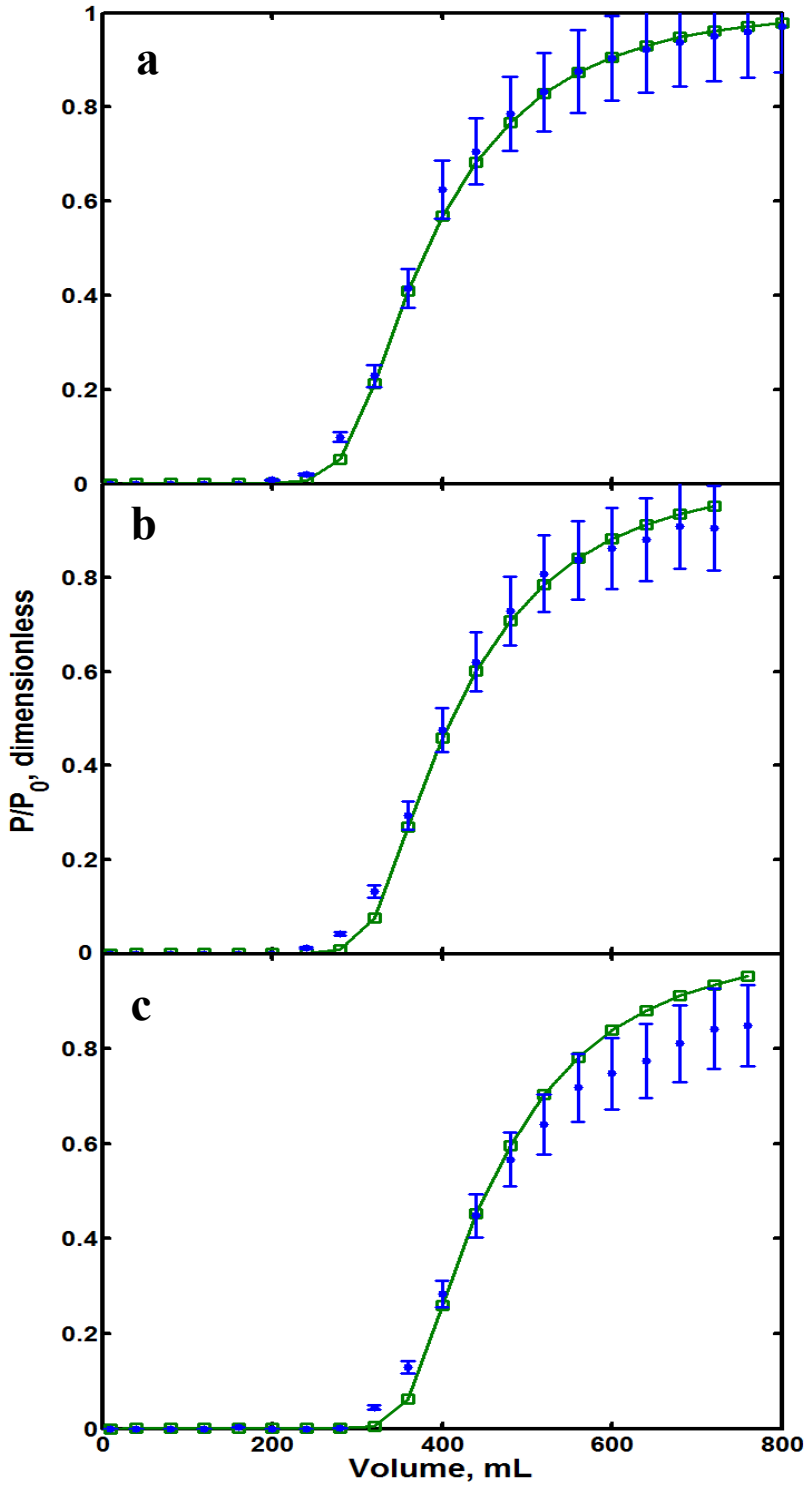

Figure 5.21 Predicted 1 mL column breakthrough curves at 310 cm h^{-1}, 232 cm h^{-1} and 155 cm h^{-1} with bead diffusivity constant re-calculated using equation 5.5. The value of constant "a" is 1.86 x 10^{-1}. The error bars on the experimental data assumes a 10% experimental error. The R^2 value for the predictions in graph a, b and c are 0.996, 0.995 and 0.972 respectively.

From the above study, the effect of bead diffusivity being a function of height is confirmed. Because the study was done with parameters estimated from an assumption, it is necessary to test whether the model has the ability to calculate the values that match the assumptions with the new bead diffusivity equation (equation 5.5). The result of the fitting using a modified model (with equation 5.5 instead of 5.3) is shown in figure 5.22 and the corresponding values for the fitted parameters are shown in table 5.14. From figure 5.22 the model still has the ability to fit the breakthrough curves correctly and more importantly the fitted value of constant "a" matches the value estimated through calculation; in addition, the adsorption parameters calculated are very similar to the ones calculated using the model with equation 5.3 (Comparing table 5.14 and 5.9 row 5).

Because the parameters have shown similarities, it is very confident that the prediction of breakthrough curves of other flowrate will follow the same rules described above and in addition, the scale up predictions will not require any correction faction to achieve the accuracy shown in figure 5.21.

Table 5.14 Fitted parameters from the general rate model with the bead diffusivity equation modified to correlate to the saturation of a resin layer (see equation 5.5). The voidage of the fitting is set to 0.54. The fitted parameters from table 5.9 row 5 (1 mL scale) is presented on the third row for comparison.

Scale	Linear velocity ($cm\ h^{-1}$)	Q_{max} ($mol\ m^{-3}_{matrix\ skeleton}$)	K_{ads} ($m^3\ mol^{-1}\ s^{-1}$)	K_d (s^{-1}) $(10)^{-3}$	Constant a (10^{-1})	k ($m\ s^{-1}$) $(10)^{-4}$
40µL	310	5.35	4.17	0.415	1.863	2.32
1 mL	310	5.33	4.27	0.450	1.66	3.30

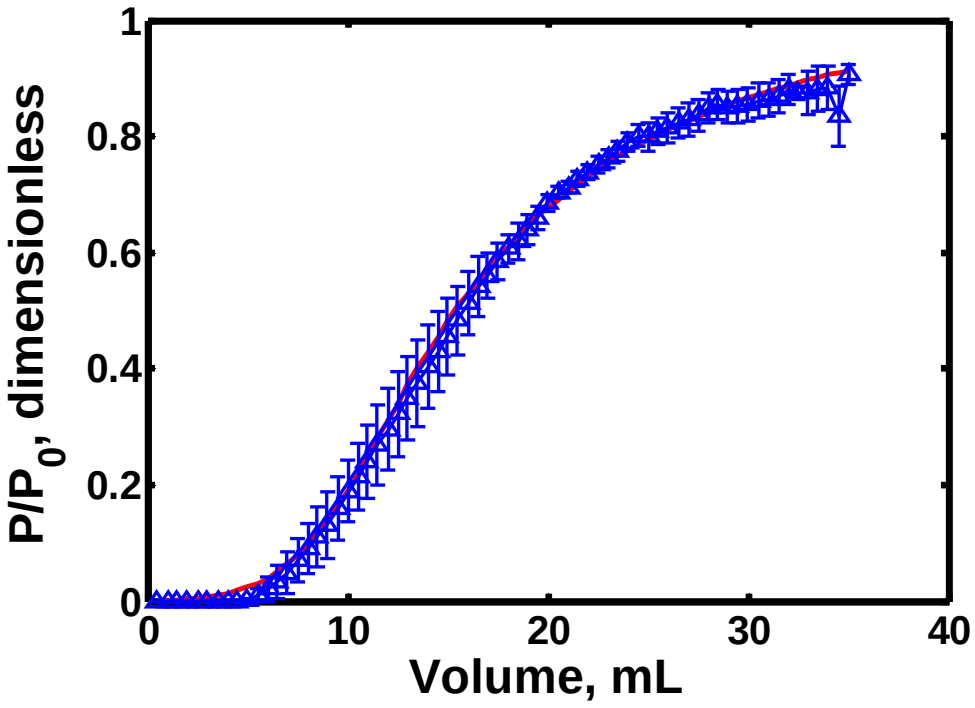

Figure 5.22 Model fitting (-) of 40 µL scale experimental breakthrough curve using five fitted parameters and equation 5.5. The fitted parameters (Q_{max}, K_{ads}, K_{dis}, D_b and K) were obtained by fitting an experimental breakthrough curve (△) at a loading rate of 310 cm h^{-1}. The error bars on the experimental data represent the standard deviation of 3 repeats. The R^2 value of the fitting is 0.998

5.7 Conclusion

In this chapter, a method to modify the general rate model was presented. The modification improved the power of the general rate model in terms of its ability to represent an adsorption system; this was done by first testing for the parameters that are sensitive to the system, followed by implementing assumptions into the model; turning ideas into mathematical terms.

The improved general rate model was used to predict the performance of chromatography at different linear velocities and different scales. A 1 mL HiTrap column and a 40 μL PhyNexus microtip were used in the studies. Through the studies, it is concluded that the system is sensitive to bead diffusivity; this parameter decays in an exponential manner and is correlated to the amount of materials being fed through the column and in addition, the maximum binding capacity, adsorption rate, de-sorption rate and mass transfer remains unchanged regardless of flowrate and scale. The maximum binding capacity, the adsorption rate, the de-sorption rate and the mass transfer coefficient of the system is approximately 56 mg mL^{-1}_{resin}, 0.08 mL mg^{-1} s^{-1} and 0.415 x 10^{-3} s^{-1} and 2.32 x 10^{-4} m s^{-1} respectively. All these values were estimated by the general rate model with one single breakthrough curve. It is also confirmed that using the modified general rate mode, it is possible to predict the performance of chromatography under different combinations of flowrate and scale (1 mL and 40 μL) by obtaining all necessary parameters from one breakthrough curve at 40 μL scale.

The model not only has the ability to predict chromatographic performance but also allows the understanding of chromatography. Through the model, it is identified that the system used in the project is an intra-particle diffusion limiting system while mass transfer of Fab' fragments into the stagnant film of the resin particles have very little effect on overall performance of chromatography.

Chapter 6 – Case studies

6.1 Introduction

In this section, the model will be put to test with two different systems. The first system is an *E.coli* homogenate with nuclease co-expressing with Fab' fragments which has a similar pI to Fab' fragments. The second system is a diluted *E.coli* homogenate with cytochrome c spiked into the solution.

The first system is a more complex one compared to that used in chapter 4 and 5 but it is four times more dilute (Fab' fragment concentration in feedstock is 35 μg mL^{-1}). The feedstock contains more whole cell proteins and a nuclease expressed by the cells. The nuclease has an isoelectric point of 9.3 and hence this protein has similar binding properties as Fab' fragments onto a cation exchange resin. Using this system the effects of binding of Fab' fragments in the presence of a major competitor at similar concentration will be investigated. This system mimics cation exchange chromatography as a primary capture step operating in a high titre process.

The second system is a semi-artificial system. The cytochrome c concentration is four times higher than the Fab' fragment concentration of the feedstock used for studies conducted in chapters 4 and 5; in addition, the molecular weight of cytochrome c (~12 kDa) is around four times smaller than Fab' fragments. The main purpose to use this system is to test the ability of the model to represent a different adsorption system with a target protein different in size and concentration. This system mimics a high titre process.

6.2 Case study I

A breakthrough curve using the Fab' fragment – nuclease homogenate was obtained at 310 cm h^{-1} with a micro-tip and is presented in figure 6.1. The method used to obtain the breakthrough curve is identical to the protocol presented in chapter 2.3.2. The nuclease is a stronger binding competitor compared to Fab' fragments judging from the earlier breakthrough of Fab' fragments (see figure 4.13).

The model developed in chapter 5.6.1 was used to calculate the values of the parameters (Q_{max}, K_{ads}, K_d and constants a and k) that best represent this adsorption system. The values of these parameters are shown in table 6.1.

From the values obtained, Q_{max} significantly decreased while constant "a" increased when comparing to the values obtained with a feedstock with less competing protein (chapter 5.4.Table 5.11). This suggests that the ability of the resin to adsorb Fab' fragments is significantly reduced because the nuclease has a stronger binding power compared to Fab' fragments. The value of constant "a" is larger than the system used in chapter 5 means that the diffusion of the Fab' fragments into the intra particle space is decaying faster. This can be explained by the fact that the nuclease attaches preferentially to the binding sites, making Fab' fragments harder to gain access into the intra-particle space hence binding cannot be achieved.

This case study not only proved that the model has the ability to solve for a solution best representing a system that is different from the one used during development. It also helped to gain a better understanding of the chromatographic adsorption system. In the presence of a highly competitive protein, the binding capacity of Fab' fragments is significantly lower; in addition the adsorption rate is slower and the rate of decay of bead diffusivity is higher than the non-nuclease expressing system. The modelled parameters suggest that nuclease in the feed stream hinders the binding of Fab' fragments onto the resin particles.

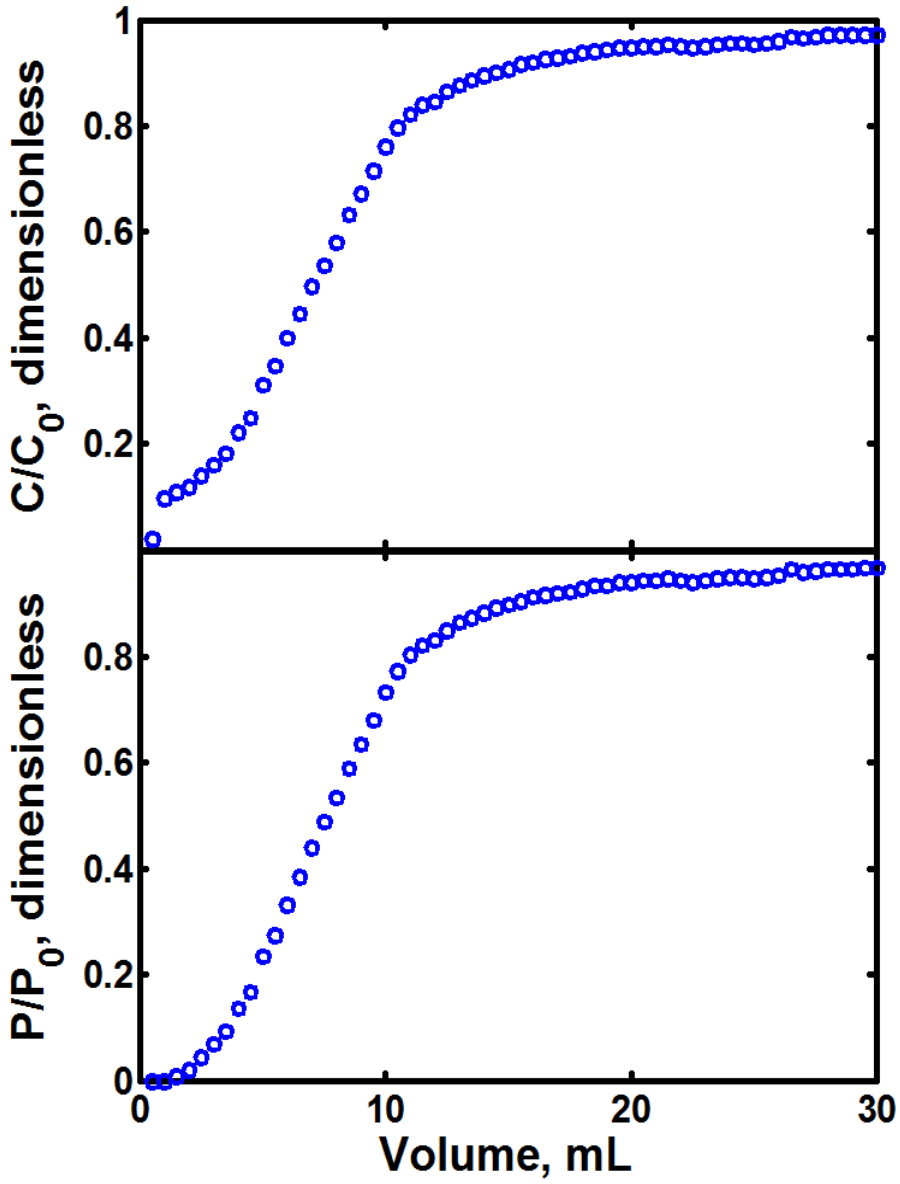

Figure 6.1 Breakthrough curve obtained using *E.coli* homogenate containing Fab' fragments and SP Sepharose FF resin. This strain of *E.coli* cell expresses nuclease and Fab' fragments. The top graph shows a breakthrough curve with no data treatment to remove the artefact caused by aggregation. The bottom graph is a breakthrough curve with the baseline correction strategy introduced in chapter 4.4. The correction factor chosen is 10%.

Table 6.1 Fitted parameters of a Fab' fragment – nuclease homogenate. The parameters are obtained by fitting five parameters with the general rate model developed in chapter 5. The fitted parameters obtained from chapter 5.4 table 5.11 are shown in row 3 for comparison

Q_{max} (mol m^{-3} $_{matrix\ skeleton}$)	K_{ads} (m^3 mol^{-1} s^{-1})	K_d (s^{-1}) $(10)^{-3}$	Constant a (m^{-1})	k (m^{-1}) (10^{-4})
1.07 (13 mg mL^{-1})	11.23 (0.22 mL $mg^{-1}s^{-1}$)	0.817	5.52	9.01
5.33 (56 mg mL^{-1})	4.27 (0.08 mL $mg^{-1}s^{-1}$)	0.450	1.66	3.3

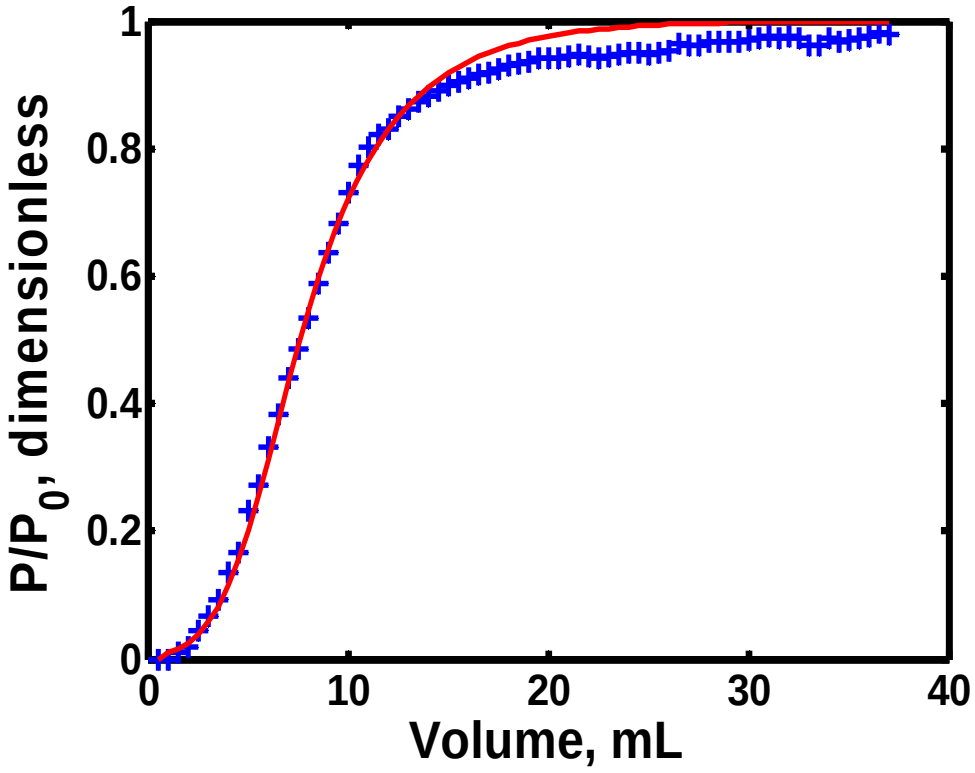

Figure 6.2 Fitting of the *E.coli* homogenate breakthrough curve. The experimental breakthrough points (+) are compared against the fitted breakthrough trend (-). The R^2 value of the fitting is 0.997.

6.3 Case study II

A breakthrough curve was obtained using micro-tips and cytochrome c in a diluted *E.coli* homogenate. The concentration of cytochrome c is 0.4 mg mL^{-1}. This system is designed to mimic a feedstock with high target protein to contaminant ratio.

Chromatography was performed using a protocol similar to the one described in chapter 2.3.2 but with minor changes. Because the pI of cytochrome c is around pH 11, the homogenate was adjusted to pH 7 instead of pH 5 stated in the protocol. The fraction size of each well in this experiment is 200 µL. Cytochrome c does not have a specific assay for quantification; however this protein can be detected between wavelengths 410 nm to 440 nm. Because the proteins in the homogenate can also be detected at these wavelengths therefore early elevation of the breakthrough curves is observed (refer to figure 6.2 a). To alleviate this problem, the optical density of the background protein needs to be taken into account; using equation 6.2 breakthrough curve for cytochrome c can be calculated and is shown in figure 6.2b.

$$OD_{\text{fractions}} - OD_{\text{homogenate}} = OD_{\text{cytochrome c}} \tag{6.1}$$

$$\frac{P}{P_0} = \frac{OD_{cytochromec}}{OD_{feedstock} - OD_{\text{hom}ogenate}} \tag{6.2}$$

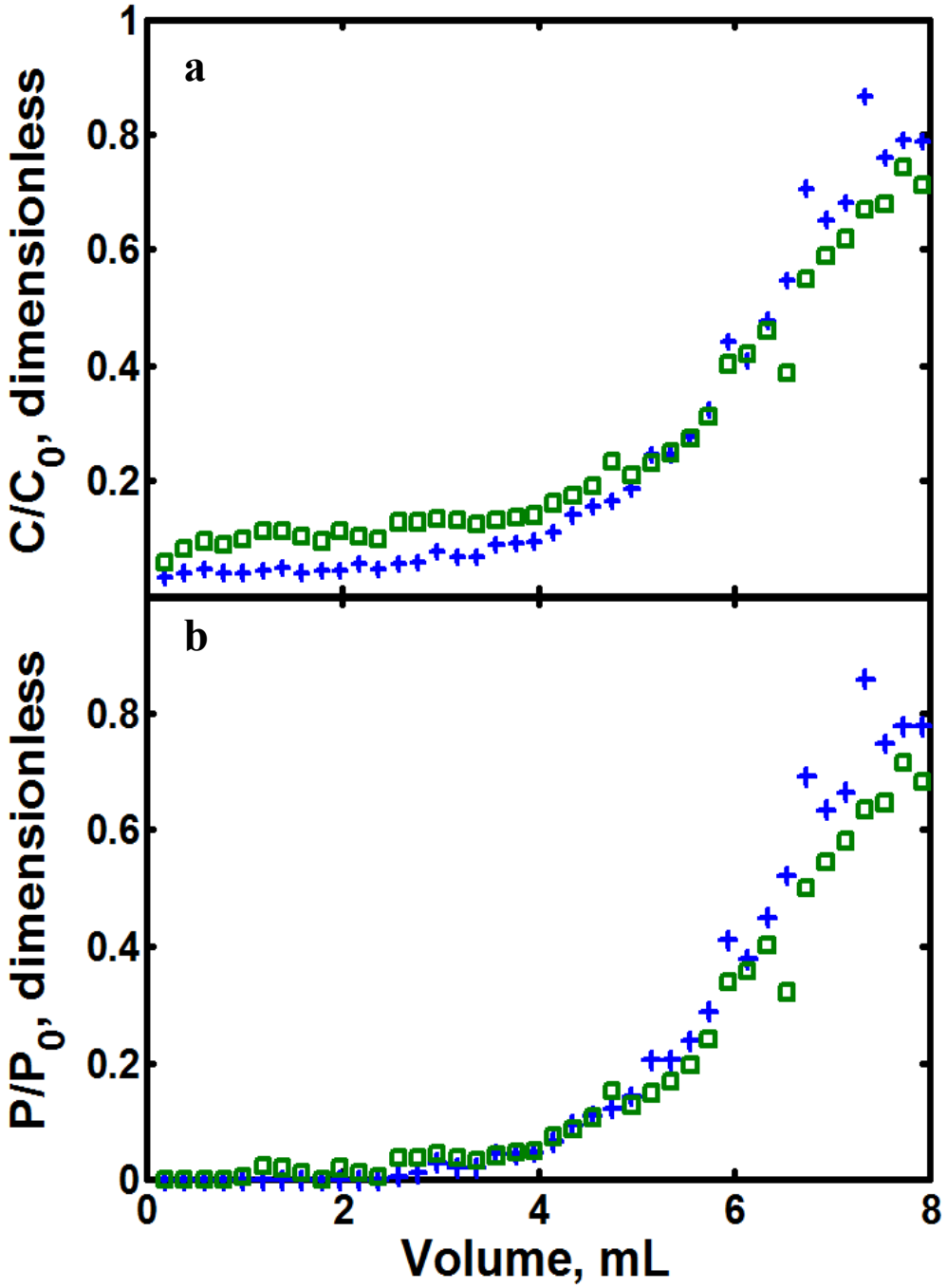

Figure 6.3 Breakthrough curves of cytochrome c at 310 cm h^{-1}. Figure a and figure b are breakthrough curves with and without baseline correction respectively. The breakthrough curves are obtained with a micro-tip with 40 µL SP Sepharose FF resin. The graphs are showing two repeats of the same experiment.

The breakthrough curve used for fitting is the average of the two experimental breakthrough curves showed in figures 6.2. The model developed in chapter 5 does not have the ability to solve for the solution. The R^2 value of the fitted solution (not shown here) is negative meaning that the model cannot represent the experimental data. This suggests that another assumption needs to be implemented into the model to take into account the extra effect caused by the change of feedstock.

In this system, the target protein concentration is higher and there are less competitors in the feedstock to the binding sites. This can turn the system into a mass transfer limiting and bead diffusivity limiting system. This implies that the target protein accumulates around the stagnant film of the resin particles waiting to diffuse into the pores of the resin particles; the rate of mass transfer is higher than the bead diffusivity rate, therefore when more feedstock flows around the resin particles the target protein cannot enter the saturated stagnant film. From the above assumption, mass transfer is a function of feedstock loaded into the column and can also be a function of resin saturation. To implement the above assumption into the model a similar equation as the bead diffusivity decay equation introduced in chapter 5 was used (refer to equation 6.3).

$$k = 9x10^{-3} e^{\frac{-bQT}{(1-\varepsilon_b)(\pi r_c^2)}} \qquad (6.3)$$

The initial value of 9 x 10^{-3} (T=0) is estimated based on the results obtained in chapter 5, assuming the mass transfer rate is ten-folds faster than a "dirtier" feed stream. This method of estimation was used because the mass transfer coefficient estimated through literature correlations (equation 3.13 and 3.14) is far from real (3.28 x 10^{-6} m s^{-1}). It is necessary to devise a better estimating method for this initial value; however in this case

study the main focus is to show that a dynamic system is unlikely to be represented by using fixed value for some of the parameters.

The fitting of the breakthrough curve is shown in figure 6.3 and the values of the parameters are shown in table 6.1. From figure 6.3, after the introduction of the mass transfer decay equation to the general rate model, the fitting greatly improved. This showed that mass transfer of the system is reducing as the amount of feedstock is being loaded into the column. Through the positive result from this fitting, it is concluded that the assumption made is very likely to be true.

Through this case study, it suggests that it is still necessary to test the model with more systems to verify its sensitivity; it is very likely that there are other parameters still not included in the model that are crucial to a certain adsorption system.

Table 6.2 Parameters fitted from the general rate model with decay equations for bead diffusivity and mass transfer coefficient

Q_{max} (mol m^{-3} $_{matrix\ skeleton}$)	K_{ads} (m^3 mol^{-1} s^{-1})	K_d (s^{-1}) $(10)^{-3}$	Constant a (m^{-1})	b (m^{-1})
32 (72.3 mg mL^{-1})	1.2 (0.0968 mL $mg^{-1}s^{-1}$)	0.78	0.238	2.56

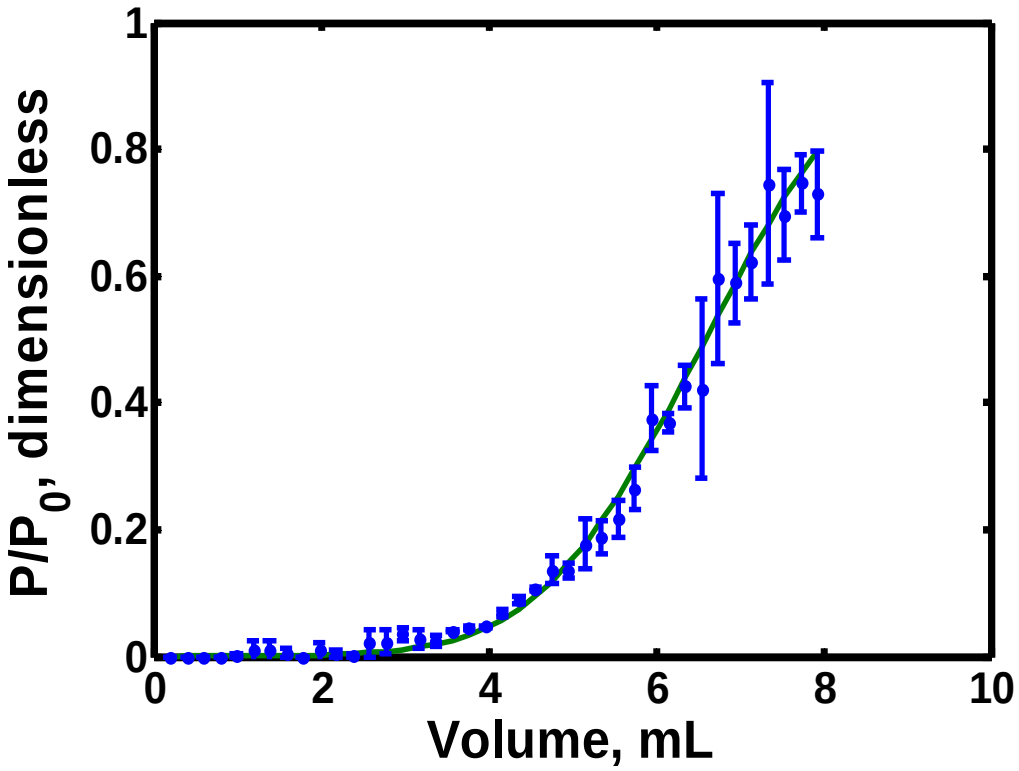

Figure 6.4 Fitting of a cytochrome c breakthrough curve using the general rate model implemented with bead diffusivity decay and mass transfer decay equations. The fitting was done by having the model to fit for five parameters (Q_{max}, K_{ads}, K_d, a, b). The error bars represent the standard deviation of two repeats. The R^2 value of the fitting is 0.990.

Chapter 7 - Conclusion

7.1 Modelling using USD method

The modelling method used in this project uses the general rate model to calculate in an iterative manner parameters from breakthrough curves. Because breakthrough curves are used, the parameters calculated through this method can better represent the system compared to a finite batch method due to the fact that the experimental data are obtained in column conditions instead of discreet experiments. In addition, the method provides a one step evaluation of an adsorption system, reducing the amount of effort required to estimate required inputs to complete the general rate model.

Traditionally the film mass transfer coefficient and the effective intra-particle diffusivity need to be estimated through correlations. This is especially the case with intra-particle diffusivity, where the correlation requires the user to estimate λ, tortuosity and molecular diffusivity. Details of these parameters were presented in theoretical consideration (Chapter 3.2.5). With the modelling method used in the project, all these parameters do not need to be calculated, but fitted by the general rate model as lumped parameters.

It is useful to summarise the modelling methodology used in the chapter 6. After obtaining the breakthrough curve, the data was entered into the original version of the general rate model to solve for the adsorption parameters (Q_{max}, K_d and K_{ads}). The quality of the fitting was evaluated by re-entering the parameters into the general rate model. Because the fitting was not satisfactory, the assumptions of the model were revised.

The first assumption studied was the values of the transport parameters. Because these parameters were taken from literature, the values obtained might not be applicable to the system. The fitting and evaluation routine was repeated with increased number of parameters (Q_{max}, K_{ads}, K_d, D_b and K) and re-assessed using the fit-evaluate routine.

The second assumption is to introduce another concept into the model, because the parameters that are sensitive for the breakthrough curve have been identified. Moreover, from the previous fit-evaluate routine a fixed value for these parameters cannot represent the system. This suggested that new functions needed to be introduced to relate these parameters into the model. In this case a time dependent function was introduced into the model to define changes of bead properties during loading. A fit-evaluate routine was used again to determine if the function improves the ability of the model to fit the experimental data.
The development of the model follows can be divided into three stages. First, fit the breakthrough curve and evaluate the goodness of fit. Second, if the fit is not satisfactory, identify the assumptions in the model that could possibly cause the mismatch between experimental data and modelled data. Third, correct the assumptions in the general rate model to better represent the system. This design cycle was applied three times to complete the model and is shown in figure 7.1. The model was tested with breakthrough curves obtained at different flowrates and further developed using the fit – evaluate routine for modification. A summary of the procedure is also illustrated in figure 7.1. The model was confirmed to be capable of predicting different flowrates at both scales separately after performing the routine describe in figure 7.1. This section of the modelling activity included the bead diffusivity decay as resin beads become more saturated during loading.

The next step taken was to evaluate the ability of the model to predict breakthrough curves from micro-scale data to millilitre scale data. In figure 7.2 a development pathway of the model for scaling-up purposes is presented. The development method follows the fit-predict-evaluate-revise assumption routine; the developed model after two correction routine has the ability to use one breakthrough curve at micro-scale to calculate the adsorption and transport parameters; using the set of parameters to predict breakthrough curves at different flowrates between the two scales.

For other systems such as mixed mode chromatography and hydrophobic interaction chromatography due to the natures of different adsorption systems, it is difficult to set up a generic modelling routine. The parameters to be changed might be different but the idea of the modelling will be similar. The first step is to attempt to fit one breakthrough curve with the general rate model; modifying the model if necessary according to the

bead chemistry and transport parameters then verify the model by predicting the breakthrough curves of the same scale (as describe by figure 7.1). Second, use the model with the capability to represent the chemistry of the adsorption system to predict the breakthrough curves at a different scale; the modification of the model in this case is to establish a link between the two scales based on the physics of the columns (as shown in figure 7.2).

In more simple terms, the model at is system-specific. In case of a different adsorption system, the variable parameters defined in the model might need to be redefined but it is uncertain which parameter(s) will be dominant for different adsorption system. A lot of work still required to be done to give a generic model.

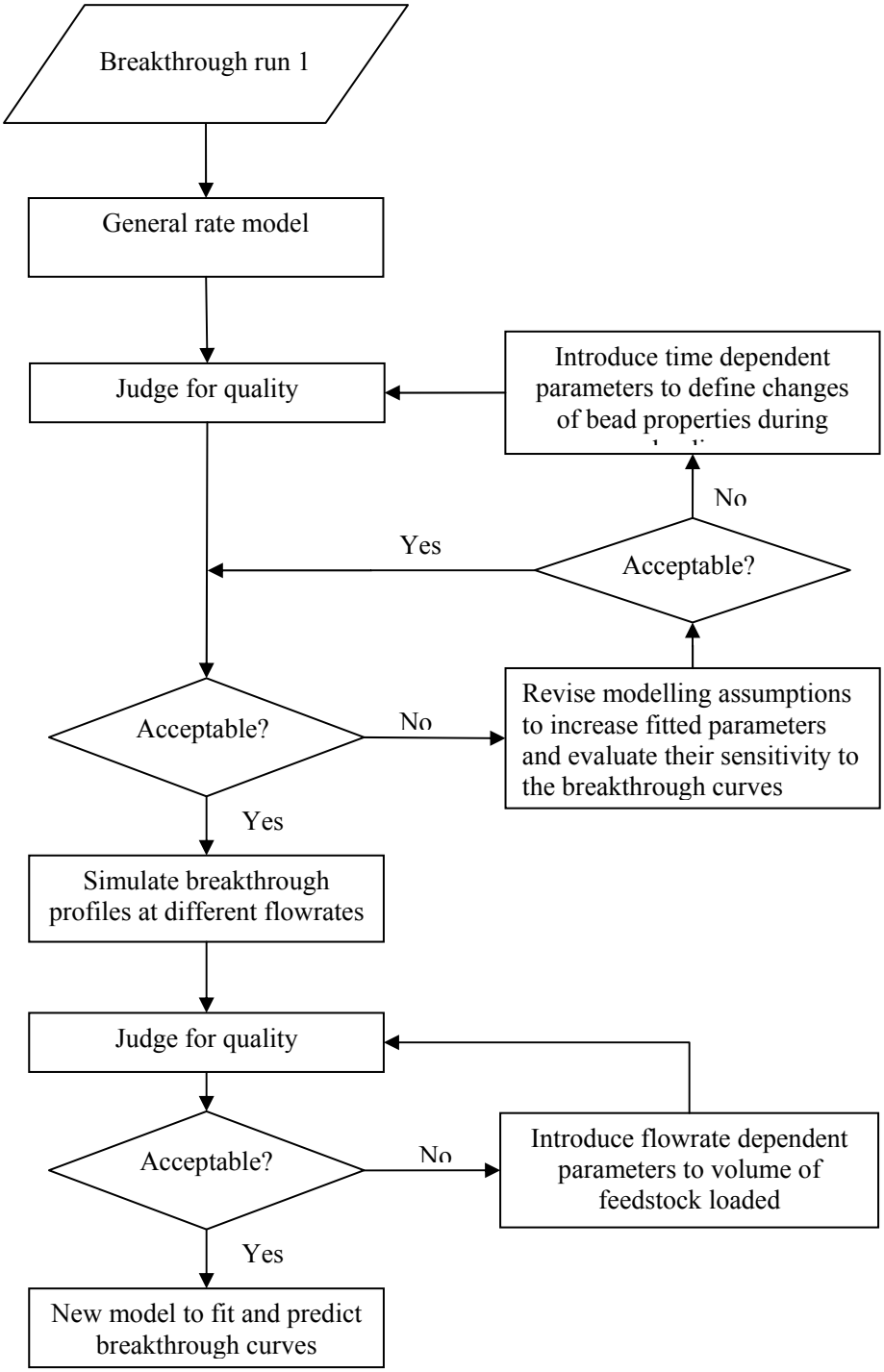

Figure 7.1 Development pathway of the general rate model to fit and predict breakthrough curves at millilitre scale data.

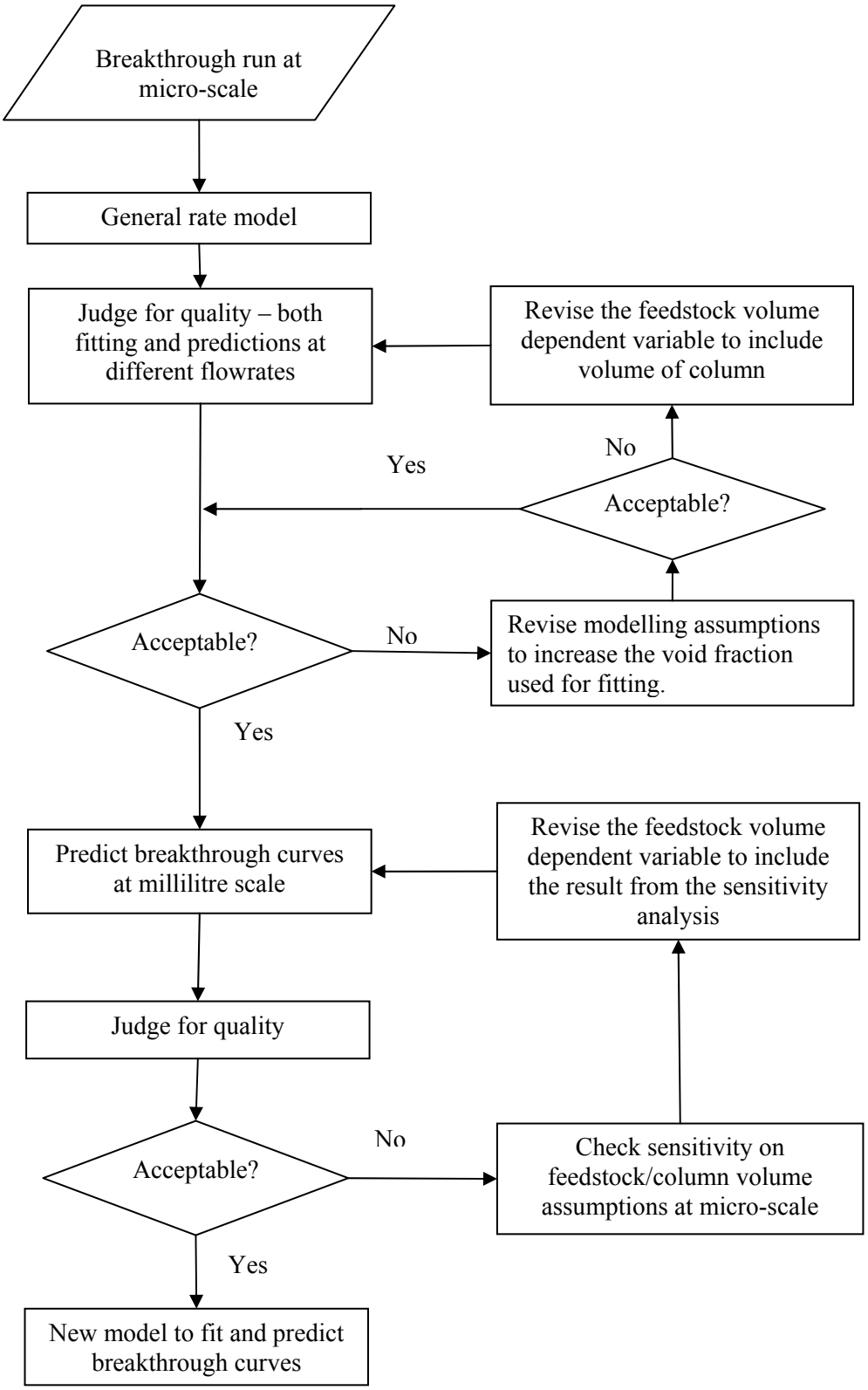

Figure 7.2 Development pathway of the general rate model to fit and predict breakthrough curves at millilitre scale data from micro-scale data.

7.2 millilitre scale vs micro-scale

A 1 mL SP sepharose FF column requires 0.12 g of Fab'fragments to saturate whereas a 40 µL PhyNexus micro-tip requires around 5.3 mg of Fab' fragments to saturate; in other words feedstock enough for one 1 mL column is enough to complete more than 20 runs with a 40 µL micro-tip.

Apart from the smaller feedstock volume requirement, the scale- up method broke the traditional geometric rule using a small scale column with a smaller internal diameter and shorter bed height. Using the constant linear velocity scale as scaling factor, the time required to complete a small scale experiment is shorter. 13 hours is required to saturate a 1 mL column at 155 cm h^{-1} whereas it only requires 4.5 hours to saturate a 40 µL micro-tip.

Although the project proved that the ultra scale-down method using a micro-tip to mimic a millilitre scale column is successful, the model still requires further verification to test for its sensitivity towards other parameters. A more detailed description of future work is presented in chapter 8.

Chapter 8 – Future Work

8.1 Improving the model

From the results chapter (chapter 5), the ultra scale-down method using a PhyNexus micro-tip is successful. The breakthrough curves obtained using the method described in chapter 2.3.2 using micro-tips represents the system running under column conditions. Using the model and method developed in chapter 5, it is possible to predict the performance of a laboratory scale millilitre scale columns from results obtained using micro-tips. This ultra scale-down method offers potential for early discovery of full scale chromatography and now requires further verification.

There are many other parameters that require attention in chromatography. A list of these parameters is listed in table 8.1. It is necessary to test if the model has the ability to take into account the effects of some of the crucial variables such as target protein concentration and molecular weight of target protein. As demonstrated in case study I a different system under different conditions will give rise to different limiting factors to the performance of chromatography. Because the model was developed using *E.coli* lysate, it is best to test these two variables using the same contaminant composition but without the Fab' fragments. This can be done by first passing the crude heat lysate through a Protein A or Protein G column to capture all the Fab' fragments present in the lysate resulting in a Fab' fragment free *E.coli* lysate. Using this method, a similiar background protein profile is achieved. Target protein can be spiked into this background lysate to create a new feedstock to obtain breakthrough curves. With this strategy, the target protein concentration and type of protein can be altered to investigate the effect of binding under these changes. Through the experiments described above, the ability of the model to take into account the effects brought to the system by the target protein can be investigated.

It will also be interesting to investigate other types of chromatography with the model. For example, affinity chromatography, hydrophobic interaction chromatography and mixed mode chromatography. Understanding these different types of chromatography with the aide of the model is beneficial to the design of a new purification strategy for a new feedstock.

All the above suggestions involve improvements of the model through different feedstock hence protein profile. Another useful function is the ability to use the model for prediction of scale-up. Currently the model can predict performance of a 1 mL column from a 40 µL micro-tip, however work still needs to be done to enable the model to predict breakthrough curves at XK 16 or even larger scale. In addition through development of the model, there are opportunities to gain a better understanding of the physics of both the column and the adsorption kinetics.

Table 8.1 Variables that have influence in the performance of chromatography

Feedstock	Resin
pH	Ligand density
Ionic strength	Particle porosity
Temperature	Resin size
Molecular weight of target protein	
Target protein concentration	
Protein aggregation	

8.2 Understanding chromatography through the modelling

The beauty of the micro-tip ultra scale-down method is its ability to mimic chromatography under column conditions. Through modelling the performance of chromatography will be translated into mathematical terms. Making use of both experimental and modelling advantage, the behaviour of adsorption of target protein under the influence of pH, ionic strength and the presence of aggregation can be compared.

Combining this technology with design of experiment (DoE) approach, a series of breakthrough curves can be obtained using micro-tips running at different ionic strength and pH. The breakthrough curves will reflect the adsorption kinetics of the target protein under complex protein environment and column conditions; which can be visualized by fitting the breakthrough curves against the general rate model developed in this project. By doing the activity described above, a trend can very likely be observed from the fitted adsorption kinetic parameters. The trend can then be translated into a mathematical model for the general rate model to enable the prediction of adsorption under the influence of ionic strength and pH.

8.3 Re-design of the small scale experimental system

At present the syringe pump device can only hold one stainless steel syringe; all experimentation is limited to one micro-tip. To alleviate this problem, a flow distributor can be attached to the device to allow three or more micro-tips to be connected to the syringe pump. A sketch of the setup is shown in figure 8.1. The figure is showing two sets of syringe-connector system.

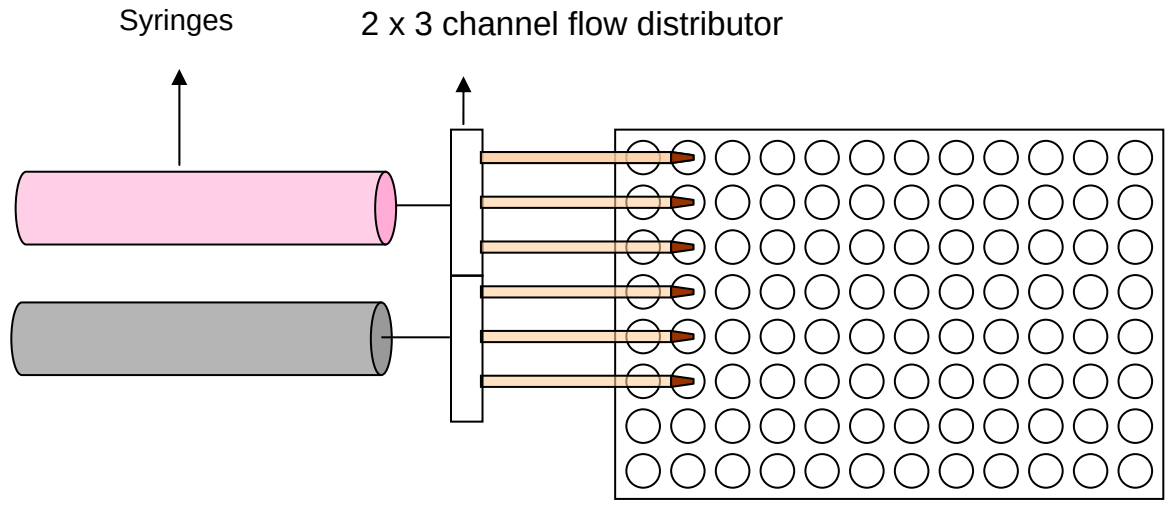

Top down view

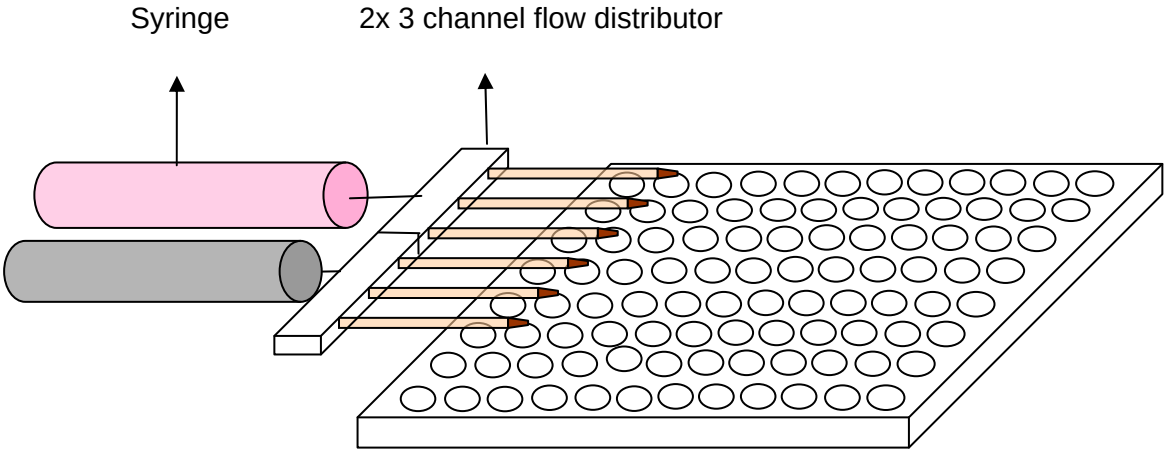

Lateral view

Figure 8.1 A sketch of one syringe pump device connected to multiple PhyNexus microtips

Using the flow distributor, the flow from the syringe will be diverged into three identical streams; the internal diameter of the channels within the flow distributor need to be identical for the flow to evenly distribute to the individual micro-tip attached.

With the addition of the flow distributor, repeats of the same experiment can be done co-currently. This reduces the experimental error caused by feedstock variation and most importantly the experimental throughput is increased by three times.

The setup also allows resin screening under column conditions using PhyNexus micro-tips. This can be achieved by connecting different pre-equilibrated resin tips to the system. The set of experiment will show the performance of each individual resin using the same feedstock running under the same flowrate.

The disadvantage of the setup is it only allows flow coming from one syringe. This means when switching from equilibration to loading buffer, the user will need to manually detach the syringe and reconnect the system with a syringe filled with feedstock. In other words, this manual switching is necessary when switching between steps in a chromatographic cycle.

8.4 Windows of operation

Windows of operation (Zhou and Titchener-Hooker 1999) serves as a tool to aid the selection of feasible operating parameters within a design space. The operating parameter chosen for chromatography are likely to be loading volume and running flowrate. These parameters are chosen because they are the easiest to control and will directly affect the outcome of chromatography.

A windows of operation can be drawn to visualise the performance of chromatography adsorption. This can be done by using the model developed in chapter 5 to calculate the yield and throughput of an adsorption under different loading volumes and flowrate. Yield

is the ratio of protein bound to the column to protein loaded into the column while throughput (g $year^{-1}$) is defined as the materials produced per campaign year. The equation of yield and throughput are shown in equations 8.1 and 8.2 respectively.

$$\text{Yield} = \frac{\text{Amount of Fab' in feedstock} - \text{amount of Fab' in effluent}}{\text{Amount of Fab in feedstock}} \quad (8.1)$$

$$\text{Throughput} = (\text{amount of Fab bound})(\text{loading time} + \text{wash} + \text{elute} + \text{re-equilibrate})^{-1} \quad (8.2)$$

In figure 8.2 an example of a window of operation of chromatography is shown. Below the yield line is an operating area that will give a yield value higher than the success criteria while the area above the throughput line will give a throughput higher than the chosen value. The shaded area represents the operating window; within this area the success criteria are met (throughput and yield).

If the model can successfully predict the performance of chromatography at different scale then logically the windows of operation can also be drawn to identify the operating window. If appropriate an economics model can then be implemented to estimate the cost and utility requirements of the unit operation.

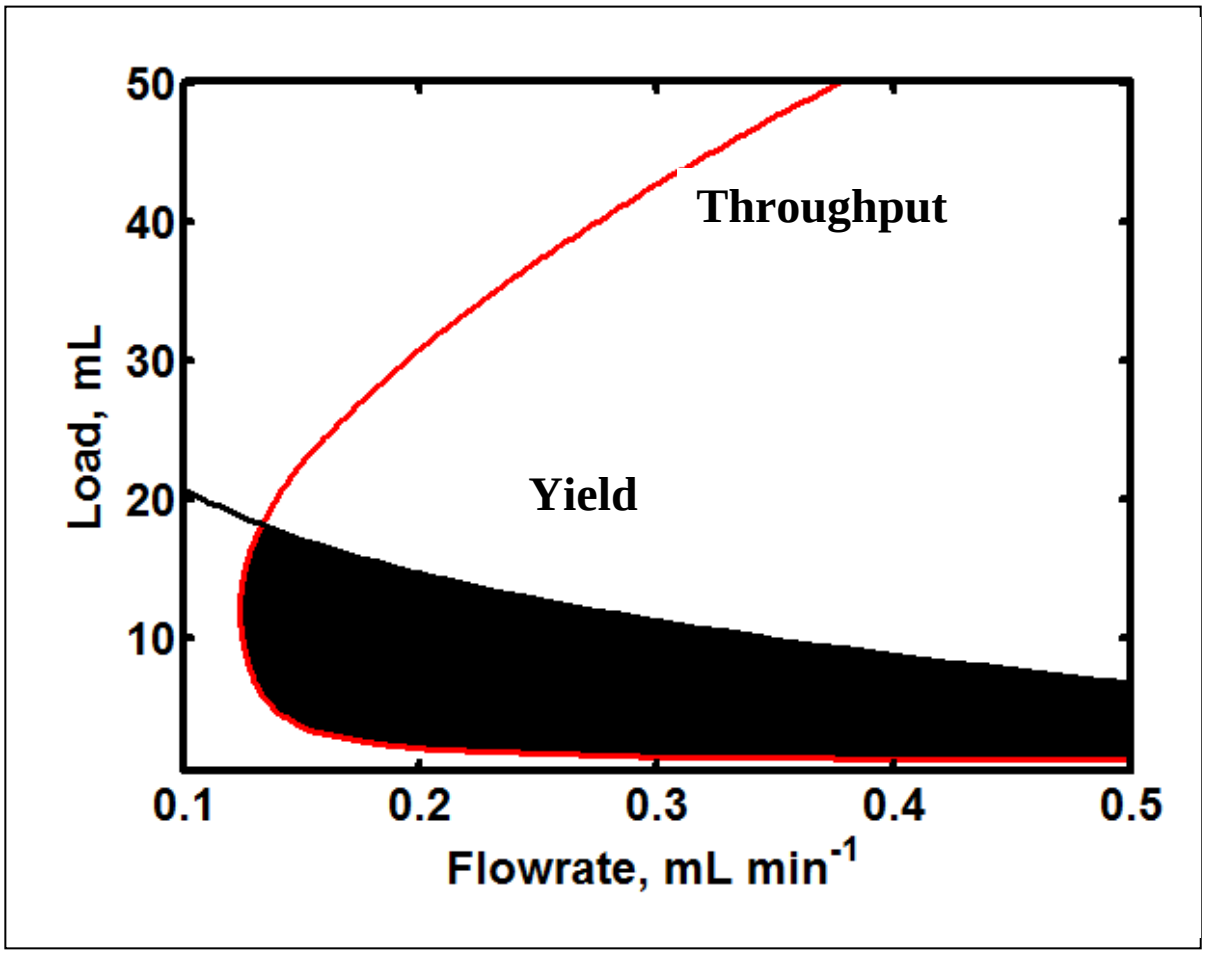

Figure 8.2 An example of a window of operation of a micro-tip. Load and flowrate are the process parameters while throughput and yield are the success criteria.

Appendix

Raw data for matrix weight analysis

Matrix volume 10 µL		
Weighing boat	Weighing boat + dried matrix	Matrix dry weight
0.6851	0.6865	0.0014
0.6431	0.6445	0.0014
0.6546	0.6563	0.0017
0.5686	0.5697	0.0011
Average		0.0014

Matrix volume 12.5 µL		
Weighing boat	Weighing boat + dried matrix	Matrix dry weight
0.6661	0.6679	0.0018
0.5802	0.5818	0.0016
0.6329	0.6342	0.0013
0.5947	0.596	0.0013
Average		0.0015

Matrix volume 15 µL		
Weighing boat	Weighing boat + dried matrix	Matrix dry weight
0.5725	0.5745	0.002
0.6685	0.6701	0.0016
0.6365	0.6383	0.0018
0.6675	0.669	0.0015
average		0.001725

Matrix volume 25 µL		
Weighing boat	Weighing boat + dried matrix	Matrix dry weight
0.6298	0.6331	0.0033
0.6829	0.6872	0.0043
0.6574	0.6611	0.0037
0.663	0.6664	0.0034
average		0.003675

Matrix volume 50 µL		
Weighing boat	Weighing boat + dried matrix	Matrix dry weight
0.6168	0.6215	0.0047
0.5956	0.6024	0.0068
0.6332	0.6409	0.0077
0.6626	0.6693	0.0067
average		0.006475

Matrix volume 100 µL		
Weighing boat	Weighing boat + dried matrix	Matrix dry weight
0.6605	0.6736	0.0131
0.6711	0.6847	0.0136
0.6406	0.654	0.0134
0.5674	0.5825	0.0151
average		0.0138

Matrix volume 150 µL		
Weighing boat	Weighing boat + dried matrix	Matrix dry weight
0.622	0.644	0.022
0.6344	0.6501	0.0157
0.6078	0.6276	0.0198
0.6462	0.6665	0.0203
average		0.01945

Parameters calculated from correlations for simulations in chapter 5.

Matrix and Bed Physical Parameters		
Molecular weight,(Da)		49000
Particle radius, R_p (m)		4.5×10^{-5}
Column diameter, (m)		7.0×10^{-3}
Column height, L (m)		2.5×10^{-2}
Bed void fraction, ε_b		0.35
Particle porosity, ε_p		0.65
Pore diameter, (m)		2.75×10^{-8}
Parameters estimated from correlations		
Molecular diameter, (m)		5.3×10^{-9}
Axial dispersion coefficient, $D_{ax}(m^2s^{-1})$	@ 310 cm h^{-1}	1.95×10^{-7}
	@ 232.5 cm h^{-1}	1.63×10^{-7}
	@ 155 cm h^{-1}	1.05×10^{-7}
Film mass transfer coefficient, k (ms^{-1})	@ 310 cm h^{-1}	1.8×10^{-5}
	@ 232.5 cm h^{-1}	1.64×10^{-5}
	@ 155 cm h^{-1}	1.42×10^{-5}
Effective intra-particle diffusivity, D_p (m^2s^{-1})		1.6×10^{-11}
+Lambda, λ		0.19
+tortuosity, τ		2.8
+Molecular diffusivity, D_m (m^2s^{-1})		7.5×10^{-11}

References

ALAHARI ARUNAKUMARI, P., JUE (MICHELLE) WANG, PHD, GISELA FERREIRA 2007. ALTERNATIVES TO PROTEIN A: Improved Downstream Process Design for Human Monoclonal Antibody Production. BioPharm International, 20(2), 5.

ASHTON, G. 2001. Growing pains for biopharmaceuticals. Nat Biotech, 19, 307-311.

BECKER, T., OGEZ, J. R. & BUILDER, S. E. 1983. Downstream processing of proteins. Biotechnology Advances, 1, 247-261.

BENSCH, M., SCHULZE WIERLING, P., VON LIERES, E. & HUBBUCH, J. 2005. High Throughput Screening of Chromatographic Phases for Rapid Process Development. Chemical Engineering & Technology, 28, 1274-1284.

BERGANDER, T., NILSSON-VÄLIMAA, K., ÖBERG, K. & LACKI, K. M. 2008. High-Throughput Process Development: Determination of Dynamic Binding Capacity Using Microtiter Filter Plates Filled with Chromatography Resin. Biotechnology Progress, 24, 632-639.

BERMUDEZ, O. & FORCINITI, D. 2004. Aggregation and denaturation of antibodies: a capillary electrophoresis, dynamic light scattering, and aqueous two-phase partitioning study. Journal of Chromatography B, 807, 17-24.

BERNINGER, J. A., WHITLEY, R. D., ZHANG, X. & WANG, N. H. L. 1991. A versatile model for simulation of reaction and nonequilibrium dynamics in multicomponent fixed-bed adsorption processes. Computers & Chemical Engineering, 15, 749-768.

BIZZARO, N. 2007. Antibodies to citrullinated peptides: a significant step forward in the early diagnosis of rheumatoid arthritis. Clinical Chemistry and Laboratory Medicine, 45, 150-157.

BLANCA LAIN, M. A. C., AND GREGORY ZARBIS-PAPASTOITSIS 2009. Development of a High-Capacity MAb Capture Step Based on Cation-Exchange Chromatography. Bioprocess technical , Vol. 7, No. 5, May 2009, pp. 26–34

BOSWELL, C. A. & BRECHBIEL, M. W. 2007. Development of radioimmunotherapeutic and diagnostic antibodies: an inside-out view. Nuclear Medicine and Biology, 34, 757-778.

BOYCHYN, M., YIM, S. S. S., BULMER, M., MORE, J., BRACEWELL, D. G. & HOARE, M. 2004. Performance prediction of industrial centrifuges using scale-down models. Bioprocess and Biosystems Engineering, 26, 385-391.

BREHM-STECHER, B. F. & JOHNSON, E. A. 2004. Single-Cell Microbiology: Tools, Technologies, and Applications. Microbiol. Mol. Biol. Rev., 68, 538-559.

BRINKMANN, U., DI CARLO, A., VASMATZIS, G., KUROCHKINA, N., BEERS, R., LEE, B. & PASTAN, I. 1997. Stabilization of a recombinant Fv fragment By base-loop interconnection and VH-VL permutation. Journal of Molecular Biology, 268, 107-117.

BROOKS, C. A. & CRAMER, S. M. 1992. Steric mass-action ion exchange: Displacement profiles and induced salt gradients. AIChE Journal, 38, 1969-1978.

CAPELLE, M. A. H., GURNY, R. & ARVINTE, T. 2007. High throughput screening of protein formulation stability: Practical considerations. European Journal of Pharmaceutics and Biopharmaceutics, 65, 131-148.

CARTER, P. J. 2006. Potent antibody therapeutics by design. Nat Rev Immunol, 6, 343-357.

CARTER-FRANKLIN, J. N., VICTA, C., MCDONALD, P. & FAHRNER, R. 2007. Fragments of protein A eluted during protein A affinity chromatography. Journal of Chromatography A, 1163, 105-111.

CHAN, G., BOOTH, A. J., MANNWEILER, K. & HOARE, M. 2006. Ultra scale-down studies of the effect of flow and impact conditions during *E. coli* cell processing. Biotechnology and Bioengineering, 95, 671-683.

CHESTER, K. A. & HAWKINS, R. E. 1995. Clinical issues in antibody design. Trends in Biotechnology, 13, 294-300.

CHHATRE, S. & TITCHENER-HOOKER, N. J. 2009. Review: Microscale methods for high-throughput chromatography development in the pharmaceutical industry. Journal of Chemical Technology & Biotechnology, 84, 927-940.

CHUNG, S. F. & WEN, C. Y. 1968. Longitudinal dispersion of liquid flowing through fixed and fluidized beds. AIChE Journal, 14, 857-866.

CLARK, A. M. & BERVEN, H. 2004. The face of the patent is not the "Whole Story": determining effective life of a pharmaceutical patent in the United States. World Patent Information, 26, 283-295.

COFFMAN, J. L., KRAMARCZYK, J. F. & KELLEY, B. D. 2008. High-throughput screening of chromatographic separations: I. Method development and column modeling. Biotechnology and Bioengineering, 100, 605-618.

CONROY, P. J., HEARTY, S., LEONARD, P. & O'KENNEDY, R. J. 2009. Antibody production, design and use for biosensor-based applications. Seminars in Cell & Developmental Biology, 20, 10-26.

COSTANTINI, V. P., AZEVEDO, A. C., LI, X., WILLIAMS, M. C., MICHEL, F. C., JR. & SAIF, L. J. 2007. Effects of Different Animal Waste Treatment Technologies on Detection and Viability of Porcine Enteric Viruses. Appl. Environ. Microbiol., 73, 5284-5291.

CROMWELL, M., HILARIO, E. & JACOBSON, F. 2006. Protein aggregation and bioprocessing. The AAPS Journal, 8, E572-E579.

DEGERMAN, M., JAKOBSSON, N. & NILSSON, B. 2006. Constrained optimization of a preparative ion-exchange step for antibody purification. Journal of Chromatography A, 1113, 92-100.

DEPHILLIPS, P. & LENHOFF, A. M. 2000. Pore size distributions of cation-exchange adsorbents determined by inverse size-exclusion chromatography. Journal of Chromatography A, 883, 39-54.

DERRICK, J. P. & WIGLEY, D. B. 1992. Crystal structure of a streptococcal protein G domain bound to an Fab fragment. Nature, 359, 752-754.

DIMASI, J. A. & GRABOWSKI, H. G. 2007. The cost of biopharmaceutical R&D: is biotech different? Managerial and Decision Economics, 28, 469-479.

DOBLHOFF-DIER, O. 1999. Safe biotechnology 9: values in risk assessment for the environmental application of microorganisms. Trends in Biotechnology, 17, 307-311.

DOBLHOFF-DIER, O. & BLIEM, R. 1999. Quality control and assurance from the development to the production of biopharmaceuticals. Trends in Biotechnology, 17, 266-270.

DOLK, E., VAN DER VAART, M., LUTJE HULSIK, D., VRIEND, G., DE HAARD, H., SPINELLI, S., CAMBILLAU, C., FRENKEN, L. & VERRIPS, T. 2005. Isolation of Llama Antibody Fragments for Prevention of Dandruff by Phage Display in Shampoo. Appl. Environ. Microbiol., 71, 442-450.

ETTRE, L. 1979. preparative liquid chromatography: History and trends-supplemental remarks. Chromatographia, 12, 302-304.

FARID, S. S. 2007. Process economics of industrial monoclonal antibody manufacture. Journal of Chromatography B, 848, 8-18.

FARID, S. S. 2007. Process economics of industrial monoclonal antibody manufacture. Journal of Chromatography B, 848, 8-18.

FARKAS, E. J. & BYLEVELD, E. 1979. Longitudinal dispersion at low liquid flow rates in fixed beds with application to elution in demineralization by ion exchange. The Canadian Journal of Chemical Engineering, 57, 527-531.

FEDKIW, P. S. & NEWMAN, J. 1982. Mass-transfer coefficients in packed beds at very low reynolds numbers. International Journal of Heat and Mass Transfer, 25, 935-943.

FELINGER, A. & GUIOCHON, G. 1996. Optimizing preparative separations at high recovery yield. Journal of Chromatography A, 752, 31-40.

FERNANDES, P. B. 1998. Technological advances in high-throughput screening. Current Opinion in Chemical Biology, 2, 597-603.

FILPULA, D. 2007. Antibody engineering and modification technologies. Biomolecular Engineering, 24, 201-215.

FOLLMAN, D. K. & FAHRNER, R. L. 2004. Factorial screening of antibody purification processes using three chromatography steps without protein A. Journal of Chromatography A, 1024, 79-85.

FOOT, E., KLEYN, D. & PALMER FOSTER, E. 2010. Pharmacogenetics--pivotal to the future of the biopharmaceutical industry. Drug Discovery Today, 15, 325-327.
G.M. FERREIRA, J. D., K. PATEL, ALAHARI ARUNAKUMARI, PHD 2007. Chromatography: A Two-Column Process To Purify Antibodies Without Protein A. BioPharm International, 20, 12.

GALLANT, S. R. 2004. Modeling ion-exchange adsorption of proteins in a spherical particle. Journal of Chromatography A, 1028, 189-195.

GAO, Y., KIPLING, K., GLASSEY, J., WILLIS, M., MONTAGUE, G., ZHOU, Y. & TITCHENER-HOOKER, N. 2010. Application of Agent-Based System for Bioprocess Description and Process Improvement. In: LOVREK, I., HOWLETT, R. & JAIN, L. (eds.) Knowledge-Based Intelligent Information and Engineering Systems. Springer Berlin / Heidelberg.

GASSER, B. & MATTANOVICH, D. 2007. Antibody production with yeasts and filamentous fungi: on the road to large scale? Biotechnology Letters, 29, 201-212.

GEISBERGER, #160, ROLAND, LAMERS, MARINUS, ACHATZ & GERNOT 2006. The riddle of the dual expression of IgM and IgD, Oxford, ROYAUME-UNI, Blackwell.

GERALD PIER, J. L., LEE WETZLER 2004. Immunology, Infection, and Immunity

GHOSE, S., ALLEN, M., HUBBARD, B., BROOKS, C. & CRAMER, S. M. 2005. Antibody variable region interactions with Protein A: Implications for the development of generic purification processes. Biotechnology and Bioengineering, 92, 665-673.

GLOCKSHUBER, R., MALIA, M., PFITZINGER, I. & PLUECKTHUN, A. 1990. A comparison of strategies to stabilize immunoglobulin Fv-fragments. Biochemistry, 29, 1362-1367.

GOSLING, I. 2005. Process simulation and modeling for industrial bioprocessing: Tools and techniques. Industrial Biotechnology, 1, 106-109.

GRAUMANN, K. & PREMSTALLER, A. 2006. Manufacturing of recombinant therapeutic proteins in microbial systems. Biotechnology Journal, 1, 164-186.
HALE, G. 2006. Therapeutic antibodies -- Delivering the promise? Advanced Drug Delivery Reviews, 58, 633-639.

GU, T., TSAI, G. & TSAO, G. 1993. Modeling of nonlinear multicomponent chromatography. In: TSAO, G. (ed.) Chromatography. Springer Berlin / Heidelberg.
Gu. TING, 1995. Mathematical modelling and scale-up of liquid chromatography, Berlin: Springer Verlag.

HARDIN, A. M., HARINARAYAN, C., MALMQUIST, G., AXÉN, A. & VAN REIS, R. 2009. Ion exchange chromatography of monoclonal antibodies: Effect of resin ligand density on dynamic binding capacity. Journal of Chromatography A, 1216, 4366-4371.

HARINARAYAN, C., MUELLER, J., LJUNGLÖF, A., FAHRNER, R., ALSTINE, J. V. & REIS, R. V. 2006. An exclusion mechanism in ion exchange chromatography. Biotechnology and Bioengineering, 95, 775-787.

HUBBUCH, J., LINDEN, T., KNIEPS, E., THÖMMES, J. & KULA, M. R. 2002. Dynamics of protein uptake within the adsorbent particle during packed bed chromatography. Biotechnology and Bioengineering, 80, 359-368.

HUDSON, P. H. P. J. 2005. Engineered antibody fragments and the rise of single domains. Nature Biotechnology, 23, 10.

JANEWAY, C. A., TRAVERS, P., WALPORT, P. M. 2001. Immunobiology, Oxford, UK, Garland Publishing

JOOSTEN, V., LOKMAN, C., VAN DEN HONDEL, C. & PUNT, P. 2003. The production of antibody fragments and antibody fusion proteins by yeasts and filamentous fungi. Microbial Cell Factories, 2, 1.

JORDAN, M. A. 1996. Bioprocess engineering principles : Pauline M. Doran Academic Press Ltd, London, 1995. 439 pps. Price £24.95 (pbk). ISBN 0-12-220856-0. Minerals Engineering, 9, 133-135.

JUE (MICHELLE) WANG, P., TIMOTHY DIEHL, MARK WATKINS-FISCHL, DEBORAH PERKINS, DEENA AGUIAR, ALAHARI ARUNAKUMARI, PHD 2008. Optimizing the Primary Recovery Step in Nonaffinity Purification Schemes for HuMAbs. BioPharm International 21, 5.

KACZMARSKI, K., ANTOS, D., SAJONZ, H., SAJONZ, P. & GUIOCHON, G. 2001. Comparative modeling of breakthrough curves of bovine serum albumin in anion-exchange chromatography. Journal of Chromatography A, 925, 1-17.

KALTENBRUNNER, O., GIAVERINI, O., WOEHLE, D. & ASENJO, J. 2007. Application of chromatographic theory for process characterization towards validation of an ion-exchange operation. Biotechnology and Bioengineering, 98, 201-210.

KARLSSON, D., JAKOBSSON, N., AXELSSON, A. & NILSSON, B. 2004. Model-based optimization of a preparative ion-exchange step for antibody purification. Journal of Chromatography A, 1055, 29-39.

KELLEY, B. D., SWITZER, M., BASTEK, P., KRAMARCZYK, J. F., MOLNAR, K., YU, T. & COFFMAN, J. 2008. High-throughput screening of chromatographic separations: IV. Ion-exchange. Biotechnology and Bioengineering, 100, 950-963.

KEMPE, H., AXELSSON, A., NILSSON, B. & ZACCHI, G. 1999. Simulation of chromatographic processes applied to separation of proteins. Journal of Chromatography A, 846, 1-12.

KEMPE, H., PERSSON, P., AXELSSON, A., NILSSON, B. & ZACCHI, G. 2006. Determination of diffusion coefficients of proteins in stationary phases by frontal chromatography. Biotechnology and Bioengineering, 93, 656-664.

KOHLER, G. & MILSTEIN, C. 1975. Continuous cultures of fused cells secreting antibody of predefined specificity. Nature, 256, 495-497.

KOTHS, K. 1995. Recombinant proteins for medical use: the attractions and challenges. Current Opinion in Biotechnology, 6, 681-687.

KRAMARCZYK, J. F., KELLEY, B. D. & COFFMAN, J. L. 2008. High-throughput screening of chromatographic separations: II. Hydrophobic interaction. Biotechnology and Bioengineering, 100, 707-720.

KRAUSS, J. 2003. Recombinant antibodies for the diagnosis and treatment of cancer. Molecular Biotechnology, 25, 1-17.

KUPPER, M., HUHN, M., SPIEGEL, H., MA, J., BARTH, S., FISCHER, R. & FINNERN, R. 2005. Generation of human antibody fragments against Streptococcus mutans using a phage display chain shuffling approach. BMC Biotechnology, 5, 4.

KURIEN, B. A. S., K.B 2006. Western blotting Methods.
LEVISON, P. R. 2003. Large-scale ion-exchange column chromatography of proteins: Comparison of different formats. Journal of Chromatography B, 790, 17-33.

LIAPIS, A. I. & GRIMES, B. A. 2008. On film mass transfer coefficient expression in ion-exchange chromatography systems. Separation and Purification Technology, 59, 342-345.

LIM, A. C., ZHOU, Y., WASHBROOK, J., TITCHENER-HOOKER, N. J. & FARID, S. 2004. A decisional-support tool to model the impact of regulatory compliance activities in the biomanufacturing industry. Computers & Chemical Engineering, 28, 727-735.

LJUNGLÖF, A., LACKI, K. M., MUELLER, J., HARINARAYAN, C., REIS, R. V., FAHRNER, R. & ALSTINE, J. M. V. 2007. Ion exchange chromatography of antibody fragments. Biotechnology and Bioengineering, 96, 515-524.

LOW, D., O'LEARY, R. & PUJAR, N. S. 2007. Future of antibody purification. Journal of Chromatography B, 848, 48-63.

LYDDIATT, A. 2002. Process chromatography: current constraints and future options for the adsorptive recovery of bioproducts. Current Opinion in Biotechnology, 13, 95-103.

MARTIN, M. & GUIOCHON, G. 2005. Effects of high pressure in liquid chromatography. Journal of Chromatography A, 1090, 16-38.

MAZOR, Y., BLARCOM, T. V., MABRY, R., IVERSON, B. L. & GEORGIOU, G. 2007. Isolation of engineered, full-length antibodies from libraries expressed in Escherichia coli. Nat Biotech, 25, 563-565.

MAZUR, P. 1970. Cryobiology: The Freezing of Biological Systems. Science, 168, 939-949.

MAZZA, C. B., REGE, K., BRENEMAN, C. M., SUKUMAR, N., DORDICK, J. S. & CRAMER, S. M. 2002. High-throughput screening and quantitative structure-efficacy relationship models of potential displacer molecules for ion-exchange systems. Biotechnology and Bioengineering, 80, 60-72.

MOLLERUP, J. M., HANSEN, T. B., KIDAL, S., SEJERGAARD, L., HANSEN, E. & STABY, A. 2009. Use of Quality by the Design for the Modelling of Chromatographic Separations. Journal of Liquid Chromatography & Related Technologies, 32, 1577 - 1597.

MOLLERUP, J. M., HANSEN, T. B., KIDAL, S., SEJERGAARD, L., HANSEN, E. & STABY, A. 2009. Use of Quality by the Design for the Modelling of Chromatographic Separations. Journal of Liquid Chromatography & Related Technologies, 32, 1577 - 1597.

MORRISON, S. L. 1992. In Vitro Antibodies: Strategies for Production and Application. Annual Review of Immunology, 10, 239-265.

MORROW, K. J. 2008. Revamping Recovery & Purification Strategies - Search Continues for Effective Alternatives. GEN news. http://www.genengnews.com: genetic engineering and biotechnology news.

MÜLLER, E. 2005. Properties and Characterization of High Capacity Resins for Biochromatography. Chemical Engineering & Technology, 28, 1295-1305.

MÜLLER-SPÄTH, T., AUMANN, L. & MORBIDELLI, M. 2009. Role of Cleaning-in-Place in the Purification of mAb Supernatants Using Continuous Cation Exchange Chromatography. Separation Science and Technology, 44, 1 - 26.

NEWCOMBE, A., NEWCOMBE, C., & FRANCIS, R. 2008. Development of an ion-exchange process. Apr 15 2008 ed.: genetic engineering and biotechnology news.

NYGREN, P.-Å., STEFAN, S. & UHLÉN, M. 1994. Engineering proteins to facilitate bioprocessing. Trends in Biotechnology, 12, 184-188.

PAVLOU, A. K. & BELSEY, M. J. 2005. The therapeutic antibodies market to 2008. European Journal of Pharmaceutics and Biopharmaceutics, 59, 389-396.

PERSSON, P., KEMPE, H., ZACCHI, G. & NILSSON, B. 2004. A Methodology for Estimation of Mass Transfer Parameters in a Detailed Chromatography Model Based on Frontal Experiments. Chemical Engineering Research and Design, 82, 517-526.

PETRIDES, D., COONEY, C. L., EVANS, L. B., FIELD, R. P. & SNOSWELL, M. Bioprocess simulation: An integrated approach to process development. Computers & Chemical Engineering, 13, 553-561.

PETSCH, D. & ANSPACH, F. B. 2000. Endotoxin removal from protein solutions. Journal of Biotechnology, 76, 97-119.

RAAG, R. & WHITLOW, M. 1995. Single-chain Fvs. FASEB J., 9, 73-80.

RAVETCH, J. V. & BOLLAND, S. 2001. IGG FC RECEPTORS. Annual Review of Immunology, 19, 275-290.

REEN, D. J. 1994. Basic protein and peptide protocols, NJ, Humana Press.
REICHERT, J. M., ROSENSWEIG, C. J., FADEN, L. B. & DEWITZ, M. C. 2005. Monoclonal antibody successes in the clinic. Nat Biotech, 23, 1073-1078.

REYNOLDS, T., BOYCHYN, M., SANDERSON, T., BULMER, M., MORE, J. & HOARE, M. 2003. Scale-down of continuous filtration for rapid bioprocess design: Recovery and dewatering of protein precipitate suspensions. Biotechnology and Bioengineering, 83, 454-464.

REYNOLDS, T., BOYCHYN, M., SANDERSON, T., BULMER, M., MORE, J. & HOARE, M. 2003. Scale-down of continuous filtration for rapid bioprocess design: Recovery and dewatering of protein precipitate suspensions. Biotechnology and Bioengineering, 83, 454-464.

RODRIGUES, M., SNEDECOR, B., CHEN, C., WONG, W., GARG, S., BLANK, G., MANEVAL, D. & CARTER, P. 1993. Engineering Fab' fragments for efficient F(ab)2 formation in Escherichia coli and for improved in vivo stability. J Immunol, 151, 6954-6961.

ROSES, A. D. 2008. Pharmacogenetics in drug discovery and development: a translational perspective. Nat Rev Drug Discov, 7, 807-817.

ROUF, S. A., DOUGLAS, P. L., MOO-YOUNG, M. & SCHARER, J. M. 2001. Computer simulation for large scale bioprocess design. Biochemical Engineering Journal, 8, 229-234.

ROUSH, D. J. & LU, Y. 2008. Advances in Primary Recovery: Centrifugation and Membrane Technology. Biotechnology Progress, 24, 488-495.

SCHELLEKENS, H. 2004. When biotech proteins go off-patent. Trends in Biotechnology, 22, 406-410.

SENTELL, K. B. & DORSEY, J. G. 1989. Retention mechanisms in reversed-phase chromatography : Stationary phase bonding density and solute selectivity. Journal of Chromatography A, 461, 193-207.

SHUKLA, A. A., GUPTA, P. & HAN, X. 2007. Protein aggregation kinetics during Protein A chromatography: Case study for an Fc fusion protein. Journal of Chromatography A, 1171, 22-28.

SHUKLA, A. A., HUBBARD, B., TRESSEL, T., GUHAN, S. & LOW, D. 2007. Downstream processing of monoclonal antibodies--Application of platform approaches. Journal of Chromatography B, 848, 28-39.

SHUKLA, A. A. & THÖMMES, J. 2010. Recent advances in large-scale production of monoclonal antibodies and related proteins. Trends in Biotechnology, 28, 253-261.
SIDHU, S. S. & FELLOUSE, F. A. 2006. Synthetic therapeutic antibodies. Nat Chem Biol, 2, 682-688.

SKERRA, A. & PLUCKTHUN, A. 1988. Assembly of a functional immunoglobulin Fv fragment in Escherichia coli. Science, 240, 1038-1041.

SOMMERFELD, S. & STRUBE, J. 2005. Challenges in biotechnology production--generic processes and process optimization for monoclonal antibodies. Chemical Engineering and Processing, 44, 1123-1137.

STICKEL, J. J. & FOTOPOULOS, A. 2001. Pressure-Flow Relationships for Packed Beds of Compressible Chromatography Media at Laboratory and Production Scale. Biotechnology Progress, 17, 744-751.

STROHL, W. R. & KNIGHT, D. M. 2009. Discovery and development of biopharmaceuticals: current issues. Current Opinion in Biotechnology, 20, 668-672.
STRUCK, M.-M. 1994. Biopharmaceutical R&D Success Rates and Development Times. Bio/Technology 12.

SUBRAMANIAN, A. 2005. Chromatographic Purification of MAbs with Non-Affinity Supports. BioPharm International, June 1, 2005.

SUSANTO, A., HERRMANN, T., VON LIERES, E. & HUBBUCH, J. 2007. Investigation of pore diffusion hindrance of monoclonal antibody in hydrophobic interaction chromatography using confocal laser scanning microscopy. Journal of Chromatography A, 1149, 178-188.

SUSANTO, A., KNIEPS-GRÜNHAGEN, E., LIERES, E. V. & HUBBUCH, J. 2008. High Throughput Screening for the Design and Optimization of Chromatographic Processes: Assessment of Model Parameter Determination from High Throughput Compatible Data. Chemical Engineering & Technology, 31, 1846-1855.

SUSANTO, A., TREIER, K., KNIEPS-GRÜNHAGEN, E., LIERES, E. V. & HUBBUCH, J. 2009. High Throughput Screening for the Design and Optimization of Chromatographic Processes: Automated Optimization of Chromatographic Phase Systems. Chemical Engineering & Technology, 32, 140-154.

TAIT, A., AUCAMP, J., BUGEON, A. & HOARE, M. 2009. Ultra scale-down prediction using microwell technology of the industrial scale clarification characteristics by centrifugation of mammalian cell broths. Biotechnology and Bioengineering, 104, 321-331.

TITCHENER-HOOKER, N. J., DUNNILL, P. & HOARE, M. 2008. Micro biochemical engineering to accelerate the design of industrial-scale downstream processes for biopharmaceutical proteins. Biotechnology and Bioengineering, 100, 473-487.

TITCHENER-HOOKER, S. C. A. N. J. 2008. Review: Microscale methods for high-throughput chromatography development in the Pharmaceutical industry. Journal of chemical technology

TYN, M. T. & GUSEK, T. W. 1990. Prediction of diffusion coefficients of proteins. Biotechnology and Bioengineering, 35, 327-338.

UNDERDOWN, B. J. & SCHIFF, J. M. 1986. Immunoglobulin A: Strategic Defense Initiative at the Mucosal Surface. Annual Review of Immunology, 4, 389-417.
VAN REIS, R. & ZYDNEY, A. 2001. Membrane separations in biotechnology. Current Opinion in Biotechnology, 12, 208-211.

VELAYUDHAN, A. & HORVÁTH, C. 1994. Adsorption and ion-exchange isotherms in preparative chromatography. Journal of Chromatography A, 663, 1-10.
VLIEGHE, P., LISOWSKI, V., MARTINEZ, J. & KHRESTCHATISKY, M. 2010. Synthetic therapeutic peptides: science and market. Drug Discovery Today, 15, 40-56.

VOET, D. A. V., J.G. 1995. Biochemistry, New York, John Wiley & Sons, Inc. .
WESTERLUND, B. 2006. Separating Proteins Using Ion-Exchange Chromatography.

WHEELWRIGHT, S. M. 1987. Designing Downstream Processes for Large−Scale Protein Purification. Bio/Technology.

WHEELWRIGHT, S. M. 1994. Commercializing Biotech products. Bio/Technology, 12, 4.

WHITLEY, R. D., COTT, K. E. V., BERNINGER, J. A. & WANG, N.-H. L. 1991. Effects of protein aggregation in isocratic nonlinear chromatography. AIChE Journal, 37, 555-568.

WIENDAHL, M., WIERLING, P. S., NIELSEN, J., CHRISTENSEN, D. F., KRARUP, J., STABY, A. & HUBBUCH, J. 2008. High Throughput Screening for the Design and Optimization of Chromatographic Processes - Miniaturization, Automation and Parallelization of Breakthrough and Elution Studies. Chemical Engineering & Technology, 31, 893-903.

WIESEL, A., SCHMIDT-TRAUB, H., LENZ, J. & STRUBE, J. 2003. Modelling gradient elution of bioactive multicomponent systems in non-linear ion-exchange chromatography. Journal of Chromatography A, 1006, 101-120.

WILLEMS, A., LEOEN, J., SCHOONOOGHE, S., GROOTEN, J. & MERTENS, N. 2003. Optimizing expression and purification from cell culture medium of trispecific recombinant antibody derivatives. Journal of Chromatography B, 786, 161-176.

YU, L. 2008. Pharmaceutical Quality by Design: Product and Process Development, Understanding, and Control. Pharmaceutical Research, 25, 781-791.

ZAPATA, G., RIDGWAY, J. B. B., MORDENTI, J., OSAKA, G., WONG, W. L. T., BENNETT, G. L. & CARTER, P. 1995. Engineering linear F(ab')2 fragments for

efficient production in Escherichia coli and enhanced antiproliferative activity. Protein Eng., 8, 1057-1062.

ZHOU, Y. H. & TITCHENER-HOOKER, N. J. 1999. Visualizing integrated bioprocess designs through "windows of operation". Biotechnology and Bioengineering, 65, 550-557.